UiO : Department of Physics
University of Oslo

Anomalous transport in a toroidal plasma

Master Thesis

Anne Schad Bergsaker

December 2012

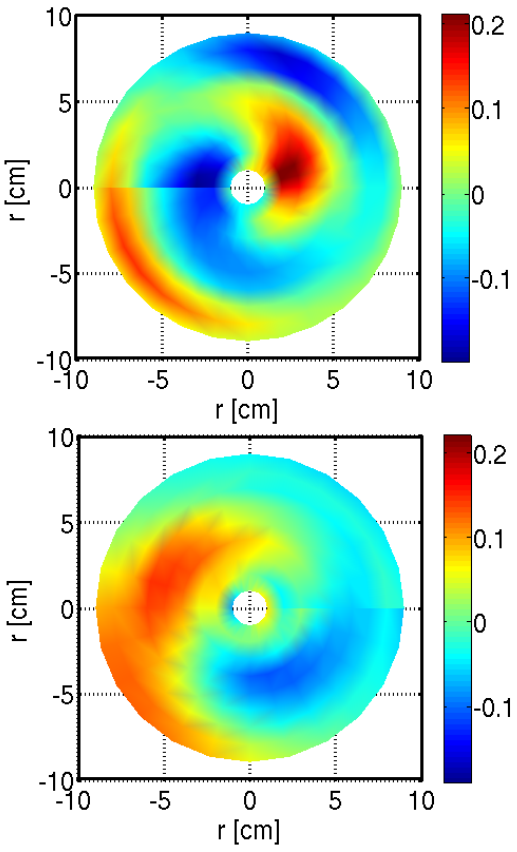

Abstract

Experimentally obtained data from the toroidal Blaamann device have been analysed. Blaamann is a simple magnetised torus with no rotational transform, and plasma is generated by a discharge from a hot filament emitting electrons. The data were obtained using a three pin Langmuir probe in combination with a stationary reference probe. Sampled floating potential and electron saturation currents from 19 different positions along the horizontal central line in a poloidal cross section, enabled us to study the turbulent transport within the plasma column.

Several statistical properties of the data were investigated. The average transport of flux is outwards, with large fluctuations in signals near the filament, but decreasing with distance from the source. A clear and systematic relation between skewness and kurtosis was also identified.

Through use of cross correlation functions and the conditional sampling technique we were able to investigate the nature of the anomalous transport, as well as identify coherent structures. These structures appear to be burst-like in nature, with a lifetime of ~ 100 μs. There is some indication that these structures are vortex-like. The coherent structures propagate around the poloidal cross section along with the rest of the plasma column, rotating with the $\mathbf{E} \times \mathbf{B}/B^2$-velocity, and at the same time transporting plasma radially out of the column, giving rise to spiral trajectories.

Acknowledgments

Firstly I would like to thank my supervisor Prof. Hans L. Pécseli for giving me this opportunity, and for all his help and advise throughout this process, and for reading through my thesis more times than I care to count. Your encouragement and guiding has been invaluable, and really I appreciate it.

I would also like to thank Prof. Åshild Fredriksen at the University of Tromsø for all her help during my stay in Tromsø, and after. Thank you for not only putting up with all my e-mails, but actually answering them as well.

Prof. em. Jan Trulsen for taking an interest in my thesis, and offering insightful comments on my results.

Thanks to Hans Brenna, Christoffer Stausland, Elling Hauge-Iversen and all the rest of you guys at the Plasma and space physics group for interesting and helpful discussions, for happy lunch hours and good company.

And to AJ for reminding me that even physicists need some time off every now and then.

Finally, the Magnifica, for making great coffee and keeping me awake and alert in these final stages.

Contents

Chapter 1

Introduction

Plasma is a partially or fully ionised gas in which a portion of the electrons and ions can move about freely. The ionisation makes plasma significantly different from classical neutral gases since the charged components have a high mobility. This allows the flow of charged particles that generates currents and magnetic fields. Forces due to electromagnetic effects are important in describing the properties and dynamics of plasmas, as electric and magnetic forces allow the particles to interact over large distances. Since plasma is in nature so different from a gas, it is often referred to as the fourth state of matter.

Even though over 90% of all visible matter in the universe consists of plasma, it was not discovered until the late 1800s, when Sir William Crookes conducted his experiments on Crookes tubes discovering what he referred to as *radiant matter* (Crookes, 1879). The term *plasma* was first used by Irving Langmuir in 1928 (Langmuir, 1928). He needed to find a name for the non-sheath region of the discharge in mercury, and he did not wish to invent a new word. Somehow he found inspiration in the medical term blood plasma, even though his colleague Tonks later specified that Langmuir did not in any way see gaseous plasma as an analogue to the liquid component of blood (Tonks, 1967).

Plasma is formed in the Earth's near as well as more distant environment, i.e. in the ionosphere and magnetosphere as well as in distant space. Study and modelling of plasmas is therefore to some extent motivated by the need to have space equipment, such as satellites and rockets functioning in an environment dominated by plasma. Industrial plasmas on the other hand are used for various processes, perhaps the most notable of which is thermonuclear fusion, which is seen as a promising new way of generating electricity. Through thermonuclear fusion, the goal is to achieve a steady state referred to as *self-sustained burn*, which means that once the process is started it will continue in principle indefinitely, generating energy. Many different devices were considered originally, where early suggestions consisted of various pinch-types (Bishop, 1958). In modern days most devices have

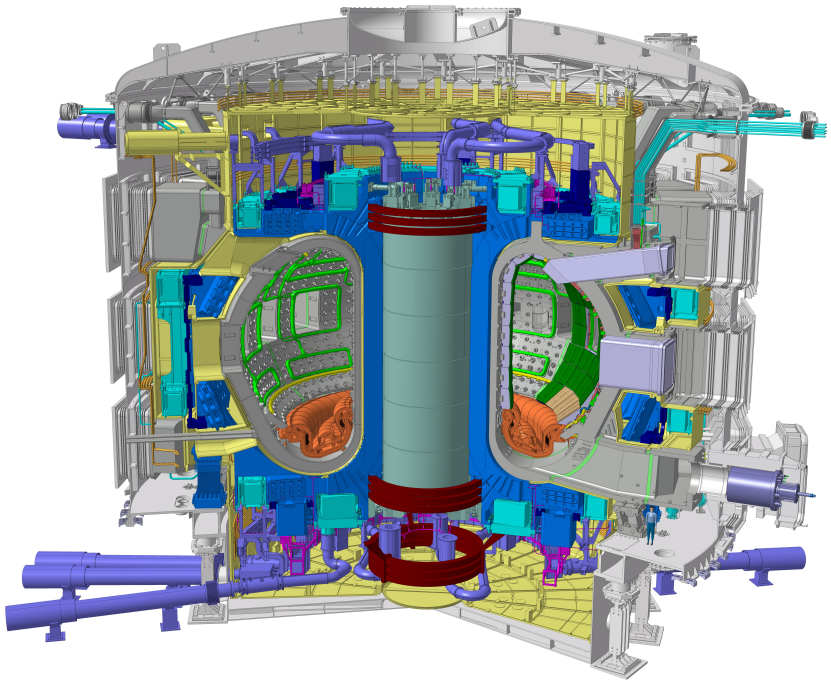

Figure 1.1: *Illustration of the future fusion device ITER currently being built in Cadarache, France. Notice the little man included on the right hand side of the sketch, giving an image of the shear size of this tokamak. Source of image: www.iter.org.*

a toroidal configuration, such as stellarators and tokamaks, the latter being the most common. In a tokamak a combined toroidal and poloidal magnetic field is used to confine a plasma. The toroidal field is generated using coils, while the poloidal field is set up by currents within the plasma itself. The result is more stable confinement than with a purely toroidal field, since the poloidal field keeps the plasma from drifting outwards towards the wall.

Figure 1.1 shows an illustration of a fusion device called ITER (originally an acronym for International Thermonuclear Experimental Reactor), currently under construction in Cadarache in southern France. When it is finished it will be the largest and most advanced experimental tokamak nuclear fusion reactor in the world, aiming to be the first ever fusion power plant producing electricity. The limiting factor for confinement of warm plasmas by magnetic fields seem to be turbulent transport. Classical collisional diffusion is also present, but this alone is not posing any serious threat to the plasma confinement. Studies of turbulent plasma transport has evolved to become an independent discipline, and the present thesis is a part of this.

The experimental data analysed in this study are from an experiment conducted with the Blaamann plasma device. It is a simple magnetised torus, which means it has a simple magnetic configuration. The magnetic field is purely toroidal, with no poloidal component, i.e. there is no rotational transform. The Blaamann device consists of a rather small toroidal tank. Originally it was constructed and set up in 1989 at the University in Tromsø, though it does not remain there today. Blaamann is not a fusion device, but a tank designed to do simple experiments on toroidal plasma. In the present study we intend to focus on anomalous, i.e. non-collisional transport within the plasma column, looking at both statistical properties of the fluctuating density, velocity and flux, as well as singling out larger events. The latter is to enable us to to investigate the possibility that we have larger coherent structures, and if so, how they are transported within the plasma. As there is no poloidal field to help with confinement, we have some loss of plasma as it is transported outwards, but this is on average balanced by the production of plasma over time (Rypdal et al., 1994).

1.1 Motivation for this study

The overall aim of this thesis is to study the anomalous transport within a toroidal plasma. Turbulent flows have a unique ability to disperse particles at a rate which greatly exceeds transport by classical molecular diffusion. The dominant mechanism within turbulent transport in plasmas is in many cases found to be transport due to low-frequency electrostatic waves that are strongly magnetic field aligned. However, in this study we will focus on analysing the turbulent fluctuations, while the driving mechanism (a plasma instability) will not be addressed.

Turbulence in itself is difficult to simulate realistically, as most systems tend to be too complex to cover all contributing factors. Experimental data offer a unique insight into the turbulent nature of plasmas, without requiring great computational resources beyond handling and treating the recorded data. Even though we only have data along the horizontal midline of a circular cross section we intend to show that much can still be deduced concerning transport within the entire cross section, and consequently the entire plasma column.

In addition, simple magnetised tori play in important role in the understanding of tokamak transport. It is easier to accomplish a good comparison between theory and experiment when dealing with a simpler case. Studying the results from a device such as Blaamann offers a chance to check theoretical models against real experimental results.

1.2 Structure of the thesis

This thesis consists of some background theory relevant to this study, as well as an outline of the various methods used. This is to illustrated how the results are obtained.

- Chapter 2
  This chapter presents a brief overview of some basic concepts within plasma physics. This is included in the thesis for the sake of completeness, emphasising the elements most useful to this study. Some of this background theory is related to general plasma physics, such as single particle motion. In addition a few topics relating to the actual experimental measurements are also included.

- Chapter 3
  This chapter offers some theoretical background material regarding anomalous transport. Two different types of turbulent transport in a magnetised plasma are presented.

- Chapter 4
  Here we present an outline of the experimental device and set-up. The relevant background parameters are presented and described, and the necessary conversion from raw data to density, velocity and flux are explained. The motion of the entire plasma column is also briefly described.

- Chapter 5
  In this chapter the methods used to analyse and study the data are described.

- Chapter 6
  A presentation of the results is given, including graphical representation of our findings. Important aspects of the results are emphasised.

- Chapter 7
  Discussion and conclusion, interpreting the results. Suggestions for future work are also presented.

Chapter 2

The basics of plasma physics

Since plasma differs significantly from all other states of matter, a brief overview of the basic concepts regarding the general description of a plasma is included in this chapter. The motion occurring within a plasma due to electric and magnetic forces is also described here, as this is very relevant to the plasma motion within Blaamann. As this is a study of experimental data, a short introduction to the mechanics of basic probes is also included, as well as concepts that are relevant for plasma confinement.

An important concept in plasma physics is *quasi-neutrality*. A plasma is said to be quasi-neutral as long as the total number of electrons on a large scale is roughly the same as the number of ions, i.e. overall the electric charge of the plasma is close to zero. There can still occur small perturbations, but this happens only on small characteristic time and length-scales, and will generally be shielded by the surrounding plasma.

When dealing with highly dilute plasmas, it is convenient to describe the motion in the plasma by single particle motion. In such cases no collective interaction needs to be taken into account, and only the background fields affecting the charged particle is needed to describe the motion. However, if the density of the plasma is sufficiently large, interactions mediated by electric and magnetic forces has to be accounted for. Interaction can be assumed to occur in essentially two different ways. One possibility is that we have collisional processes, i.e. interaction between only two particles at a time. The other possibility is that we have a large number of particles that simultaneously affect the motion of one selected reference particle.

2.1 Basic plasma parameters

There are four parameters that prove useful when describing a plasma. These are the thermal velocity, the plasma frequency, the Debye length and the plasma

parameter. Therefore brief definitions of all four are included here. In this study we use the definition where the temperature is given in eV, which is equivalent to a temperature in Kelvin satisfying the relation $\kappa T = e\phi$.

2.1.1 Thermal velocity

The thermal velocity is the typical velocity of the thermal motion of the particles in a fluid or gas. Hence it is also a measure of temperature. The definition used here is

$$u_{th,s} = \left(\frac{eT_s}{m_s}\right)^{1/2}, \tag{2.1}$$

where e is elementary charge, T_s is the temperature given in eV and m_s the mass of particle species s. This definition has excluded a numerical constant for simplicity. The expression is found numerically from conservation of energy, i.e. from $\frac{1}{2}m_s\langle u^2\rangle = \frac{3}{2}eT_s$ for monoatomic gases with three degrees of freedom, and $u_{th}^2 = \langle u^2\rangle$.

2.1.2 The plasma frequency

A characteristic time scale is the inverse of the plasma frequency, ω_{pe}, defined as

$$\omega_{pe} = \left(\frac{e^2 n}{\epsilon_0 m_e}\right)^{1/2}, \tag{2.2}$$

where n is the number density and m_e is the electron mass. Consider a slab of plasma within which the electrons have been slightly displaced with respect to the ions. This small perturbation in the charge density distribution sets up an electric field. Since the electrons are much smaller and lighter than the ions, they are also much more mobile. The result is that the electrons start to oscillate about the equilibrium position with a characteristic frequency ω_{pe}. The corresponding plasma period is then $\tau_p = 2\pi/\omega_{pe}$.

2.1.3 The Debye length

The characteristic length scale in a plasma is the *Debye length*, λ_{De}.

$$\lambda_{De} = \left(\frac{\epsilon_0 T_e}{en}\right)^{1/2} \tag{2.3}$$

A plasma particle moving with the thermal velocity u_{th} will travel one Debye length in one plasma period. Physically, this distance characterises a shielding

distance. When a single charge q is introduced into a plasma, the surrounding particles of opposite charge will attempt to screen off the electric potential arising due to q. The result is that further away from the charge, this minor perturbation is close to undetectable, and only the collective behaviour of all the particles in the plasma can be observed. At a distance of one Debye length from q, the electric potential of this charge is reduced by a factor of e^{-1}, i.e. the charge is shielded by the surrounding plasma.

2.1.4 The plasma parameter

From the Debye length and the plasma density the plasma parameter can be constructed.

$$N_p = n\lambda_{De}^3 \tag{2.4}$$

This dimensionless quantity is related to the average number of particles contained within a sphere with radius λ_{De}. As long as the number of particles within the Debye sphere is large, any small perturbation within it will not be noticed a certain distance from it. This is because the many other particles within the sphere shield off any small perturbation, thus the overall electric field is not noticeably influenced. However, if the number of particles within the Debye sphere is low, any change of the charge distribution within it might have a significant effect on the surroundings, and the electric field might be perturbed. Thus the plasma parameter is a tool that enables us to predict whether a plasma will be dominated by the discrete nature of the particles, or their collective behaviour. We have that $\lambda_{De}^3 \sim n^{-3/2}T^{1/2}$, which means that $N_p \sim n^{-1/2}T^{3/2}$. This means that N_p will increase either if T increases or n decreases. Thus any plasma with $N_p \gg 1$ will be hot and dilute.

2.2 Single particle motion

The simplest version of a plasma imaginable is a plasma consisting of only one particle. This may seem like a gross oversimplification, but it turns out that the behaviour that can be deduced for a single particle in magnetic and electric fields, is also applicable to more complex plasmas.

2.2.1 $\mathbf{E} \times \mathbf{B}$-drift

The most significant force affecting a particle travelling through a combined electric and magnetic field is the Lorentz force,

$$\mathbf{F} = q(\mathbf{E} + \mathbf{U} \times \mathbf{B})\,. \tag{2.5}$$

Consider a particle with charge q and mass m moving with a velocity $\mathbf{U}$ through a uniform B-field. The equation of motion for the particle is then

$$m\frac{d}{dt}\mathbf{U}_\perp = q\mathbf{U}_\perp \times \mathbf{B}\,. \tag{2.6}$$

The magnetic field cannot impart any energy to a charged particle, since the force is perpendicular to the displacement. As the acceleration is perpendicular to $\mathbf{U}_\perp$, we have that $\mathbf{U}_\perp$ is constant in magnitude but not in direction. The result is that the particle will gyrate in a circular orbit with a radius given by the initial velocity, the Larmor radius

$$r_L = \frac{mU_\perp}{qB}\,, \tag{2.7}$$

and a frequency known as the cyclotron frequency

$$\Omega_c = \frac{qB}{m}\,. \tag{2.8}$$

If one should also introduce a constant electric field with a component perpendicular to the magnetic field, the resulting equation of motion would be

$$m\frac{d}{dt}\mathbf{U} = q(\mathbf{E}_\perp + \mathbf{U} \times \mathbf{B})\,. \tag{2.9}$$

By introducing a new velocity $\mathbf{U}_* \equiv \mathbf{U} - \mathbf{E}_\perp \times \mathbf{B}/B^2$, where $\mathbf{U}$ is the original velocity, it can be shown that the resulting velocity consists of two parts. One accounting for the gyromotion due to the magnetic field, and one accounting for the average motion of the gyro-centre. The latter is given below and is generally known as the $\mathbf{E} \times \mathbf{B}$-velocity.

$$\overline{\mathbf{U}}_{E\times B} = \frac{\mathbf{E}_\perp \times \mathbf{B}}{B^2} \tag{2.10}$$

Physically this drift occurs because of the effect the two different fields have on a charged particle. Assume that the charge q is positive. The electric field will then accelerate it along the direction of its field lines. Because the particle now has a velocity with a component $\perp\mathbf{B}$, its trajectory will be curved by the B-field, and it will eventually have completed a semicircle. This in turn will mean that the particle is moving against the E-field, which will cause it to decelerate and eventually stop. Then the whole cycle starts over again, causing a motion across both electric and magnetic field lines (see Figure 2.1). Notice that this drift does not cause charge separation as electrons and ions drift in the same direction.

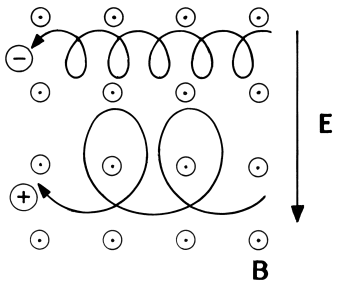

Figure 2.1: *Sketch of $E \times B$-drift for electrons and ions. Source: (Pécseli, 2012)*

2.2.2 Curvature drift

When the magnetic field is non-uniform additional drifts arise. They are most easily derived by generalising equation (2.10) to describe the drift due to any given force, **F**, as shown here.

$$\mathbf{U}_D = \frac{\mathbf{F} \times \mathbf{B}}{qB^2} \,. \tag{2.11}$$

Notice that as long as the force, **F**, has no first order dependence on the charge of a particle, the resultant drift will cause charge separation, i.e. electrons and ions moving in opposite directions.

A special case of this drift is the curvature drift. Assume that a charged particle with the same charge and mass as mentioned earlier has a significant velocity component parallel to a curved magnetic field. The particle will then experience a centrifugal force due to the curvature of the magnetic field lines. The expression for this force is given as

$$\mathbf{F}_C = m\, U_{||}^2 \frac{\overline{\mathbf{R}}}{\overline{R}^2} \,. \tag{2.12}$$

Notice that this force points away from the centre of curvature. We can assume that there is little motion along the magnetic field lines except for what is caused by the thermal motion, thus $U_{||}$ can be represented by u_{th}. This gives a resultant drift perpendicular to the magnetic field, given as

$$\overline{\mathbf{U}}_{DC} = \frac{m u_{th}^2}{qB} \frac{\mathbf{R} \times \mathbf{B}}{BR^2} \,. \tag{2.13}$$

In a toroidal device with only toroidal B-field this drift will be in the vertical direction, with electrons and ions moving in opposite directions.

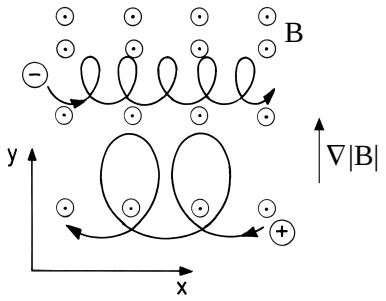

Figure 2.2: *Sketch of ∇B-drift for electrons and ions. Source: (Pécseli, 2012)*

2.2.3 ∇B-drift

When the magnetic field has a gradient perpendicular to the direction of $\mathbf{B}$, the resulting gyromotion is affected. The Larmor radius will not be constant over the course of one gyration, and thus the guiding centre drifts. See Figure 2.2.

It can be shown that the average drift velocity is

$$\overline{\mathbf{U}}_{\nabla B} = \frac{mU_\perp^2}{2qB}\frac{\mathbf{B}\times\nabla|B|}{B^2}\,, \tag{2.14}$$

and as can be seen from the expression, the resulting drift is perpendicular to both $\mathbf{B}$ and ∇B (Pécseli, 2012).

In a toroidal field the effect of the non-uniform magnetic field will cause a drift in the same direction as the curvature drift, with electrons and ions moving in opposite directions. Thus it would appear that the two are linked. Assuming that the magnetic field has a toroidal component only, the ∇B can be rewritten as

$$\frac{\nabla|B|}{|B|} = -\frac{\mathbf{R}}{R^2}\,,$$

leading back to (2.13).

The plasma drift velocities (2.13) and (2.14) are relevant for the Blaamann plasma since $\mathbf{B} = \mathbf{B}(\mathbf{r})$ there, due to the toroidal geometry.

2.2.4 Polarisation drift

Consider a case where we have a homogeneous time stationary magnetic field and a spatially uniform electric field $\perp \mathbf{B}$ that varies slowly in time. (By slow we mean compared to a gyroperiod.) For simplicity we assume that $\mathbf{E}$ only varies in intensity and not direction. A particle moving through such a field will have a time-varying $\mathbf{E}\times\mathbf{B}/B^2$-velocity, i.e. it will experience acceleration which in

the particles own frame of reference can be interpreted as a form of an artificial gravitational acceleration, $\mathbf{g}$. This gravitational acceleration is given as the time derivative of the $\mathbf{E} \times \mathbf{B}/B^2$-velocity

$$\mathbf{g} = -\left(\frac{1}{B^2}\right)\frac{d}{dt}(\mathbf{E} \times \mathbf{B})\,.$$

The resulting force $\mathbf{F} = m\mathbf{g}$ gives rise to the following velocity

$$\mathbf{U}_p = \frac{m}{eB^2}\frac{d}{dt}\mathbf{E}\,. \tag{2.15}$$

This drift velocity is called the polarisation drift and it is dependent on charge. Electrons and ions will move in opposite directions.

Equivalently, this can be used to describe the drift of a particle moving through a spatially inhomogeneous time-stationary electric field, since the particle will experience this as $\frac{d}{dt}\mathbf{E} \neq 0$ in its own frame of reference.

In Blaamann we have an electric field that consists of a time-stationary radial background field, $\mathbf{E}_0$, with an additional fluctuating component, causing an $\mathbf{E} \times \mathbf{B}/B^2$ as well as a polarisation drift.

2.3 Fluid model

When treating a plasma consisting of many particles, it is possible to treat this as an N-body problem, taking into account all the forces acting on every single particle, including interaction effects. However, when investigating macroscopic processes, it is much simpler to treat a plasma as a conducting fluid, and it turns out that the two different models yield the same results as long as the analysis is carried out consistently to the same order (Goldston and Rutherford, 1995).

The fluid model treats the plasma as a collection of fluid elements, thus only evaluating bulk parameters. These include particle density, flow velocity, current density, charge density and temperature over a collection of particles within a fluid element. Since this study is based on experimental data containing measurements of bulk parameters, and the spatial resolution is such that any microscopic effects would not be detected, it will be reasonable to treat the plasma tube contained within the Blaamann plasma tank as an electromagnetic fluid.

2.4 Plasma sheath and presheath

Any quasi-neutral plasma contained in a vacuum chamber will be joined to surfaces by a thin positively charged layer called a *sheath*. These arguments will in principle also apply to probe surfaces and similar.

2.4.1 Sheath region

Assume we have a plasma contained within a vacuum chamber, and that there is only a negligible electric field present. This means that the potential within the plasma is ~ 0. When electrons and ions collide with the wall they recombine, and are thus lost. As electrons are significantly more mobile than ions, they are lost more quickly, resulting in a build-up of positive charge near the wall. Therefore a potential must exist to contain the more mobile charged species, allowing the flow of positive and negative particles to the wall to be balanced (Chen, 1984). The non-neutral potential region between the quasi-neutral plasma and the wall is called a *sheath*, and is typically a few λ_{De} wide. An ion entering the sheath will then be accelerated towards the wall, while an electron will be reflected back into the plasma. The electron density near the wall will always be less than the ion density, as it decays on the order of a Debye length, shielding the electrons from the wall.

The Bohm sheath criterion states that the velocity of an ion in the sheath must be greater than or equal to the *Bohm velocity*, u_B

$$u_s \geq u_B = \left(\frac{eT_e}{M}\right)^{1/2}, \tag{2.16}$$

where T_e is given in electronvolts. The Bohm velocity is in itself the acoustic velocity of ions, and thus ions are supersonic in the sheath. (Chen, 1984; Lieberman and Lichtenberg, 2005)

2.4.2 The presheath

In order to ensure continuity of ion flux, there must be a finite electric field in the plasma over the same area, generally much wider than the sheath. This region is called the *presheath*. The presheath itself is not field free, but $\mathbf{E}$ is very small here, so there is a small potential drop. This potential drop accelerates the ions to the Bohm velocity, causing a transition from subsonic flow velocity in the bulk plasma to supersonic flow in the sheath. At the exact boundary between the sheath and the presheath, the ions have a velocity equal to the Bohm velocity.

In Blaamann we will have sheaths and presheaths both surrounding the outer wall, but also around the Langmuir probes used to measure floating potential and electron saturation current. The nature of the sheath and presheath regions must be taken into account when using the data to find the corresponding density fluctuations.

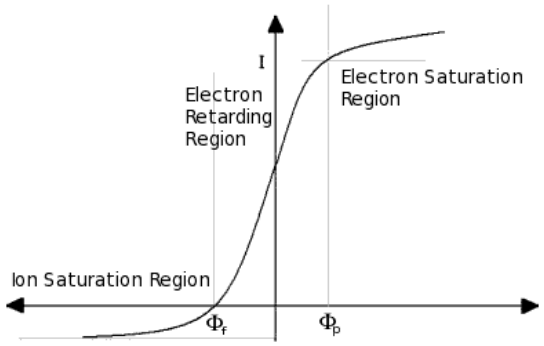

Figure 2.3: *I-V characteristic for a Langmuir probe.*

2.5 Langmuir probes

In 1926 Langmuir and Mott-Smith introduced the probe that was later to be known as the Langmuir probe (Mott-Smith and Langmuir, 1926). It is a metal probe inserted in a discharge, and biased with a positive or negative voltage drawing electron or ion current. The probe is surrounded by a sheath, but as the probe is very small it causes only minor perturbations in the plasma.

The voltage and current of a Langmuir probe gives an I-V characteristic, as shown in Figure 2.3. The probe is biased with a voltage V relative to the ground, drawing a corresponding current, I. The plasma itself has a potential Φ_p relative to the ground. For probe voltages $V \geq \Phi_p$ the probe draws mainly current from the more mobile electrons, which is defined as positive current flowing from the probe into the plasma. Increasing the value of potential on the probe will eventually lead to a saturation, i.e. that the probe measures only current from the electrons. This is known as the electron saturation current. For $V < \Phi_p$ the electrons are repelled, more so for lower values of the probe potential. Decreasing the potential will eventually give a situation where the electron current and the ion current are equal, thus resulting in a total current $I = 0$. This potential is referred to as the floating potential, Φ_f. The reason for the name is that at this potential an insulated probe, which cannot draw any current, will float. For probe potentials less than the floating potential the current is increasingly dominated by ion current (negative into the plasma), approaching the ion saturation current. The magnitude of the ion saturation current will normally be much less than the electron saturation current due the large mass of the ions compared to the electrons.

There is a significant uncertainty when using electron saturation current as a measure of density. The accuracy depends on how well the electron distribution corresponds to the assumed Maxwellian distribution. Sheath heating in a capacitive discharge may cause the electron distribution to get a high energy tail, thus

leaving the bulk electrons significantly colder than assumed through equilibrium discharge with a Maxwellian distribution (Lieberman and Lichtenberg, 2005).

In this study cylindrical probes were used to measure floating potential and electron saturation current. However, electron diffusion across magnetic field lines is greatly inhibited.

$$D_{\perp} = \frac{D_{||}}{1 + \omega_c^2 \tau_c^2} \,,$$

where ω_c is the gyration frequency, τ_c is the mean collision time, and $D_{||}$ is the drift coefficient along $\mathbf{B}$ while $D_{\perp}$ is the drift coefficient $\perp \mathbf{B}$. Because of this a cylindrical probe drawing electron current will behave similarly to a plane probe measuring conditions where there is no magnetic field. The only difference is that the effective probe area becomes equal to the probe cross section along the field lines, rather than the actual surface area of the cylindrical probe. Since the probe only collects electrons from a thin plasma layer corresponding to two times the probe cross section (front and back), it can be treated like a plane probe.

Chapter 3

Turbulent plasma transport

It has been shown by Rypdal et al. (1994) that no classical mechanisms can account for the transport of charge from the filament to the wall in Blaamann. Both experimental and theoretical evidence suggests that the charge transport is due to turbulent processes, and that this turbulence is also what causes the cross field plasma transport. However, the question is whether this turbulence in mainly diffusive or burst-like is nature.

This chapter outlines the mechanisms of turbulent diffusion as well as plasma blob transport.

3.1 Classical diffusion

In classical diffusion collisions between particles cause them to wander significant distances from their respective starting positions. In a non-uniform plasma the result of such motion is a net migration of particles from an area with high density to one with lower density, thus levelling out any large scale density gradients. Mathematically it is described by the diffusion equation in one spatial dimension

$$\frac{\partial n}{\partial t} = \frac{\partial}{\partial x}\left(D\frac{\partial n}{\partial x}\right), \tag{3.1}$$

where D is the diffusion coefficient.

A simple and illustrative way of describing diffusion is the *random walk* model. Assuming a number of particles are moving randomly along a straight line with a step length of Δx taken at equal intervals of time Δt, we can estimate the average motion. If there are many similar particles that all start out from $x = 0$, all with an equal chance of moving to the left or to the right, the average position of the group of particles will be

$$\langle x \rangle = 0$$

at any given time. However, after some time the group will have spread out. Even though it will have spread a nearly equal distance on either side, the root-mean-square position will not be zero. It can be shown that this quantity increases in time as

$$\frac{d}{dt}\langle x^2\rangle = \frac{(\Delta x)^2}{\Delta t}\,,$$

which gives

$$\langle x^2\rangle = \frac{(\Delta x)^2 t}{\Delta t}\,,$$

where the aforementioned diffusion coefficient is related through $D \sim (\Delta x)^2/\Delta t$. Thus in classical diffusion the spread of the particles goes as $\langle x^2\rangle \sim t$.

This can be generalised to three dimensions, with the diffusion equation becoming

$$\frac{\partial n}{\partial t} = \nabla\cdot(D\nabla n)\,. \tag{3.2}$$

Note that since charged particles can move freely along magnetic field lines, diffusion parallel to the magnetic field is reduced by collisions. However, diffusion across the magnetic field is enhanced by collisions. We will focus on transport across $\mathbf{B}$.

As D has dimension $[D] = length^2/time$, it seems reasonable that we can estimate the diffusion coefficient for diffusion due to electron-ion collisions by a typical step length and the time between collisions. The latter is merely the inverse of the collision frequency, ν_{ie}. A typical step length will be given by the Larmor radius, but it is important to keep in mind that r_L is much greater for ions than for electrons. In a magnetic field conservation of momentum demands that the gyro-centre of two particles with equal but opposite charge must move the same distance after a collision, because we must have $q_1\Delta\mathbf{r}_c^{(1)} + q_2\Delta\mathbf{r}_c^{(2)} = 0$. $\mathbf{r}_c$ is the position of the respective gyro-centres. This means that even though an ion in principle could move a typical step length $\sim r_{Li}$, it is bound by the electron Larmor radius. Thus both electrons and ions will have a typical step length of $\sim r_{Le}$ (Pécseli, 2012).

For a fully ionised plasma we have $D_\perp \sim r_{Le}^2\nu_{ei}$. Inserting (2.7) for r_{Le} and $\nu_{ei} \sim \omega_{pe}/N_p$, we find that

$$D_\perp \sim \frac{n}{B^2\sqrt{T}}\,.$$

This means that increasing the magnetic field strength will reduce collisional diffusion, as will increasing the temperature or reducing the density. Physically we have that when the magnetic field strength is increased, the Larmor radius decreases. This means that both electrons and ions gyrate in smaller circles, and the distance travelled due to a collisions is smaller. Thus more collisions are needed

for a charged particle to be able to escape the bulk plasma. Similarly, if the temperature is increased we get an increase in N_p, giving a corresponding decrease in collision frequency. If there are less collisions, the motion of charged particles across magnetic field lines will be slower. Increasing the particle density will naturally give a greater collisions frequency, as there will be more particles to collide with. Consequently we will have an increase in collisional diffusion across $\mathbf{B}$.

The scaling remains accurate (with a different numerical factor) for collisions with neutrals. Ions will then not be bound by the electron Larmor radius, but the electron and ion dynamics are locked by the requirement of quasi-neutrality, and as an order of magnitude the coefficient retains the electron Larmor radius as an effective length scale, with appropriate collision frequency.

3.2 Turbulent diffusion

One of the most important properties of turbulent flows is their ability to disperse particles at a rate which by far exceeds transport by classical molecular diffusion. This is a property of both neutral fluids and plasmas alike. Whenever there is a density gradient in a plasma, a drift wave instability will eventually occur, setting up a transverse isobar wavefront in the plasma between dense and less dense areas. During the linear growth phase, the drift wave instability is closely connected with particle transport along the direction of the density gradient. The question is how the saturated turbulent fluctuating field (assuming that such a state exists) transports particles.

First we make some general remarks on this problem, and present some of the basic results on turbulent diffusion. The outline is independent of the dimensionality of the problem and the ideas apply equally well for three dimensional and two dimensional turbulence, assuming the plasma to be homogeneous and isotropic. Particle displacement will be expressed in terms of a velocity, but this velocity can be obtained from an electrostatic electric field in magnetized plasmas as $\mathbf{u}(\mathbf{r},t) = \mathbf{E}(\mathbf{r},t) \times \mathbf{B}_0/B_0$ for homogeneous magnetic fields. We assume low frequency turbulence in which relevant frequencies are $\omega \ll \Omega_{ci}$, where Ω_{ci} is the ion cyclotron frequency. This model will then assume two dimensional turbulence in the plane $\perp \mathbf{B}_0$. Polarisation drifts along $\partial\mathbf{E}/\partial t$ are ignored, i.e. to the accuracy $\langle\omega\rangle/\Omega_{ci} \approx 10^{-3}$.

Many experiments have demonstrated that turbulent transport is an important mechanism in for instance fusion plasma experiments (Liewer, 1985), and significant efforts have been made to understand this mechanism for anomalous transport also in the context of drift wave turbulence (Horton, 1999).

3.2.1 Single particle turbulent diffusion

We start by considering the simplest possible problem, namely the one where a single particle is released in a homogeneous and isotropic turbulent velocity field, $\mathbf{u}(\mathbf{r}, t)$. Assuming that the particle is convected passively by the flow, we want to determine its mean square displacement with respect to the origin of release. For simplicity we take this to be at the origin (Roberts, 1957).

Since, by assumption, $d\mathbf{r}(t)/dt = \mathbf{u}(\mathbf{r}(t), t)$, we have in a given realisation of the flow that the particle position is given as

$$\mathbf{r}(t) = \int_0^t \mathbf{u}(\mathbf{r}(t'), t')dt' \,. \tag{3.3}$$

The *average* position $\langle \mathbf{r}(t) \rangle$ vanishes, since we have assumed $\langle \mathbf{u}(\mathbf{r}(t), t) \rangle = 0$. This is actually not quite as self evident as it might appear, since we can assume from the outset only that $\langle \mathbf{u}(\mathbf{r}, t) \rangle = 0$, but this is concerning a function of a spatial as well as a temporal variable, while $\langle \mathbf{u}(\mathbf{r}(t), t) \rangle$ is a function of time alone.

The mean square displacement is a positive quantity, and we find

$$\mathbf{r}(t) \cdot \frac{d\mathbf{r}(t)}{dt} = \frac{1}{2}\frac{dr^2(t)}{dt} = \mathbf{u}(\mathbf{r}(t), t) \cdot \int_0^t \mathbf{u}(\mathbf{r}(t'), t')dt' = \int_0^t \mathbf{u}(\mathbf{r}(t), t) \cdot \mathbf{u}(\mathbf{r}(t'), t')dt' \,. \tag{3.4}$$

Taking the ensemble average, we have

$$\frac{d}{dt}\left\langle r^2(t) \right\rangle = 2\int_0^t \langle \mathbf{u}(\mathbf{r}(t), t) \cdot \mathbf{u}(\mathbf{r}(t'), t') \rangle \, dt' \,. \tag{3.5}$$

For time stationary turbulence we have a dependence of time separations only such as

$$\langle \mathbf{u}(\mathbf{r}(t), t) \cdot \mathbf{u}(\mathbf{r}(t'), t') \rangle = R_L(t - t')\langle u^2 \rangle$$

with the subscript L reminding us to sample the velocity field along a Lagrangian orbit, i.e. follows the path of the single particle. We introduced R_L as the normalised Lagrangian velocity correlation function, $R_L(0) = 1$. By the assumption of time stationary Lagrangian velocities, we implicitly assume that all spatial positions visited by the randomly moving particle are statistically similar, i.e. we assume the turbulent velocity field to be spatially homogeneous.

When integrating (3.4) as

$$\left\langle r^2(t) \right\rangle = 2\langle u^2 \rangle \int_0^t \int_0^{t''} R_L(t'' - t')dt'dt''$$

it is an advantage to introduce the variables $\tau \equiv t'' - t'$ and $s \equiv t''$, giving the Jacobian

$$J = \begin{vmatrix} \dfrac{\partial \tau}{\partial t''} & \dfrac{\partial \tau}{\partial t'} \\ \dfrac{\partial s}{\partial t''} & \dfrac{\partial s}{\partial t'} \end{vmatrix} = \begin{vmatrix} 1 & -1 \\ 1 & 0 \end{vmatrix} = 1$$

so that $dt''dt' = d\tau ds$. Transforming the variables as indicated, we note that we can change the order of integration as

$$\begin{aligned} \int_0^t \int_0^s R_L(\tau) d\tau ds &= \int_0^t \int_\tau^t R_L(\tau) ds d\tau \\ &= \int_0^t R_L(\tau) \int_\tau^t ds d\tau \\ &= \int_0^t R_L(\tau)(t-\tau) d\tau \end{aligned}$$

to give

$$\left\langle r^2(t) \right\rangle = 2t\langle u^2 \rangle \int_0^t (1 - \tau/t) R_L(\tau) d\tau \,. \tag{3.6}$$

Two relevant limiting cases of (3.6) can be distinguished here (Roberts, 1957).

1. Very short times, where it can be assumed that the correlation function $R_L(\tau) \approx 1$. In this limit we find

   $$\left\langle \mathbf{r}^2(t) \right\rangle \approx \langle u^2 \rangle t^2$$

   which is often called the *ballistic limit* since it is the result we would have obtained by assuming the particle to follow straight lines of orbit, $\mathbf{r}(t) = \mathbf{u}t$, and simply average over all velocities. This kind of motion will be burst-like. One can experience finding auto-correlation functions that are not differentiable for $\tau = 0$, and in such cases the ballistic limit does not exist. Such cases require that $\langle (d\mathbf{u}/dt)^2 \rangle$ diverges. With finite particle inertia we would expect that $d\mathbf{u}/dt$ should be finite at all times. The absence of a ballistic limit simply indicates a very rapidly changing velocity field, and the interval where $R_L(\tau) \approx 1$ may be negligible.

2. Very large times, $t \to \infty$, where it can be assumed that $\int_0^t R_L(\tau) d\tau \approx \tau_L$, introducing the Lagrangian integral correlation time

   $$\tau_L \equiv \int_0^\infty R_L(\tau) d\tau \,. \tag{3.7}$$

In this limit we find the important result

$$\left\langle r^2(t) \right\rangle \approx 2t\tau_L \langle u^2 \rangle \,. \tag{3.8}$$

At least formally this looks like the result one obtains by using the classical diffusion equation with a diffusion coefficient $D \equiv 2\tau_L \langle u^2 \rangle$ to obtain the mean square particle displacement. Such cases have

$$\left\langle \mathbf{r}^2(t) \right\rangle \sim t \,.$$

The limit of times much larger than the Lagrangian correlation time is consequently called the diffusion limit. This limiting case is consistent with a random walk with a typical length step $\tau_L \sqrt{\langle u^2 \rangle}$ per time τ_L, consistent with a mixing length model.

By the assumption of a stationary random process for the turbulent velocity field, i.e. averages depend on time differences only and not absolute times, we are in effect implying that the process is also spatially homogeneous. Otherwise the particle would occupy, from time to time during its random motion, spatial regimes where the statistical properties of $\mathbf{u}(\mathbf{r}, t)$ differed from the rest of the flow. Was this the case, we would experience sequences of the Lagrangian temporal velocity signal, where the statistical properties were distinguishable from the rest.

In reality we will never experience a fully homogeneous random vector field. However, for some finite time interval where a particle is, by high probability, confined to a *locally* homogeneous field we might use such idealised approximations. In the Blaamann plasma we might assume local spatial homogeneity in a "doughnut-shaped" region around the origin $(x, y) = (0, 0)$ (see Figure 4.5). Within this region it might be possible to observe the diffusion limit, in principle. We will find, however, that no such diffusion limit will be identified with the analysis tools used in this project.

Note that $\mathbf{r}(t)$ is not a time-stationary random process, although it is derived from $\mathbf{u}(\mathbf{r}, t)$ which can be assumed to be so. The initial time (the time when the particle was released) has a special role for $\mathbf{r}(t)$.

Introducing the Lagrangian power spectrum,

$$S_L(\omega) \equiv (1/2\pi) \int_{-\infty}^{\infty} R_L(t) e^{-i\omega t} dt \,,$$

with

$$R_L(t) = \int_{-\infty}^{\infty} S_L(\omega) e^{i\omega t} d\omega \,,$$

we can write the result (3.6) on the form

$$\left\langle r^2(t)\right\rangle = t^2 \left\langle u^2\right\rangle \int_{-\infty}^{\infty} \left(\frac{\sin(\omega t/2)}{\omega t/2}\right)^2 S_L(\omega) d\tau \,. \tag{3.9}$$

The function $\sin^2(\omega t/2)/(\omega t/2)^2$ originates from the Fourier transform of the "triangular" function $1 - \tau/t$ entering the convolution (3.6). For large times it is evident that dispersion of the test particle is primarily due to the low frequencies in the Lagrangian spectrum. We have

$$\lim_{t\to\infty} \frac{\sin \omega t/2}{\omega/2} = \pi\delta(\omega)\,,$$

so we recover $\tau_L = S_L(\omega = 0)$. Note that oscillations in the Lagrangian spectrum with frequencies being multiples of $1/t$ do not contribute to the particle displacement. This is because they return the particle to its starting point after a time t. Often it is assumed that low frequencies in (3.9) corresponds to large wavelengths (or rather large scales), but we should be aware that there is no a priori reason to expect this.

By (3.9) our problem seems to be solved once and for all, at least for the case of homogeneous isotropic turbulence. However, it is not so, since we do not know the spectrum $S_L(\omega)$, and it is very complicated to obtain it experimentally. It has been a major enterprise over the years to find ways of predicting $S_L(\omega)$ on the basis of the more readily measurable *Eulerian* correlation function. Amazingly good results can be obtained, at least as far as predictions of $\langle \mathbf{r}^2(t)\rangle$ are concerned. However, this might as well imply that this is a very robust result, and that almost any reasonable guess on R_L will give acceptable results. After all, we *must* require that $R_L(0) = 1$ and that $R_L(t \to \infty) \to 0$, and with a little common sense all reasonable guesses of R_L tend to look more or less the same.

The asymptotic stage of turbulent transport is diffusion-like but the intermediate steps are very different as illustrated in Figure 3.1.

3.3 Plasma blob transport

An alternative method of transport within plasma across magnetic field lines is blob transport. A blob is a plasma structure that is elongated along the magnetic field. It is significantly denser and warmer than the surrounding plasma, and highly limited in size across magnetic field lines. It travels in the radial direction from strong magnetic fields to weaker, i.e. in the direction of $-\nabla B$. In a torus this would mean motion towards the outer wall on the low field side. They are also referred to as *mesoscale structures* because their perpendicular size is intermediate between

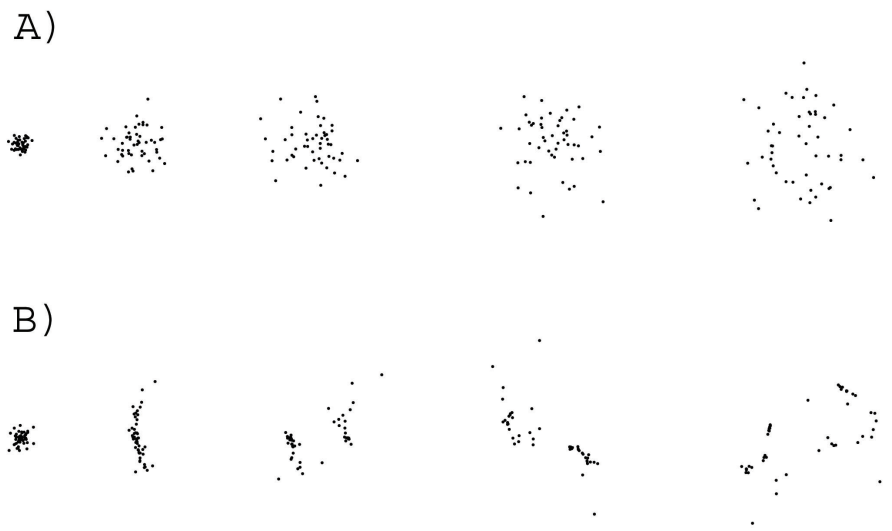

Figure 3.1: *The motion of a set of particles over time when we have (A) simple Brownian motion, and (B) when there is turbulent diffusion. The figure is originally produced by Jakob Mann and Søren Ott at the Risø National Laboratory.*

Ω_{ci} and the macroscopic machine dimensions. There exists also the equivalent plasma holes, which then are less dense and warm than the background plasma. These tend to move in the opposite direction, i.e. towards stronger B-field.

Both theory and simulations predict that blobs are created as a result of turbulence in the main plasma region or because of coherent magnetohydrodynamic instabilities, the latter being the less likely of the two (D'Ippolito et al., 2011; Krasheninnikov et al., 2008). Exactly how turbulence causes these blobs to come into existence is not yet well understood, as turbulence in itself is still a subject of active research. However, what starts out as a small density perturbation grows due to the turbulence, and eventually disconnects from the rest of the plasma. Approximately equal parts blobs and holes are formed, meaning that the formation zone is characterised statistically by a density distribution that has a skewness[1] close to 0.

After the blob has been created it will move radially outwards. The reason for this can be analysed mathematically. Consider an isolated blob initially at rest, elongated along $\mathbf{B}$ and localised in the poloidal plane. We start out with the charge continuity equation for low frequency quasi-neutral fluctuations

$$\nabla \cdot \mathbf{J} = 0 \Longrightarrow -\nabla \cdot \mathbf{J}_{\perp} = \nabla \cdot \mathbf{J}_{||}\,,$$

[1]Skewness will be explained and defined in Chapter 5

where $\mathbf{J}_\perp$ is the perpendicular current density and $\mathbf{J}_{||}$ is the magnetic field-aligned current density. The perpendicular current can be written as a sum of the plasma inertia current and the current due to guiding centre drifts. If the magnetic field is non-uniform, we will have guiding centre drifts due to ∇B and curvature, causing a current

$$\mathbf{J}_B = \frac{P}{B}\mathbf{b} \times (\kappa + \nabla \ln B)\,, \tag{3.10}$$

where $\mathbf{b}$ is a unit vector in the direction of $\mathbf{B}$, P is the plasma pressure and $\kappa = (\mathbf{b}\cdot\nabla)\mathbf{b}$ the magnetic field curvature vector. As κ is pointing inwards towards the centre of the torus and the magnetic field oriented along the toroidal direction (counter clockwise when viewed from above), the current density $\mathbf{J}_B$ sets up an electric field within the blob, pointing downwards. The resultant $\mathbf{E} \times \mathbf{B}$-drift will then be radially outwards towards the outer edge of the torus.

Inserting (3.10) into the continuity equation gives

$$\nabla \cdot \left(\frac{\rho_m}{B} \frac{d}{dt} \frac{\nabla_\perp \phi}{B} \right) + \frac{1}{B}\mathbf{b} \times (\kappa + \nabla \ln B) \cdot \nabla P = \nabla \cdot \mathbf{J}_{||}$$

where the first term is the plasma inertia current (Garcia, 2009). ρ_m is the plasma mass density and ϕ the electrostatic potential. The left hand side of this equation gives a relationship between speed of the blob C_b and parameters such as size across field lines, ℓ, pressure amplitude within the blob, ΔP, and curvature radius of the magnetic field, R.

$$\frac{C_b}{C_s} \sim \left(\frac{2\ell}{R} \frac{\Delta P}{\Pi} \right)^{1/2}.$$

Π is the background plasma pressure. This shows that a larger or denser blob will move faster than a smaller, more dilute blob. Numerical simulations of blob structures with a Gaussian pressure distribution have shown that a blob starting out from rest will have a radial drift at the centre of the structure, but as the blob accelerates, the structure itself changes shape, and an asymmetric wavefront forms with a steep front and a trailing wake, giving it a characteristic mushroom-like shape. In some cases the blob will distort further, and eventually dissolve completely.

The experimental definition of a blob has varied in literature, depending on the data available. Generally, the very minimum required for a positive identification of a blob is a single point measurement of a density distribution which is positively skewed and non-Gaussian in the outer midplane, as this is indicative of a large positive density perturbation passing the probe. However, distinguishing between a non-Gaussian blob-like structure and the Gaussian background tends to be difficult, since the blob itself has developed from this Gaussian background turbulence.

In the presence of blobs in toroidal plasma, the skewness of the density distribution tends to increase with increased distance from the blob birth zone. In some cases the skewness will be negative closer to the plasma centre, indicating plasma holes having propagated inwards. Near the birth zone the blobs tend to be small and hard to detect, but closer to the outer wall, blobs are expected to be large and dominant. Because of the asymmetry due to magnetic curvature in a toroidal device giving a toroidal field, it is somewhat unclear whether blobs exist in the inside regions of the torus, and also in which direction they might propagate.

Blobs contribute large positive burst in the density time signal. Probe measurements of identifiable blobs have shown that the probability distribution of particle density signals are positively skewed and have heavy tails due to the many large bursts in the time series, hence also the kurtosis is expected to be greater than 3, which is the kurtosis of a random Gaussian process. However, though a density distribution with positive skewness and large kurtosis are characteristic when we have blob transport, they are not necessarily evidence of the presence of blobs in the plasma.

Chapter 4

The Blaamann experiment

4.1 The plasma tank

In 1989 the Blaamann plasma experiment (see Figure 4.1) was constructed at the University of Tromsø. The purpose of the device was to offer the opportunity to study the behaviour of turbulent weakly magnetised plasma, as well as instabilities and anomalous transport. This was done by confining plasma on magnetic field lines within a toroidal vacuum chamber and measuring spatial and temporal changes in density, potential difference and electron temperature across a poloidal cross section. A thorough description of both how Blaamann was built and how it works in detail can be found in Rypdal et al. (1994) and Brundtland (1992). Here we will give a brief description in order to illustrate how the experiment in question was conducted, and how the data were obtained.

Schematic set-up of the experiment is shown in Figure 4.2a) (from above) and b) (from the side). The experiment consists of a stainless steel vacuum chamber shaped like a torus with major radius $R = 651.5$ mm and minor radius $r = 133.5$ mm, hence the width of the chamber is small compared to the major circumference. The chamber itself is comprised of four 90 degree bends connected together with conflat flanges, and each section has a sector chamber for improved access. 24 circular coils (marked blue) provide a toroidal magnetic field of up to 0.4 T. This field is almost homogeneous with a magnetic ripple $\delta B/B$ that varies from 0.002 in the central part of the poloidal cross section to 0.01 near the outer wall. Eight horizontally positioned coils centred around the major axis can provide small radial and vertical magnetic fields (marked red and white respectively). All along the surface of the tank is a series of square copper tubes working as water cooling. In addition there is also a vacuum pump and a power supply. The entire set-up is held in place by a supporting rack as indicated by the dark grey sections in Figure 4.2. The entire device weighs about 350 kg.

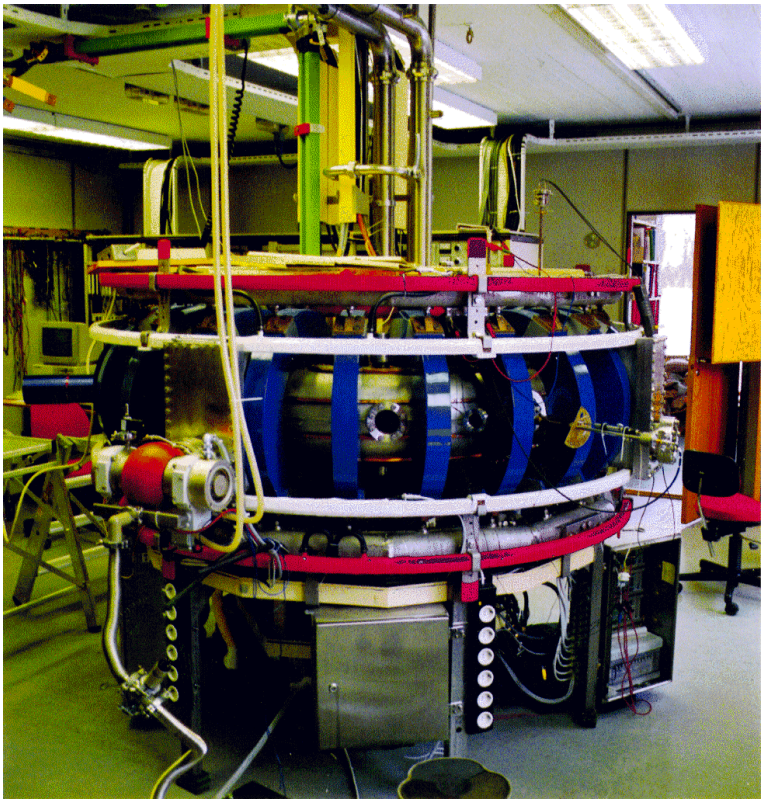

Figure 4.1: *The Blaamann plasma tank, set up at the University of Tromsø. Notice the desk chair next to the device, giving an idea of the size of this tank.*

The Blaamann device was operated under steady-state conditions. Due to the magnetic configuration of Blaamann, plasma confinement is somewhat limited. Plasma losses are due to diffusion and drifts given by the velocities (2.13) and (2.14). The losses are however, on average, balanced by plasma production due to the discharge by the negatively biased hot filament (Rypdal et al., 1994).

4.2 Probe diagnostics

Weakly ionised plasma is produced by a negatively biased hot tungsten cathode emitting electrons (thermionic discharge) which ionises the neutral gas. The degree of ionisation is $\sim 1\%$. The primary electrons flow in both directions along the toroidal axis, but are also subject to ∇B and curvature-drift in the vertical direction, with ions moving upwards and electrons moving downwards. Due to the radial electric field caused by the potential within the plasma, a poloidal $\mathbf{E}\times\mathbf{B}/B^2$-

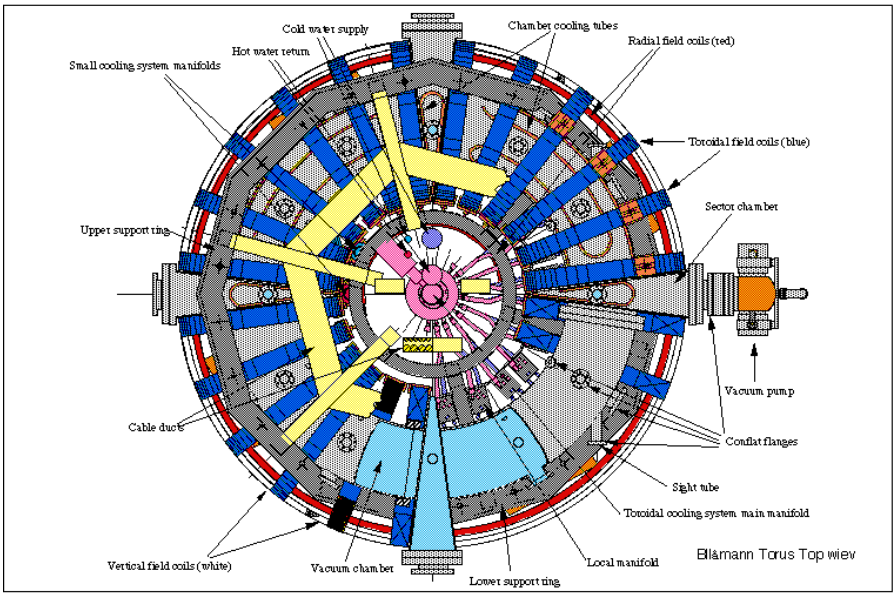

(a)

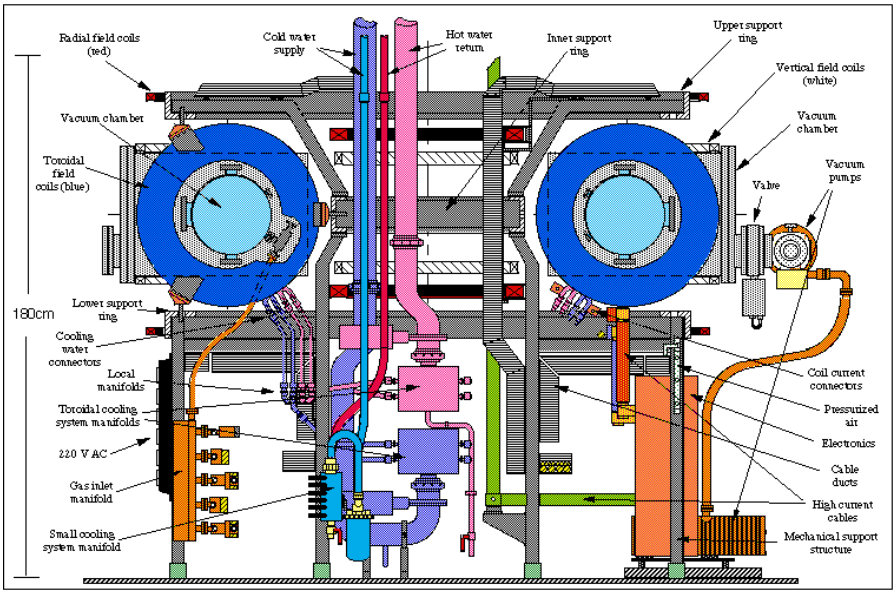

(b)

Figure 4.2: *Sketch of the toroidal plasma tank seen from (a) above and (b) from the side. Figures produced by Terje Brundtland.*

drift is also set up, causing a rotation of the plasma column. A circular poloidal limiter extending 2.5 cm inwards from the wall receives any discharge current between the filament and the ground. Since there is no toroidal electric current nor poloidal magnetic field except the radial and vertical fields which can be imposed, there is no rotational transform. A steady state situation is achieved where the plasma generation and losses are balanced. Note that this condition should here be understood to mean in an averaged sense.

The experiment in question was carried out in August 2003. It was conducted using helium plasma held at a constant background pressure of $\sim 2.0 \times 10^{-4}$ mbar and with a discharge current of 1.0 A. The toroidal field current was 350 A, resulting in a magnetic field strength of 1540 G (0.154 T) at a reference point in the centre of a poloidal cross section. The filament was biased at 140 V with respect to the surrounding walls. The electric field $\mathbf{E}$ and the plasma density n have both a dc and a fluctuating component, while the magnetic field is considered to be constant in time. We assume quasi-neutrality, i.e. $n = n_e \approx n_i$.

Measured background parameters are shown in Figure 4.3, where the time averaged dc electron potential, dc electron density and dc electron temperature have been measured using a motorised Langmuir probe that does measurements in a tight grid within the poloidal cross section. Measuring several times and averaging over each set gives the resulting data shown in Figure 4.3. The plasma displays a negative and almost parabolic potential well near the centre of the circular cross section of the tank, due to the abundance of electrons. This gives rise to a radial electric field directed inwards, which in turn sets up a clockwise rotation of the plasma column due to poloidal $\mathbf{E} \times \mathbf{B}/B^2$-drift, as indicated in Figure 4.5. This angular velocity is nearly constant throughout the entire plasma column, with some small deviations near the outer limit due to the inhomogeneity of the $\mathbf{B}$-field. Hence the background plasma rotates almost like a rigid body. The electron temperature and density exhibit maxima near the same area as the potential minimum. Peak values of the time-averaged densities were $n_0 \approx 2 \times 10^{17}$ m^{-3}, electron temperatures $T_{e0} \approx 6$ eV and the local minimum of the time averaged plasma potential was $\phi_0 \approx -50$ V. Basic plasma parameters for this experiment are listed in Table 4.1.

For this analysis we used a local Cartesian coordinate system (x, y, z), as indicated in Figure 4.2, with the centre of the coordinate system situated in the centre of the poloidal cross section. The toroidal magnetic field is $||\hat{\mathbf{z}}$, and the x-axis is in the direction of the major radius, with positive direction being away from the centre of the torus. The y-axis is our vertical axis within the cross section. By radial direction we will mean with respect to the centre of this local Cartesian coordinate system in the (x, y)-plane.

The probe diagnostics were obtained using a four pin Langmuir probe, but

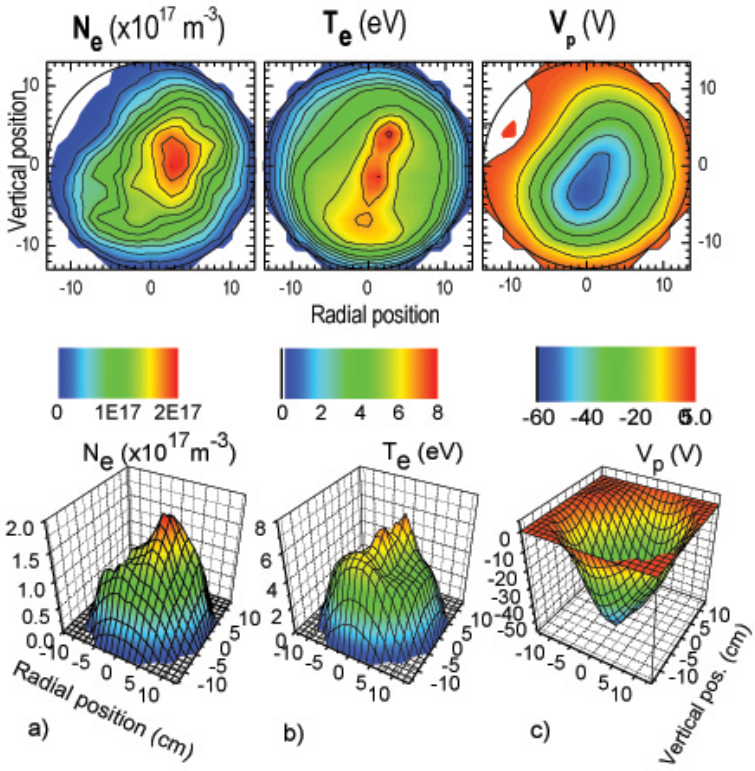

Figure 4.3: *The dc electron density N_e, dc electron temperature T_e and dc plasma potential V_p for a poloidal cross section. All parameters are time averaged and obtained using a computer controlled motorised Langmuir probe. The coordinate (0, 0) is taken to be the middle of a poloidal cross section. The vertical filament is placed near where N_e has a sharp maximum, and T_e displays an elongated peak. Figure provided by Åshild Fredriksen.*

only three of the pins were actually in use. In addition to this there was also a fixed reference probe. All probes were 5 mm long and had a radius of 0.125 mm. The constellation is shown in Figure 4.5. The reference probe was positioned at 5 cm above the horizontal centre line of the poloidal cross section indicated by a small circle in the figure, and measured floating potential. The four pin probe was movable along the horizontal midplane and consisted of two pins measuring potential and one measuring electron saturation current, with the fourth pin being obsolete. Measurements were done along the horizontal centre line in positions from $x = -9$ cm to $x = +9$ cm, in leaps of one cm, giving a total of 19 different positions. At every position 5 datasets were collected. The data was digitized using a 12-bit digitizer at a sampling rate of 250 kHz with 10^4 samples per set,

Table 4.1: Summary of basic plasma parameters, assuming singly charged helium ions.

Electron plasma frequency, ω_{pe}	1.8×10^{10} s^{-1}
Electron Debye length, λ_{De}	50×10^{-6} m
Reference electron temperature, T_e	5 eV
Ion temperature, T_i	0.05 eV
Sound speed, C_s	11×10^3 m s^{-1}
Electron thermal velocity, u_{the}	0.94×10^6 m s^{-1}
Ion thermal velocity, u_{thi}	10^3 m s^{-1}
Electron cyclotron frequency, ω_{ce}	27×10^9 s^{-1}
Ion cyclotron frequency, Ω_{ci}	3.7×10^6 s^{-1}
Average electron Larmor radius	35×10^{-6} m
Average ion Larmor radius	0.27×10^{-3} m
Ion-electron collision frequency, $\nu_{e,i}$	80×10^3 s^{-1}
Electron-neutral He cross section, $\sigma_{e,n}$	6×10^{-20} m^2
Ion-neutral He cross section, $\sigma_{i,n}$	65×10^{-20} m^2
Electron-neutral mean free path, $\ell_{e,n}$	0.7 m
Ion-neutral mean free path, $\ell_{i,n}$	64×10^{-3} m
Electron-He collision frequency, $\nu_{e,n}$	1.4×10^6 s^{-1}
Ion-He collision frequency, $\nu_{i,n}$	16×10^3 s^{-1}

resulting in time series lasting for 40 ms.

The measurements of floating potential are used to obtain an estimate for the vertical component of the fluctuating electric field at $y = 0$, which is equivalent to the poloidal field at the given measuring positions. The **E**-field in the vertical direction is given by

$$E_y = -\frac{\partial \phi}{\partial y} \approx -\frac{\phi(x, y + \Delta y) - \phi(x, y - \Delta y)}{2\Delta y} = -\frac{V_1 - V_2}{d}\,, \tag{4.1}$$

where d is the distance between the two probes, here 7 mm. As long as the potential fluctuates on a large enough scale, this estimate will be sufficiently accurate. However, should we have fluctuations in the electric field with a wavelength of the same order of magnitude as d or smaller, our estimate becomes inaccurate.

The measured data of the y-component of the fluctuating electric field can in turn be used to find an approximation for the magnitude and variation of the $\mathbf{E} \times \mathbf{B}/B^2$-velocity in the x-direction for $y = 0$, given as

$$\tilde{u}_{E\times B,x} = \frac{\tilde{E}_y}{B}\,. \tag{4.2}$$

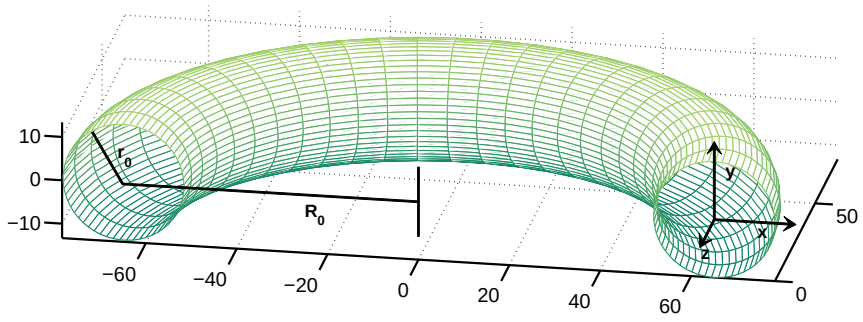

Figure 4.4: *Schematic drawing of a torus, with major and minor radius corresponding to Blaamann's measures. The coordinate system illustrated is the one used throughout this analysis.*

This velocity is in turn equivalent to a radial velocity in the x-direction of Figure 4.5, with positive $\tilde{u}$ being in the positive x-direction.

The electron saturation current is used as an estimate for the fluctuating electron density, since this gives similar results as the ion saturation current, and is easier to obtain near the bottom of the potential well (Fredriksen et al., 2003b). Because the potential well is so negative, any estimate of the ion saturation will be highly inaccurate. In addition, the ion saturation current will be affected by hot electrons near the filament.

The electron current in the area surrounding the probe is given as

$$I^- = \Gamma_e e A \,, \tag{4.3}$$

where e is the elementary charge, Γ_e is the electron flux and A is the area of the sheath edge. The sheath itself is only a few λ_{De} thick. From Table 4.1 it is evident that $\lambda_{De} \ll d$, where d is the probe diameter. Thus the area of the sheath can be approximated by the area of the probe.

The electron flux at the probe is

$$\Gamma_e = \frac{1}{4} n_s \overline{u}_e e^{V/T_e} \,,$$

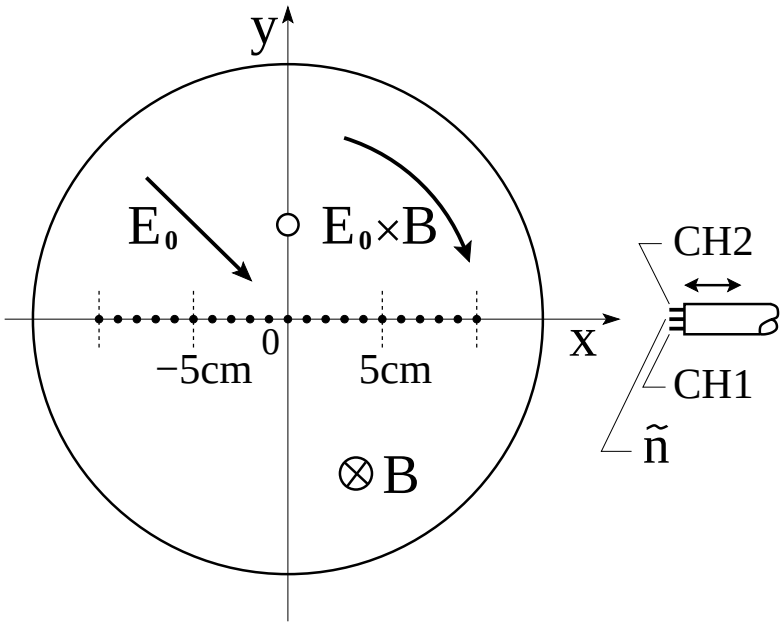

Figure 4.5: *Poloidal cross section with probe constellation, background electric field,* $\boldsymbol{E}_0$ *and magnetic field,* $\boldsymbol{B}$*. The small black dots mark positions where measurements were made, and the larger circular marker situated above the horizontal centreline marks the position of the reference probe, which was stationary during the entire experiment.*

where n_s is the density at the sheath edge, i.e. the density the probe would measure (due to the nature of the presheath this density is not the same as the density in the bulk plasma), $\overline{u}_e$ is the mean electron speed, T_e is electron temperature in eV and V is the probe potential.

The density at the sheath edge, i.e. the density that gets through to the probe, relates to the density in the plasma through the Boltzmann relation

$$n_s = \tilde{n} e^{-\Phi_p/T_e} \,.$$

The potential drop across the presheath is given by ion energy conservation

$$\frac{1}{2} M u_B^2 = e\Phi_p \,,$$

where u_B is the Bohm velocity, i.e. the ion velocity at the plasma sheath (see eq. (2.16)). Solving for the plasma potential gives

$$\Phi_p = \frac{T_e}{2} \,.$$

Thus the density at the sheath edge relates to the density in the main plasma through

$$n_s = \tilde{n}e^{-1/2} \approx 0.61\tilde{n}\,.$$

Assuming the electron velocity to have a Maxwellian distribution

$$f(u) = n\left(\frac{m}{2\pi eT}\right)^{3/2} \exp\left(-\frac{mu^2}{2eT_e}\right)$$

gives an average electron velocity of

$$\bar{u}_e = \left(\frac{8eT_e}{\pi m_e}\right)^{1/2},$$

where m_e is the electron mass. m_e is known and T_e is measured. With the temperature given in Table 4.1 this velocity is approximately $\bar{u}_e \approx 1.5 \times 10^6$ m/s. It has been experimentally shown that even though the electron temperature fluctuates, with the low pressure that we have, these fluctuations do not significantly affect the density (Fredriksen et al., 2003a). Therefore the electron temperature can be approximated by a fixed value. In deriving the electron velocity we have assumed that the electrons have three translational degrees of freedom.

Due to the highly limited electron motion across magnetic field lines, the cylindrical probes can be treated like plane probes. This means that the effective surface area of the probe can be estimated as two times the cross section of the probe, i.e. the product of the diameter of the pins times their length. The circular end section is so small that it is neglected here. Thus we have

$$A \approx 2ld$$

which gives the final expression for the electron current. (Lieberman and Lichtenberg, 2005)

$$I^- = \frac{1}{4}e\left(\frac{8eT_e}{\pi m_e}\right)^{1/2} 2ld\tilde{n}\,\exp\left(\frac{(V-\Phi_p)}{T_e}\right).$$

Since the electron saturation current is the current that is measured when $\Phi_p = V$, the exponential disappears, and we have

$$I^-_{sat} = e\tilde{n}\left(\frac{eT_e}{2\pi m_e}\right)^{1/2} 2ld\,. \tag{4.4}$$

Solving for the fluctuating density $\tilde{n}$ gives

$$\tilde{n} = \frac{I^-_{sat}}{eld}\left(\frac{\pi m_e}{2eT_e}\right)^{1/2}. \tag{4.5}$$

The fluctuating particle flux within the plasma is given as the product of the fluctuating density and the velocity.

$$\tilde{\Gamma}_x(x,t) = \tilde{n}(x,t)\tilde{u}_x(x,t) \tag{4.6}$$

The flux will also have a component $n_0(x)\tilde{u}_x(x,t)$ due to the background density. However, this will on average be zero, and is therefore not investigated in this study.

4.3 Plasma rotation and drifts

As mentioned a spatially averaged radial electric field component $E_0(r)$ gives rise to a rotation of the plasma column. Assuming a parabolic potential and a homogeneous magnetic field given by its value near the centre of the device, one can estimate a rotation frequency $\Omega_0/2\pi \approx 8 \times 10^3$ Hz.

Estimating the individual rotation frequencies for the electrons and ions requires more consideration. The ion rotation frequency can be found from

$$\left(1 + 2\frac{\Omega_+}{\Omega_{ci}}\right)\left(\frac{\Omega_0}{\Omega_{ci}} - \frac{\Omega_+}{\Omega_{ci}} - \left(\frac{\Omega_+}{\Omega_{ci}}\right)^2\right) = \left(\frac{\nu_{i,n}}{\Omega_{ci}}\right)^2 \frac{\Omega_+}{\Omega_{ci}} \tag{4.7}$$

where the right hand side accounts for collisional friction due to the stationary neutral gas, and the left hand side includes the effect of centrifugal forces on the ions (Odajima, 1978). There would be a similar expression for the electron rotation frequency. However, given the low collision frequency, ν_{en}, compared to the electron cyclotron frequency, ω_{ce}, found in Table 4.1, we can assume that the electrons rotate with Ω_0, and ignore friction and centrifugal forces.

The result of this difference in rotation frequency for the ions and electrons is charge separation. Consider a localised plasma density enhancement or depletion at some finite radial position. Such a perturbation will be polarised due to the charge separation, giving rise to electric fields. These electric fields will in turn cause radial motion of the density perturbation, with depletions and enhancements moving in opposite directions.

In order to estimate the polarisation of a local plasma density perturbation, we need the difference in rotation frequency between the electrons and the ions.

$$\Delta\Omega \approx \Omega_0 - \Omega_+$$

which gives the relative displacement of the electrons with respect to the ions as approximately

$$\Delta\Omega tr$$

for a density perturbation δn at a position r at a time $t > 0$. The resulting electric field is then

$$E \approx te\,\delta n\, r\Delta\Omega/\varepsilon_0\varepsilon_r$$

where ε_r is the relative dielectric constant. Assuming that this can be estimated using the standard form for flute type slow plasma variations gives $\varepsilon_r \approx 1 + \delta n M c^2\mu_0/B^2$. For large perturbations this approaches $\varepsilon_r \approx \delta n M c^2\mu_0/B^2$, and for small perturbations we have $\varepsilon_r \approx 1$. For the first case we find a radial velocity of the density perturbation

$$E/B \approx tr\,\Omega_{ci}\Delta\Omega$$

independent of density, noting that the position varies with time, i.e. $r = r(t)$. In the other limit we find

$$E/B \approx tr\,\delta\Omega_{pi}^2\,\Delta\Omega/\Omega_{ci}$$

with $\delta\Omega_{pi}^2 \equiv \delta n e^2/M\varepsilon_0$. Taking a perturbation $\delta n/\overline{n} \approx 0.1$ at a position $x = 50$ mm, we find $\varepsilon_r \approx 300$, so the first case is relevant in the central parts of the plasma.

Using the parameters from Table 4.1 we find that both $\Omega_0/\Omega_{ci} \ll 1$ and $\nu_{i,n}/\Omega_{ci} \ll 1$, indicating that the difference in rotation velocities for the electrons and the ions has a small contribution to the azimuthal current. However, the polarisation of a localised density perturbation can become important as it increases with time.

To estimate this polarization we make the series expansion from the solution of (4.7) to find

$$\Omega_+ \approx \Omega_0 - \Omega_0^2/\Omega_{ci} - \Omega_0(\nu_{i,n}/\Omega_{ci})^2$$

giving

$$\Omega_{ci}\Delta\Omega \approx \Omega_0^2 + \Omega_{ci}\Omega_0(\nu_{i,n}/\Omega_{ci})^2$$

where the last term is small with parameters from Table 4.1. We therefore have

$$E/B = dr/dt \approx tr\,\Omega_0^2$$

with solution

$$r(t) = a\exp\left(\frac{1}{2}\Omega_0^2 t^2\right)$$

where $a = r(0)$. This result indicates that a density perturbation can propagate significant radial distances during one rotation of the plasma column. In a fixed frame, the density perturbation will appear to follow a spiralling orbit. Also the ∇B-gradient drift will contribute to the polarisation of a local plasma density enhancement or depletion. To estimate the relative magnitude of the two polarisations we compare the ∇B-velocity $\approx 0.6\times10^2$ m s^{-1} with $r\Delta\Omega \approx 2.5\times10^2$ m s^{-1},

where we used $R \approx R_0$ for estimating the ∇B-velocity and $r \approx 50$ mm for the differential rotation velocity. Other parameters were taken from Table 4.1. The two polarisation effects seem to be of the same order of magnitude, but the ion ∇B-drift is in the positive y-direction on both the low and high magnetic field sides, and is therefore partially compensated by the plasma rotation. The polarisation due to the differential rotation gives a drift that is always in the radial direction. We also note that a collisional drag will reduce the effect of the ∇B-gradient drift, while it will increase the differential rotation, see (4.7).

The radial drift deduced from these arguments come in addition to the bulk plasma rotation. If we follow a blob moving in the plasma column, it will follow a "spiral-like" orbit in the laboratory frame of reference.

4.4 Fluctuating velocities

In the following we identify the fluctuating plasma velocity component $\perp \mathbf{B}$ as $\tilde{\mathbf{E}} \times \mathbf{B}/B^2$, where we ignore polarisation drifts to the accuracy $\langle\omega\rangle/\Omega_{ci} \approx 10^{-3}$. For homogeneous magnetic fields and electrostatic fluctuations we have

$$\frac{\nabla \cdot \left(\tilde{\mathbf{E}} \times \mathbf{B}\right)}{B^2} = -\frac{\nabla \cdot \left(\nabla\tilde{\phi} \times \mathbf{B}\right)}{B^2} = 0\,.$$

For the present case, however, we have $\mathbf{B} = \mathbf{B}(\mathbf{r})$ so that $\nabla \cdot \tilde{\mathbf{E}} \times \mathbf{B}/B^2 \neq 0$, and the plasma flow is slightly compressible. These velocities should be compared to gradient and curvature drifts. We will find that root-mean-square $\mathbf{E}\times\mathbf{B}/B^2$-drifts are largest by about an order of magnitude. All these velocities are, however, small compared to the sound speed, see Table 4.1.

With our set-up and the parameters given in Table 4.1 we can estimate the velocities associated with ∇B- and curvature drifts. The common factor in the two drift velocities is

$$\frac{\nabla B}{B} = -\frac{\mathbf{R}}{R^2} = -\frac{1}{R}\hat{\mathbf{r}} \approx -1.53\hat{\mathbf{r}}\,,$$

with magnitude in m^{-1}. The curvature drift is given by equation (2.13), and for an electron this would be approximately $\bar{U}_{DC} \approx 50$ m/s directed downwards. Equivalently for the ∇B-drift, assuming the perpendicular velocity $U_\perp$ is comparable to the average electron velocity is approximately $\bar{U}_{\nabla B} \approx 64$ m/s, also directed downwards for electrons. We will later find a fluctuating velocity with rms value ~ 500 m/s. As a reference we have $C_s \approx 10^4$ m/s.

Chapter 5

Methods

In analysing the radial flux data from the Blaamann experiment we looked at a number of different aspects and features of the datasets. The data files contain six variables, where two are derived (velocity and flux), and the other four are raw data (measurements of floating potentials and saturation currents). The main focus of this study is to investigate the nature of the plasma transport within Blaamann by looking at the density, velocity and flux fluctuations in the plasma column.

5.1 The probability density function

The measured time series by themselves are difficult to interpret directly. In order to get an overall impression of the data we estimated the respective probability density functions (PDF) of the flux, velocity and density. This was done by grouping the data into bins, and counting the number of observations within each bin, just like one would make a histogram. In order to normalise the function, the counter for each bin was divided by both the total number of data points and the size of the bin, thus ensuring that the area under the graph is equal to one.

We have five datasets for almost every position, with four sets for positions 0 cm and -1 cm. In addition, one of the sets recorded for position -1 cm had to be eliminated, due to some disturbance occurring during the first 2 ms of data. The PDF of each variable was estimated by grouping all the sets together into one long time series and estimating the PDF for each position. This means that each PDF is estimated from 50.000 points (40.000 for probe position $x = 0$ cm, and 30.000 for $x = -1$ cm). The PDF is estimated for all positions, giving a set of 19 functions showing how the distribution changes with probe position. The PDF in each position is normalised individually.

A joint PDF for the velocity and the density was also found, in order to il-

lustrate how these two quantities relate. This was done similarly to the ordinary PDFs, but corresponding data points from density measurements and velocity measurements were investigated simultaneously. Each event would then fall within a square of a grid where density values were along the x-axis and velocity values along the y-axis. The result is then equivalent to a three dimensional histogram.

5.1.1 Theoretical model for the local particle flux

Assuming that the individual components that make up the flux signal, i.e. the density and velocity, are Gaussian in nature, Carreras et al. (1996) have deduced a theoretical joint distribution function for the fluctuating density and the velocity signals.

$$f(\tilde{n}, \tilde{u}_r) = \frac{1}{2\pi} \frac{\sqrt{1-\gamma^2}}{W_u W_n} \exp\left[-\left(\frac{\tilde{u}_r^2}{2W_u^2} + \frac{\tilde{n}^2}{2W_n^2} + \gamma \frac{\tilde{u}_r \tilde{n}}{W_n W_u} \right) \right] \tag{5.1}$$

W_u and W_n are the standard deviations of the velocity and density respectively, in the absence of correlation. γ is the signed correlation between density and velocity, which means $|\gamma| < 1$. By introducing $\Gamma = \tilde{n}\tilde{u}_r$ it can be shown that (5.1) gives the following theoretical distribution for the fluctuation-induced turbulent flux.

$$p(\Gamma) = \frac{1}{\pi} \frac{\sqrt{1-\gamma^2}}{W_u W_n} K_0 \left(\frac{|\Gamma|}{W_u W_n} \right) \exp\left(-\gamma \frac{\Gamma}{W_u W_n} \right) \tag{5.2}$$

K_0 is the modified Bessel function of the second kind. γ will be estimated from the correlation coefficient for density and velocity for each position. W_u and W_n are taken to be equal to σ_n and σ_u, i.e. the respective standard deviations of the experimentally obtained density and velocity.

We intend to test the results of this model against the PDFs of flux obtained from the experimental data.

5.2 Moments

Describing my data more quantitatively than a PDF requires calculating the lower order moments, thus finding specific numbers to describe the shape of the distributions. We will concentrate on the first four moments, as they are the ones that are most easily interpreted and understood.

The first moment is the mean, μ, approximated as

$$\mu = \langle x \rangle = \frac{1}{N} \sum_{i=1}^{N} x_i \tag{5.3}$$

for a dataset consisting of N measurements, where x_i denotes the ith data point. The mean will only tell around which value the time series oscillates over the course of the entire series. A standard normal distribution has $\langle x \rangle = 0$.

The higher order central moments are given as

$$\mu_n = \langle (x - \langle x \rangle)^n \rangle \tag{5.4}$$

and are all centred around the sample mean.

The second moment is the biased variance. This is related to the width of the corresponding PDF, thus giving the spread of the data around the mean.

$$\mu_2 = \sigma^2 = \langle (x - \langle x \rangle)^2 \rangle \tag{5.5}$$

For a random Gaussian process σ can take any value.

Variance can be normalised by dividing by $\langle x \rangle^2$, making σ^2 dimensionless, whereas the estimated mean is the only moment we cannot normalise. $\langle x \rangle$ will therefore be in arbitrary units, while the higher order moments are dimensionless.

The third moment is the skewness, which indicates if and how a distribution of numbers may be skewed compared to the mean. If the distribution is perfectly symmetric the skewness will be zero, as is the case for a Gaussian random process. If the left tail of the distribution is more pronounced than the right tail, the skewness is said to be negative, and similarly if the right tail is more pronounced the skewness is considered to be positive. The expression given underneath is normalized with respect to the standard deviation. A large skewness indicates a clear deviation from the Gaussian distribution.

$$\mathscr{S} = \frac{\mu_3}{\mu_2^{3/2}} = \frac{\langle (x - \langle x \rangle)^3 \rangle}{\langle (x - \langle x \rangle)^2 \rangle^{3/2}} \tag{5.6}$$

The fourth moment is the kurtosis, and is given beneath in its normalized form. It is a measure of how tall and slim or alternatively how short and wide the distribution is compared to the normal distribution. In addition, it is a measure of the weight of the tails. A set of data that are have a Gaussian distribution will have a normalized kurtosis of three. A kurtosis of less than three indicates a distribution that is wider and shorter than the normal distribution and that has less heavy tails, whereas a kurtosis of more than three is indicative of a distribution that is more peaked and has longer tails than the normal.

$$\mathscr{K} = \frac{\mu_4}{\mu_2^2} = \frac{\langle (x - \langle x \rangle)^4 \rangle}{\langle (x - \langle x \rangle)^2 \rangle^2} \tag{5.7}$$

A finite database can only provide an estimate for averages, not the true values. With the large database available at each spatial position we can ignore this

uncertainty and assume that for instance (5.3) is an exact relation for a finite but large N-value.

Consider a random variable x and assume that you have found an estimate $\frac{1}{N}\sum_{j=1}^{N} x_j$ for the average $\mu \equiv \langle x \rangle$. The error e on the estimate is given as

$$e \equiv \left\langle \left(\langle x \rangle - \frac{1}{N}\sum_{j=1}^{N} x_j \right)^2 \right\rangle .$$

We find

$$e = \langle x \rangle^2 + \frac{1}{N^2}\left\langle \left(\sum_{j=1}^{N} x_j \right)^2 \right\rangle - 2\left\langle \langle x \rangle \frac{1}{N}\sum_{j=1}^{N} x_j \right\rangle .$$

The last sum is easy: each term in the sum becomes $\langle x \rangle$ and we have N of these, so we find all in all $-2\langle x \rangle^2$ for this term. The second term is written as

$$\frac{1}{N^2}\sum_{k=1}^{N}\sum_{j=1}^{N}\langle x_j x_k \rangle .$$

The double sum contains two sorts of terms: N terms where $j = k$ and $N(N-1)$ terms where $j \neq k$. In the former case we have

$$\langle x_j^2 \rangle = \langle x^2 \rangle$$

for each term, in the latter case we find

$$\langle x_j x_k \rangle = \langle x_j \rangle \langle x_k \rangle = \langle x \rangle^2 .$$

Consequently we have

$$e = \langle x \rangle^2 + \frac{1}{N^2}(N\langle x^2 \rangle + N(N-1)\langle x \rangle^2) - 2\langle x \rangle^2$$

giving

$$e = \frac{1}{N}(\langle x^2 \rangle - \langle x \rangle^2) .$$

We have $e \to 0$ for $N \to \infty$ as expected, in such a way that the root-mean-square error decreases as $1/\sqrt{N}$. The discussion can be extended to other averages.

5.2.1 Skewness-kurtosis relations

In order to discuss the possibility for a systematic relation between the skewness and the kurtosis of the plasma flux signal we begin by introducing a simple two-level model, where we assume that the flux is "burst-like", i.e. it is either vanishing

or it assumes a constant positive value $\gamma > 0$ in a short time interval. This means that the time variation of the flux event has a so called "top-hat" shape. The temporal duration of the flux event $\Delta\tau$ is finite, so Gaussian or exponential pulses, for instance, are excluded. The random process is assumed to be time stationary, and the probability for encountering a plasma burst at some position is constant in time. At some fixed position at any given time it is assumed that the probability for being in the interval $\Delta\tau$ is $0 \leq \alpha \leq 1$. It is essential for the following discussion that flux events do not overlap. This analysis addresses a plasma flux signal, since this is what we are concerned with here, but the arguments can just as easily be applied for a density or velocity signal.

If we have a long time record of duration $\mathcal{T}$, we have $\alpha = \mu\Delta\tau$ where $\mu \approx \langle N\rangle/\mathcal{T}$ is the number density of the appropriate flux-pulses in the record. Uncertainties arise due to end-effects, which can be made arbitrarily small by increasing $\mathcal{T}$.

After averaging over different realisations, the probability density for the plasma flux in this basic model is

$$P(\Gamma) = (1-\alpha)\delta(\Gamma) + \alpha\delta(\Gamma - \gamma)\,, \tag{5.8}$$

where the first term accounts for the cases where the flux vanishes, i.e. at times where no plasma burst is intercepted at the detection position, and the second term gives the probability distribution within a flux tube (the "top hat"). For the case given by (5.8) we can obtain

$$\langle \Gamma^m \rangle = \alpha\gamma^m$$

with $m = 1, 2, 3, \ldots$, giving the average value

$$\langle \Gamma \rangle = \alpha\gamma\,,$$

the variance

$$\sigma^2 \equiv \langle (\Gamma - \langle\Gamma\rangle)^2 \rangle = \alpha(1-\alpha)\gamma^2\,,$$

the skewness

$$\mathscr{S} = \alpha(1 + 2\alpha - 3\alpha^2)\gamma^3/\sigma^{3/2}$$

and kurtosis

$$\mathscr{K} = \alpha(1 - 4\alpha + 6\alpha^2 - 3\alpha^3)\gamma^4/\sigma^4\,,$$

implying here the exact relation $\mathscr{K} = \mathscr{S}^2 + 1$ for any α. This can easily be demonstrated by insertion. For this particular signal we have $\mathscr{S} = 0$ when $\alpha = 1/2$.

The "top-hat" model also gives a relation between normalized variance and skewness in the analytic form

$$\sigma^2/\langle\Gamma\rangle^2 = 1 + \frac{1}{2}\left(\mathscr{S}^2 + \mathscr{S}\sqrt{\mathscr{S}^2+4}\right) .$$

Note that this expression assumes $\langle\Gamma\rangle \neq 0$, so it will not apply for positions near the center of the plasma.

Generally it can be shown that $\mathscr{K} \geq \mathscr{S}^2 + 1$ holds for any probability distribution, with the exception of PDFs with $\sigma = 0$ which are singular in the present context. (We use here the definition where $\mathscr{K} = 3$ for a Gaussian distribution.) More generally we actually have

$$\mathscr{K} = A\mathscr{S}^2 + B\,, \tag{5.9}$$

where A and B are constants. The simple analytical model (5.8) and its generalisations have been widely discussed in, e.g. studies of concentration fluctuations in turbulent environments (Jørgensen et al., 2010).

The model (5.8) can be generalised by allowing for a more general temporal form of the burst event containing a random parameter a with PDF $P(a)$. More parameters can readily be included. We denote this form $G_a(\tau)$ for $0 \leq \tau \leq \Delta\tau$ and $G_a(\tau) = 0$ otherwise. One example could be $G(\tau) = a\sin^p(\pi\tau/\Delta\tau)$ for $0 \leq \tau \leq \Delta\tau$, where p is a fitting parameter. With this generalisation we find

$$P(\Gamma) = (1-\alpha)\delta(\Gamma) + \alpha\frac{1}{\Delta\tau}\int_0^\infty\int_0^{\Delta\tau}\delta(\Gamma - G_a(\tau))d\tau P(a)da\,, \tag{5.10}$$

where it is assumed that a burst event is encountered at any time $\tau \in \{0;\Delta\tau\}$ with equal probability. The previous results for $\langle\Gamma\rangle$, σ^2, $\mathscr{S}$ and $\mathscr{K}$ are now generalised. We find, for instance,

$$\langle\Gamma^m\rangle = (\alpha/\Delta\tau)\int_0^\infty\int_0^{\Delta\tau} G_a(\tau)^m d\tau P(a)da\,.$$

The expression (5.10) can be formulated differently, but it turns out that this form is the most convenient here. For completeness, we might add that (except for the top-hat signal) the distribution of amplitudes $P(a)$ is not simply related to the probability density of the signal amplitude, since a is the amplitude of a local maximum. If we have the joint probability density of the flux and its two first derivatives $\Gamma(t), d\Gamma(t)/dt, d^2\Gamma(t)/dt^2$ as $P_J(\Gamma,\Gamma',\Gamma'')$ then $P(a) = \int_0^\infty P_J(a,\Gamma' = 0,\Gamma'')d\Gamma''$.

Extensions of the idealised model (5.8) have been presented by e.g. Jørgensen et al. (2010), basically relying on generalisations included in (5.10). They found

that a parabolic relation like (5.9) remained but with $A > 1$ and $B > 1$. The numerical value of A and B depend on the structure shape $G_a(\tau)$.

Garcia (2012) discusses a model where pulses are superimposed randomly. The pulses can in principle have infinite support, i.e. are not constrained to a finite temporal or spatial domain. The position of one pulse or structure is there assumed to be independent of the position of all the others. This model will consequently have the possibility of overlapping of two or more structures. Such models have been widely used for modelling random signals (Pécseli, 2000; Pécseli and Trulsen, 1993). The model discussed by for instance (5.6) assumes that the basic pulses or structures do not overlap: such a model seems much more reasonable here, since it is unlikely that one plasma burst can begin before the previous one has terminated.

5.3 Correlation functions and power spectra

A correlation function describes how two measurements made at different times t_1 and t_2 are related, and measures how closely a dataset resembles itself at a later time. It can also be used as a measure of predictability of a signal based on past data in the time series. It is defined as

$$C(t_1, t_2) \equiv \frac{\langle Y(t_1)Y(t_2)\rangle}{\langle Y^2\rangle}\,, \tag{5.11}$$

where σ_Y^2 is the variance and $\langle Y(t_1)Y(t_2)\rangle$ is the autocovariance function of dataset Y. Here the two events are from within the same time series. In such a case the function is called an autocorrelation function, i.e. it shows how a time series is correlated with itself.

The cross correlation function gives the correlation between two different time series, and can be considered as a measure of how well one measured quantity can be used to predict the development of another. It is important to remember that one might not know which variable is the cause and which is the effect. The cross correlation function is given as a similar expression as (5.11).

$$C(t_1, t_2) \equiv \frac{\langle X(t_1)Y(t_2)\rangle}{\sqrt{\langle X^2\rangle\langle Y^2\rangle}} \tag{5.12}$$

Assuming that we have a time stationary process, the above expressions can be simplified by introducing τ which denotes the difference between t_1 and t_2, i.e. $\tau = t_2 - t_1$.

$$C_{YY}(\tau) = \frac{\langle Y(t+\tau)Y(\tau)\rangle}{\sigma_Y^2} \tag{5.13}$$

With the current data it is reasonable to assume that we have time stationary events, as there is little reason to assume that the PDF changes greatly throughout the time series.

Similarly for the cross correlation function we have

$$C_{XY}(\tau) = \frac{\langle X(t)Y(t+\tau)\rangle}{\sqrt{\sigma_X^2\sigma_Y^2}}\,. \tag{5.14}$$

The discrete form of the above expression for the cross correlation function is

$$C_{XY}(\tau) = \frac{\frac{1}{n}\sum_{i=1}^{n-\tau} X(i)Y(i+\tau)}{\sqrt{\sigma_X^2\sigma_Y^2}}\,. \tag{5.15}$$

It is equivalent for the autocorrelation function.

As we have several datasets for each probe position, it is convenient to combine the results into one correlation function. The correct way of finding the average is given below, where the average of the covariance function between the two variables X and Y, and the variance of X and Y all are found separately. The factor $1/5$ is omitted from each average, as they cancel each other.

$$C_{XY}(\tau) = \frac{\sum_{j=1}^{5}\left(\frac{1}{n}\sum_{i=1}^{n-\tau} X(i)Y(i+\tau)\right)_j}{\sqrt{\sum_{j=1}^{5}\sigma_{X,j}^2\sum_{j=1}^{5}\sigma_{Y,j}^2}} \tag{5.16}$$

Physically, a correlation function is a measure of a signals ability to interfere with either itself (auto correlation) or with another (cross correlation), and for the auto correlation function this interference is always greatest at $\tau = 0$. The cross correlation function can reach its maximum value for any τ depending on how the two signals are connected, and how the two probes are positioned according to one another. The correlation function yields physical information on e.g. time scales of a process, or delay between two related processes.

In the current analysis it is most instructive to investigate how the physical quantities, i.e. floating potential, density, velocity and flux are correlated with the reference probe. The reference probe is situated a quarter of a revolution from the positive probe positions, given that we follow the direction of the $\mathbf{E}\times\mathbf{B}/B^2$-drift, and three quarters of a revolution from the negative probe positions. Any correlation between the reference probe and data from the moveable probe indicates that some structure with enhanced values for density or velocity (or both) has passed one of the probes and then the other, i.e. a coherent structure of some sort.

From the auto correlation function of a variable at a given position, the power spectrum can be found by calculating the Fourier transform of said function. This

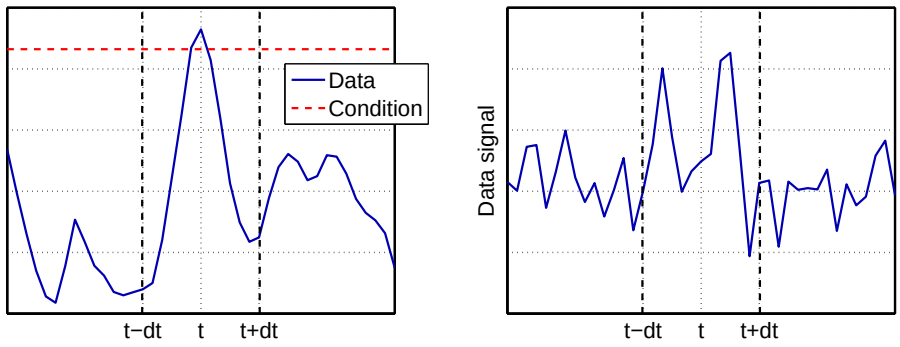

(a) (b)

Figure 5.1: *Illustration of selection of data using conditional sampling.*

is done numerically using Fast Fourier Transform (FFT), and gives the frequencies present in the autocorrelation function. Physically this means that the power spectrum gives the frequencies at which larger coherent structures are detected at a given probe's position.

5.4 Conditional sampling and averaging

A useful tool when studying the presence of large coherent structures is conditional sampling (Johnsen et al., 1987; Øynes et al., 1995). Generally this is a method where only small intervals of a time series are sampled and used to study the data. The way the intervals are selected is by imposing some condition on the amplitude of the time series, i.e. that only when there is a larger burst is an interval of appropriate length surrounding this point selected.

Here we will mostly use a version of conditional sampling often referred to as cross-parametric conditional sampling. This means that the condition C is imposed on a reference signal Φ_1 rather than on the time series we wish to study, and this is used to select a subset of data from the signal of interest, Φ_2. Only when the condition is met within the reference signal, say at time t_0, are both signals sampled, and only within a time interval of $\{t_0 - \tau, t_0 + \tau\}$, where τ is adjusted according to the duration of the average larger coherent structure (see Figure 5.1). τ tends to be related to the correlation time. The result is then a new time series consisting of several intervals where the signal is exactly the same as in the original, but in between the said intervals are only zeros. That way we find the response in Φ_2 to larger bursts in Φ_1.

Each of the intervals selected from Φ_2 can then be used to find an average

response, given as

$$\Phi_{ca} = \langle \Phi_2 | C \rangle \,, \tag{5.17}$$

thus giving the conditionally averaged signal that is expected in Φ_2, given that condition C is met in Φ_1. This averaging over conditionally sampled subsets extracts the coherent parts of the dataset, suppressing the uncorrelated parts. In other words, the turbulent fluctuations are averaged out, giving the average response in Φ_2 to a spike in Φ_1.

It is important to make sure that none of the intervals selected from either of the two datasets overlap, as that would mean that some measurements are sampled twice in the conditional averaging. If intervals were to overlap there would be no guarantee that they are independent of each other. As we have already mentioned, we are already assuming that a model with no overlapping bursts is applicable to our data, thus it is not unreasonable to set this additional condition of only sampling individual events that are clearly separated from the previous and the next event within a time series.

Typically we will use conditions which are related to the standard deviation of the reference signal, e.g. C is $\Phi_1 \geq 1.5\sigma$. We will spend some time investigating the effect of changing this condition for a higher or lower value.

The conditional averaging technique offers similar results as the cross correlation functions, which seems reasonable as they both in some way give a relation between a reference signal and another time series. The conditional average with $|\Phi_1| > 1.5\sigma$ is a first approximation of the cross correlation function between the reference signal and the signal of interest. However, conditional averaging is also sensitive to polarisation, as long as the conditional limit is set to be either a positive or a negative number, and not both, i.e. if the condition is e.g. $\Phi_1 > 1.5\sigma$. Such a condition ensures that only large positive bursts are selected, ignoring all others. This is useful when studying fluctuating data, as one is allowed to select only flow with enhanced positive speed, density, etc. If the condition is set to $|\Phi_1| > 1.5\sigma$ however, the sensitivity to polarity disappears.

The conditional variance is defined as

$$V_{con} = \frac{\langle (\Phi_2 - \langle \Phi_2 | C \rangle)^2 | C \rangle}{\langle (\Phi_2 | C)^2 \rangle} \,, \tag{5.18}$$

and gives the level of reproducibility of the entire event, i.e. shape, position and trajectory. V_{con} can only take positive values between 0 and 1. A low variance means a high level of reproducibility, whereas a variance close to 1 means little or no reproducibility. We use here the same definition of conditional variance as Øynes et al. (1998).

5.4.1 Reference signals

The conditional sampling and averaging technique can be used to study any kind of physical quantity measured as a time series. In this study it would be possible to use it to investigate the velocity and density signals, as well as the flux. However, we will concentrate on the flux signal as it gives the most information with regards to the transport of plasma within the tank. However, there is no limit on how many conditions we can impose on the data when conditionally sampling fragments, thus we can add conditions not only on the reference signal but also on the other signals. Since we will want to distinguish between transport in and out of the plasma, one additional condition will be $\Gamma \gtrless 0$. Finally, distinguishing between density enhancements and depletions and propagation in and out of the plasma, will be interesting, and thus another condition will be $u \gtrless 0$, or equivalently $n \gtrless 0$.

The flux signal is the product of the fluctuating component of velocity and density. Therefore it seems likely that it will be more closely related to a reference signal that is either a measure of velocity or density, rather than one that is a measure of floating potential. As mentioned the electric field is directly proportional to a velocity, and is also related to potential through

$$E_y = -\frac{\partial \phi}{\partial y}\,.$$

In general we have that the potential is a function of space and time. Introducing the coordinate $\xi = y - u_0 t$ which gives position relative to the background motion we can write the potential as $\phi(y - u_0 t, t)$. Differentiating this signal with respect to ξ is equivalent to differentiating with respect to y, since

$$\frac{\partial \xi}{\partial y} = 1\,.$$

Thus we have

$$\frac{\partial \phi}{\partial y} = \frac{\partial \phi}{\partial \xi}\,.$$

However, since we have floating potential ϕ as a time series, we only have the option of differentiating with respect to time. As it turns out, this is not a problem.

$$\frac{\partial \phi}{\partial t} = -u_0 \frac{\partial \phi}{\partial \xi} + \frac{\partial \phi(\xi, t')}{\partial t'} \approx -u_0 \frac{\partial \phi}{\partial \xi} = u_0 E_\xi$$

Here we have assumed that $\partial\phi/\partial t'$ is small, i.e. implicitly we assume that the time evolution is slow in the rotating frame of reference. The time derivative of ϕ is proportional to E_y as long as the fluctuations are small, meaning that we can treat u_0 as a constant. Therefore we can assume that the time derivative of the signal

from the reference probe will be proportional to an electric field, and thus also to a velocity signal.

$$E_y \sim \frac{\partial \phi}{\partial t}\,,$$

which will be assumed in the ensuing analysis.

Chapter 6

Results

The aim of this study is to investigate statistical properties of the data from Blaamann, and to use this to infer a conclusion regarding the turbulent transport of plasma within a simple magnetised torus. In this chapter our results are presented and described.

6.1 The raw data

As mentioned these data consist of a number of sets collected at 19 different positions. Originally there were five sets for each position. However, for both positions 0 cm and -1 cm the final set is empty, i.e. no data. In addition, one set collected at -1 cm had to be eliminated due to some disturbance causing very large harmonic oscillations in the data during the first 2 ms of the set. Possibly the probe was situated in the middle of the plasma beam, thus causing the disturbance, but there is really know way of knowing the cause for certain.

The raw data in itself offers little insight into the transport and motion of plasma within the toroidal tank. However, a few samples of the data collected at several different positions are included here for completeness, and in order to illustrate what the various time series look like (see Figure 6.1). It is clear that the signals fluctuate between much larger values nearer the centre, which is closer to the filament, with the greatest fluctuations found for $x = -1$ cm. The data collected near the centre will most likely be very chaotic, and are not as valuable to our analysis as the datasets collected a little further out. However, they are useful in illustrating the large amount of fluctuations occurring near the centre. Further out we have much smaller fluctuations. Note that there is not a symmetric decrease in levels. The smallest fluctuations are found for $x = -9$ cm, with the corresponding position on the outside demonstrating somewhat greater variation.

The density signal oscillates very quickly, whereas the velocity shows some signs

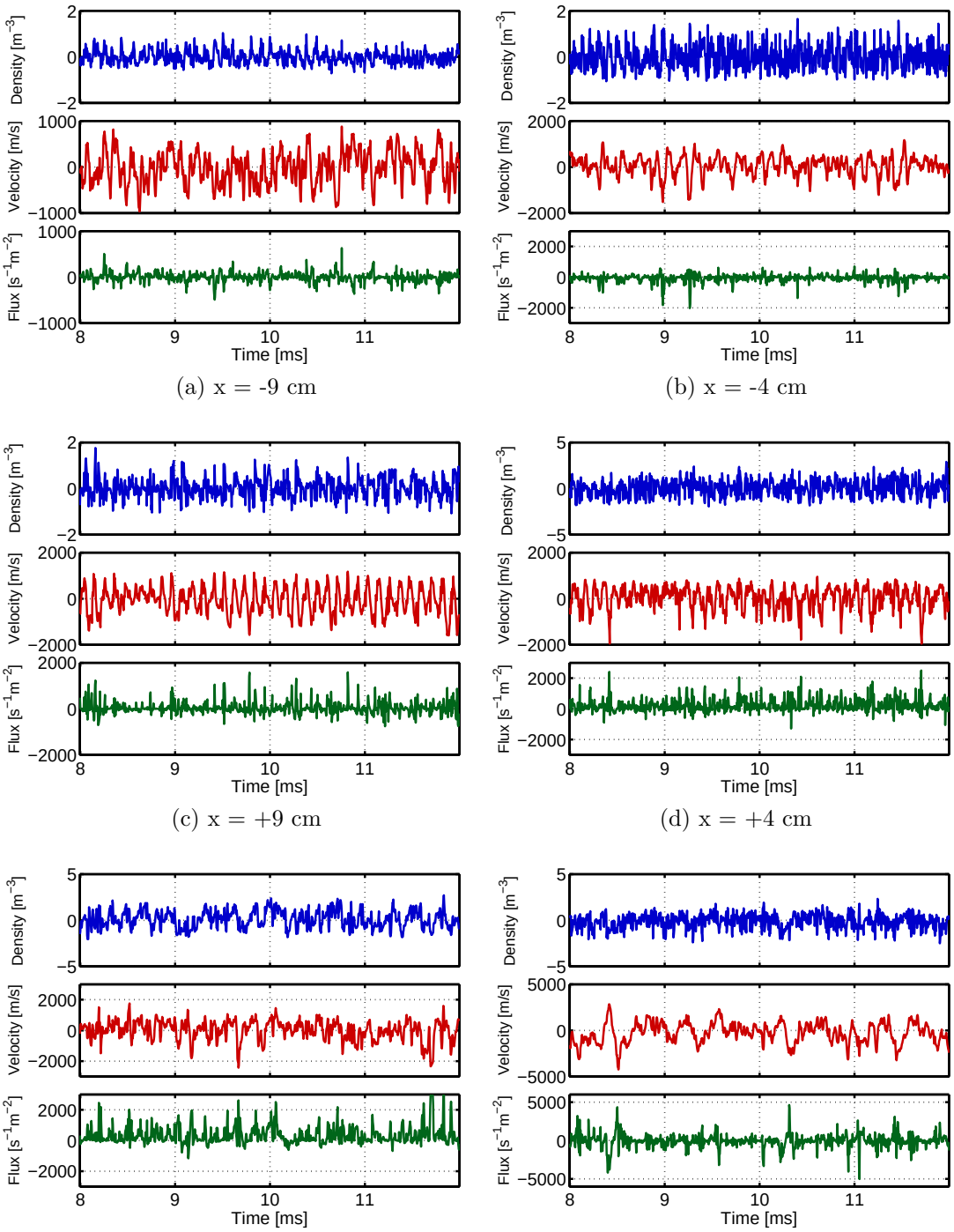

(a) x = -9 cm

(b) x = -4 cm

(c) x = +9 cm

(d) x = +4 cm

(e) x = +1 cm

(f) x = -1 cm

Figure 6.1: *Samples of raw data showing density, velocity and flux in six different positions along the local x-axis.*

of occasional harmonic bursts with a somewhat lower frequency, as can be seen for instance in Figure 6.1d) in the interval 10-12 ms. Such bursts will be studied more closely using the conditional sampling technique.

It is also worth noticing the larger positive flux events in d) ($x = 4$ cm) at approximately 8.5 ms, 10.5 ms and 11.5 ms with corresponding negative spikes in velocity and density. This indicates that we here have a density depletion moving in the negative direction, i.e. inwards. Note that for negative positions a negative velocity corresponds to a velocity in the direction of the wall, i.e. outwards. Equivalently for $x = -4$ cm there are two clear negative spikes in the flux signal, one at 9.0 ms and one about 300 μs later, corresponding to negative spikes in velocity and positive spikes in density, which means these are density enhancements moving outwards.

6.2 PDFs

The first approach in studying the data from Blaamann was to find the probability density functions of the measured and derived quantities. The result of this is shown in Figure 6.2, where we have included the PDFs of velocity, flux and density, as well as the distribution we found for one for the probes measuring floating potential (channel 1). The equivalent distribution of the data from channel 2 is not included as it is nearly identical to the one for channel 1 and thus would not contribute with any additional insight.

As we can see, the floating potential has generally larger fluctuations for positive x-values, i.e. on the outer side of the torus, with the widest PDFs at $x = 7-8$ cm from the centre. There is also a slight asymmetry for the positive positions, with a skewness leaning towards positive values for the floating potential for positions near the wall, and towards negative values closer to the centre and the filament. For negative positions, the PDFs are more peaked, and also more symmetric.

The density distributions are rather varied for the different positions. For the innermost positions the PDF is rather symmetric and peaked, with most fluctuations within an interval of ± 1 m^{-3}. However, as one moves towards the centre, the PDFs become increasingly skewed, leaning towards negative values. They are also less peaked, with fluctuations occurring within a larger interval of densities. Nearing the filament, the skewness changes towards positive values. The distributions also widen a great deal, indicating more large scale fluctuations of density in this region. Nearing the outermost positions, the skewness changes again, leaning once more towards negative values. For the outermost point the PDF is nearly symmetric.

The PDFs for the velocity are all fairly symmetric, and there is less variation in width as well. The only exceptions are two of the positions closest to the filament,

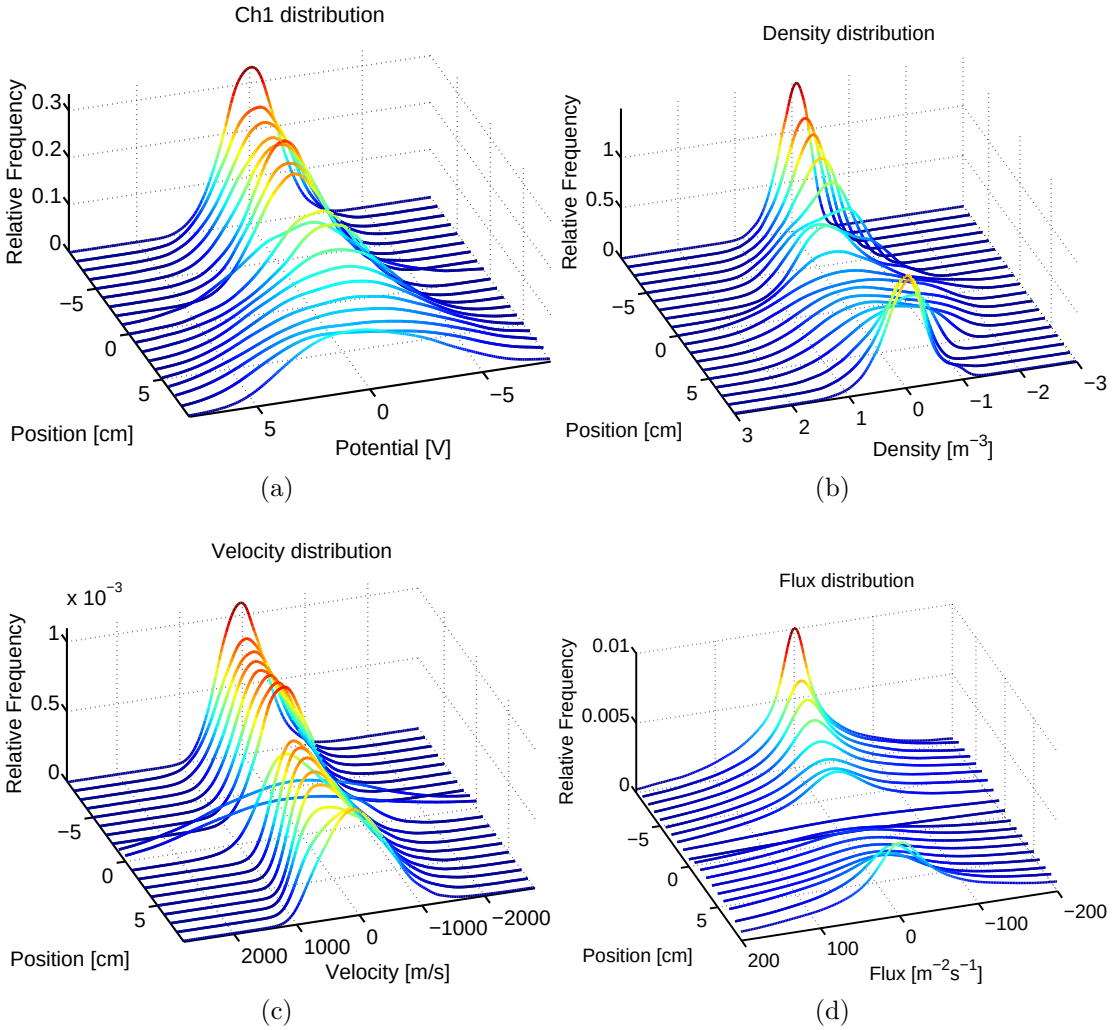

Figure 6.2: *Probability densities for (a) floating potential measured through channel 1, (b) density, (c) velocity and (d) flux. Each PDF is normalised individually for each position. All PDFs have been smoothed.*

namely -1 cm and 0 cm. Here the velocity is very widely distributed over a large interval. However, this is to be expected as there will be much chaotic motion caused by the filament itself. Velocities fluctuate in general within an interval of ± 1000 m/s.

The flux distributions are mostly symmetric around zero, with a slight negative skewness for negative values, and vice versa for positive values. However, it is evident that the PDFs are significantly more peaked near the outer positions, while fairly wide closer to the centre of the poloidal cross section. Thus there will be more flux occurring near the centre, as this is where we find the greater values, while further away from the centre small fluxes are far more likely. This is to be expected as there is bound to be more motion near the filament, as the helium gas is being ionised in this area.

Since a toroidal cross section will not have a homogeneous $\mathbf{B}$-field causing the $\mathbf{E} \times \mathbf{B}/B^2$-velocity to be compressible, we have little reason to expect perfect symmetry of the PDFs around $x = 0$.

6.2.1 Comparison with theoretical model for the flux distribution

The theoretical PDF for the fluctuating flux signal based on the model of Carreras et al. (1996) is shown Figure 6.3. It shows a clear similarity to the PDF based on the experimental data, shown in Figure 6.2d), with the most peaked distribution being found for $x = -9$ cm. The general dependence on probe position is similar for the two distributions. However, this theoretical PDF appears to be somewhat more peaked and narrow than the one based on our data. There is also some inconsistency between the average flux that we get with this model. The greatest average flux is found for $x = -9$, and generally the flux is greater for $x < 0$ than for $x > 0$, which is quite the opposite of what we find for our experimental data, as will be shown in Section 6.3.

The model given by (5.2) gives a fairly good estimate for our experimental results, but it is somewhat inaccurate. This is most likely because it oversimplifies the nature of the velocity and density signals. Even though their respective distributions may be somewhat similar to a Gaussian distribution, at least for some probe positions, they deviate greatly from such a distribution in other points. Thus we have little reason to expect this simple model to fit perfectly with our results.

6.2.2 Joint PDF for velocity and density

In order to illustrate how the velocity and the density are related a joint PDF for these two variables was created. It is shown in Figure 6.4. These PDFs are the

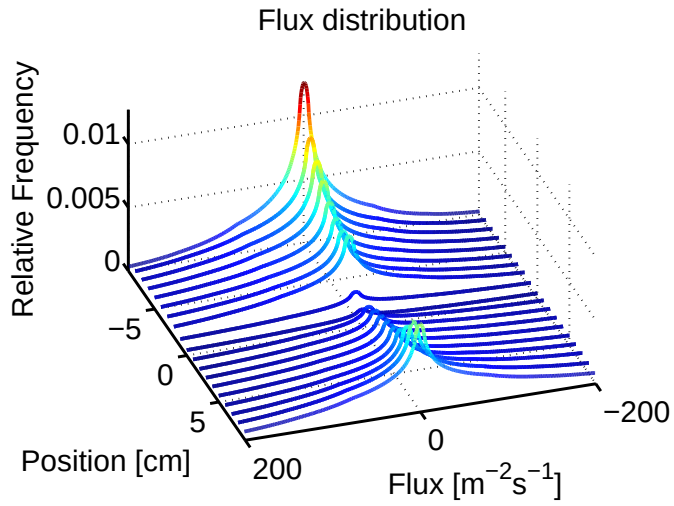

Figure 6.3: *Theoretical PDF in each probe position for the fluctuating flux, based on (5.2). A simple smoothing algorithm has been used.*

mean of all the sets, but divided into one for positions $x > 0$ and $x < 0$. The purpose of this figure is to show how especially the large values of density relate to large values for velocity, as these are the events causing large spikes in the flux signal.

We can see that in both cases that the peak is situated around 0 to low positive values for both velocity and density. The PDF for $x < 0$ is less spread out than it is for $x > 0$. This indicates that there are more large flux events for positive x than for negative. In addition it is worth noticing that in both cases the joint PDF is somewhat elongated like an ellipsis. However, the two are tilted in opposite directions. For $x < 0$ we have slight tails stretching out towards combinations of either positive values for density and negative values for velocity, or towards negative densities and positive velocities. For $x > 0$ we find the opposite case. The tails of the distribution are stretched out towards combinations of values of the same sign for density and velocity. This indicates that one would most likely find more large positive flux events than negative for $x > 0$, and correspondingly more large negative flux events for $x < 0$, consistent with an average flux directed out of the plasma.

By inspection of Figure 6.4 for $x > 0$ we note that a large positive value of $\Gamma \equiv \tilde{n}\tilde{u}$ is most likely to be found if either $\tilde{u}$ is large and negative with moderate negative $\tilde{n}$, or $\tilde{u}$ is moderate and positive while $\tilde{n}$ is large and positive. Large negative $\tilde{n}$ or large positive $\tilde{u}$ are rare.

The PDFs change somewhat from position to position, and hence it is useful to look at the result from individual positions as well. In Figure 6.5 the joint PDF

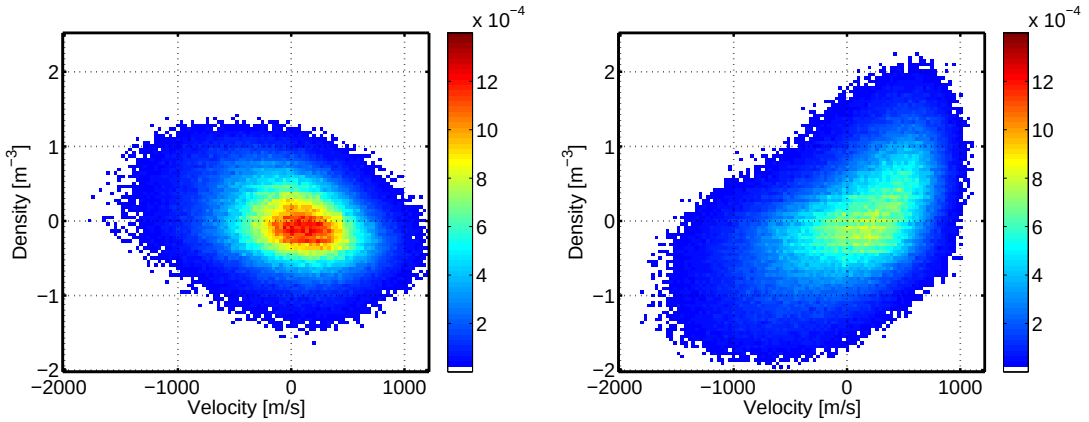

(a) $x < 0$ (b) $x > 0$

Figure 6.4: *Joint probability density function for velocity and density. (a) shows the averaged joint PDF for positions* $(-1) - (-9)$ *cm and (b) shows the PDF for the corresponding positions* $1 - 9cm$.

found for four different individual positions are shown. These are the average distributions found by averaging over all five datasets in one position. We see the same tendency as we did in the PDFs averaged over 9 positions on both sides of the centre of the cross section. However, the PDFs are more spread out for positions ± 4 cm than for ± 9 cm, indicating the presence of greater flux events closer to the centre. For the most extreme positions it is much more likely that the velocity and density will have low values, resulting in small flux, which corresponds well with the individual PDFs for flux shown in the previous section.

These joint distributions are equivalent to the PDF presented by Carreras et al. (1996) (see eq. (5.1)). However, we can see from Figures 6.4 and 6.5 that the assumption that velocity and density should have Gaussian distributions is incorrect in our case. One could possibly argue that the PDF of $x = -9$ cm shown in Figure 6.5a) can nearly be considered to be a combination of two Gaussian variables, but the PDFs found for the other positions are not, as they are clearly asymmetrical.

We recall here that the plasma column is not circularly symmetric, and that the $\mathbf{E} \times \mathbf{B}/B^2$-velocity is not incompressible. Consequently we have no reason to expect that the joint PDFs are the same for $x < 0$ and $x > 0$.

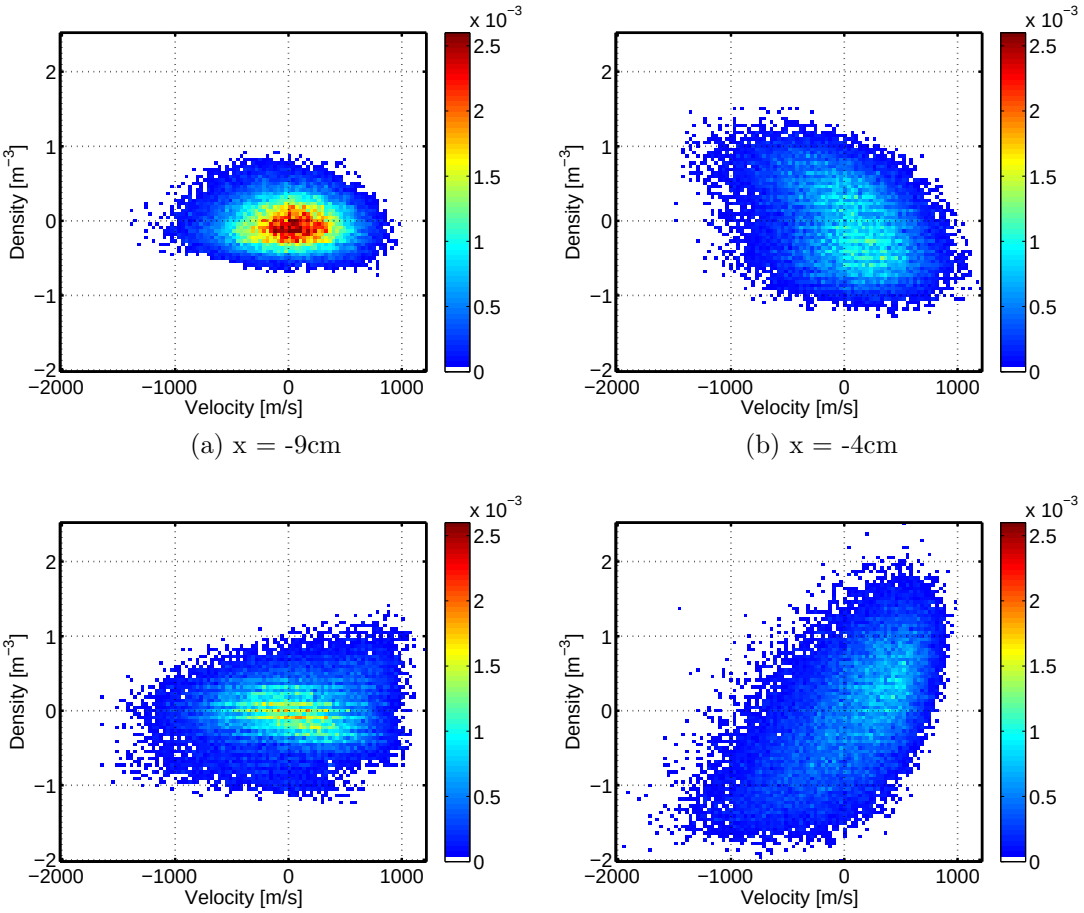

(a) x = -9cm (b) x = -4cm

(c) x = +9cm (d) x = +4cm

Figure 6.5: *Joint PDF for velocity and density at different radial positions. All distributions have the same colour scale, in order to illustrate the difference in size and magnitude. The white areas represent combinations of velocity and density that were not observed at all.*

6.3 Moments

Closely related to the PDFs of the various variables are the moments. Even though much can be deduced by simple inspection of the PDFs, it is useful to see the numerical values of the moments presented individually. Figure 6.6 shows how the moments for the flux signal vary with position. Note that positive flux indicates that we have either a density enhancement moving with a positive velocity along the x-axis, or a density depletion moving with negative velocity. Even though these two phenomena are quite different, in terms of flux they are equivalent. For positive x this corresponds to a density enhancement moving outwards towards the wall, or a density depletion moving inwards. For negative x it is negative flux which corresponds to density enhancements moving outwards or depletions moving inwards. From Figure 6.6a) it seems as though the average flux is, for all positions, directed outwards towards the wall of the tank, as we have negative averages for $x < 0$ and positive for $x > 0$. The average numerical value of the flux is however much larger for $x > 0$ than for $x < 0$.

As can be seen from Figure 6.6b), the normalised variance is very large near the centre and also close to the tank wall. In the centre the probe is very close to the filament, and is thus greatly affected by this. The flux is therefore more chaotic here, and thus the variance is large in this area. Near the wall we have very small average flux, and thus the normalised variance will be large here. In this area we also have that the average plasma density is low, and therefore these results are not as accurate and will in general have a larger error than the data collected nearer the centre. Generally, the variance for $x > 0$ is less than for $x < 0$, so even though the mean is numerically less for negative x, the data itself is more widely spread.

The skewness shown in Figure 6.6c) shows a change in sign corresponding to that observed for the mean, which supports the hypothesis that flux is generally directed outwards. A positive skewness for $x > 0$ indicates that not only is the mean somewhat shifted with respect to zero, but the whole distribution is asymmetric, with a larger portion of data points for positive fluxes than negative, and correspondingly for $x < 0$.

The kurtosis is generally significantly larger than what it is for a standard normal distribution. This means that the flux distribution for each position is more narrow and peaked and has heavier tails than the normal distribution. This is especially evident for the negative positions, indicating that there is a larger probability of small flux events than what one would find for a Gaussian random process.

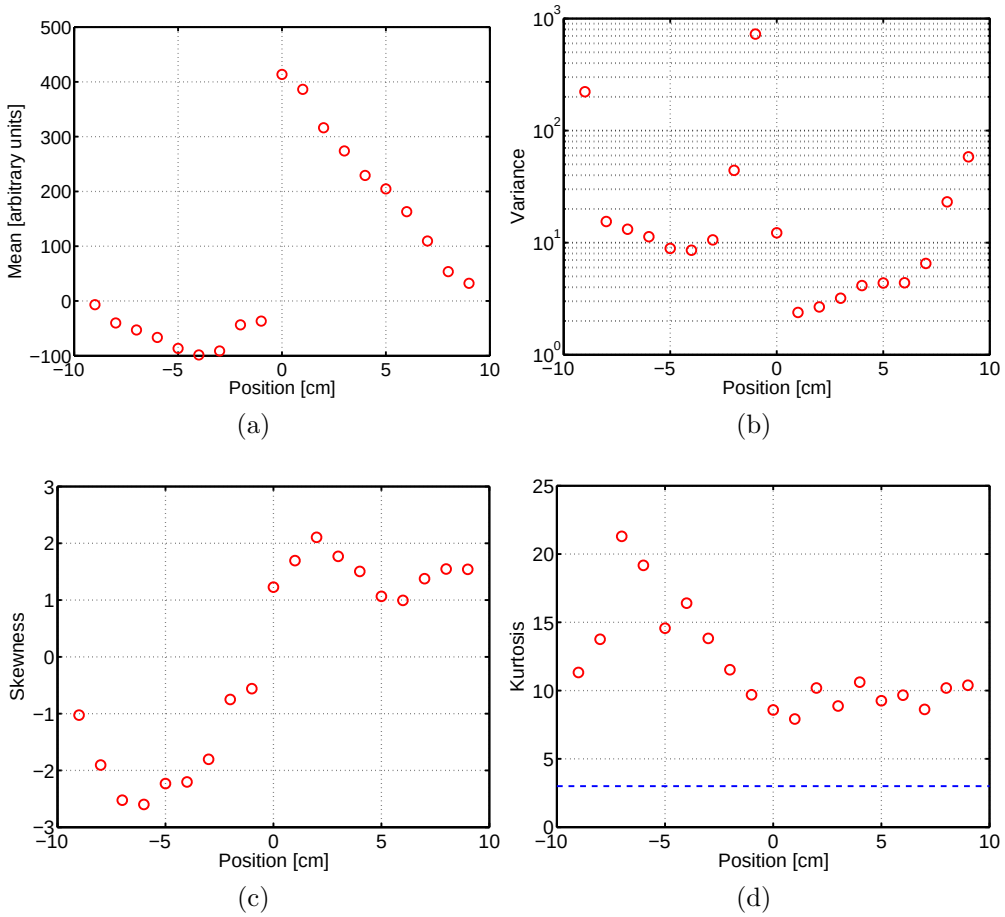

Figure 6.6: *Estimates for (a)average mean, (b)normalised variance (note that the scale on the y-axis is logarithmic), (c)skewness and (d)kurtosis along the horizontal midline of the poloidal cross section. For illustrative purposes the kurtosis of the standard normal distribution is included as a dotted blue line in (d). Skewness and kurtosis are dimensionless by definition, and the variance is made dimensionless by normalising with respect to the corresponding mean. Only the sample mean is in arbitrary units.*

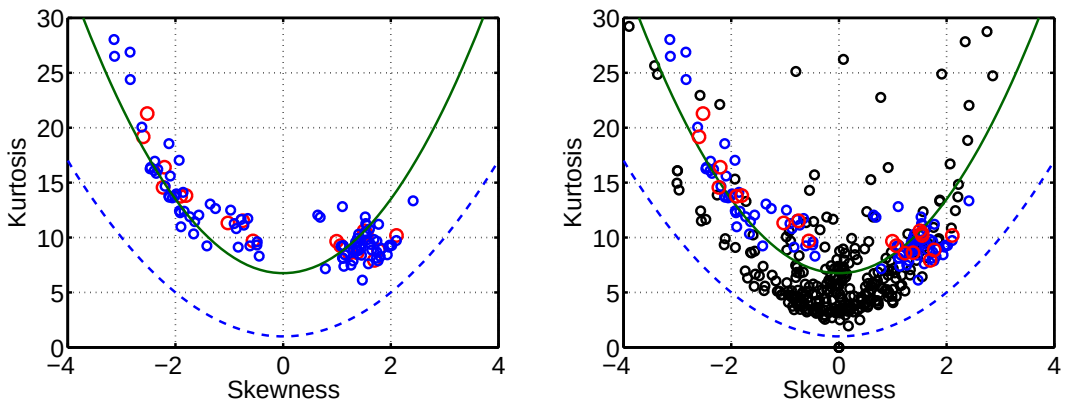

(a) (b)

Figure 6.7: *(a)Skewness/kurtosis relation with both data points from each dataset separately (blue), and grouped according to position (red). The green curve is the fitted curve, and the blue curve is the curve corresponding to a two level model. (b) The same relation but including data from datasets of argon plasma (black), also recorded in an experiment conducted using Blaamann. The green curve is the fitted curve based on the original data from the helium plasma experiment, and the blue dashed curve corresponds to the two level model, and is the absolute theoretical minimum of any data point. The black point in* $(0, 0)$ *is a remnant from missing data sets, and can be disregarded.*

6.3.1 Skewness/kurtosis relation for plasma flux

In investigating the relation between skewness and kurtosis for the flux, both the original data from this particular experiment was used, supplemented by data from another experiment conducted using Blaamann, but with argon plasma rather than helium. The experimental set-up for the argon experiment was somewhat different. About half the data was recorded with a low gas pressure (1.0×10^{-4} mbar, which is half of what we had for the helium plasma), and the rest with high pressure (1.0×10^{-3} mbar). In addition, measurements were made for several different values of the toroidal field current, which ranged from 100 A up to 600 A. 23 datasets exist for each configuration, with probes positioned similarly to what was done in the helium experiment.

The results using only our original data is shown in Figure 6.7a), where both the skewness and kurtosis of each individual set is included (marked as blue circles), as well as the resulting moments found when combining the individual sets into one large set for each radial position (red circles). As indicated in Section 5.2.1, we might expect to see some relation between the skewness and the kurtosis resembling

a parabola. Looking at the figure, we see clear evidence of such a relation.

Both the points corresponding to one individual set, and the ones which are the average of the results from each radial position are close to or on the same parabola. The green line is a curve fitted according to the data points and set to be on the form $\mathscr{K} = A\mathscr{S}^2 + B$. The mathematical expression for this curve is

$$\mathscr{K} = 1.685\mathscr{S}^2 + 6.753$$

The dotted blue line is the theoretical line for the perfect two-level model, i.e. $\mathscr{K} = \mathscr{S}^2 + 1$. As expected, all data points are above this line.

Looking at the skewness kurtosis relation for all the data available, including the data from the argon plasma experiments, shown in Figure 6.7b), we see that there is also here a clear parabolic relation. However, the data from the argon plasma do not follow the same parabola as the data from the helium plasma, i.e. different values for the constants A and B in $\mathscr{K} = A\mathscr{S}^2 + B$. The argon data also has several points that do not follow any clear parabola, but instead appear to be scattered anywhere within the area above the characteristic parabolic shape that most of the rest of the data follow.

We believe that the seemingly robust skewness-kurtosis relations of the form $\mathscr{K} = A\mathscr{S}^2 + B$ can be adequately explained by a model as the one outlined in Section 5.2.1 and the change in numerical coefficients is caused by a change in shape of the basic flux-structures when we change the filling gas from helium to argon.

Note that a Gaussian random process reduces to one point $(\mathscr{S}, \mathscr{K}) = (0, 3)$ in the representation of Figures 6.7a) and b).

One model obtained for correlated joint Gaussian distributions of fluctuating densities and velocities Carreras et al. (1996) implies a skewness-kurtosis relation for the fluctuating plasma fluxes which can also be tested with our data. Those results predict $|\mathscr{S}| \leq 2\sqrt{2} \approx 2.8$ and $9 \leq \mathscr{K} \leq 15$, again with a parabolic relation like $\mathscr{K} \approx 9 + (3/4)\mathscr{S}^2$. Although it is not an optimal fit, it turns out that this result is at least within the uncertainty for the helium data, but it is completely off for argon.

We also investigated the possibility of a relation between the probe position, and where along the parabola a data point from a given probe might be situated. However, this did not yield any satisfactory results, as there did not appear to be any link between probe position and corresponding skewness/kurtosis relation.

6.3.2 Skewness/variance relation for plasma flux

A theoretical relationship between normalised variance and skewness was briefly mentioned in Section 5.2.1. This has also been investigated, though the results

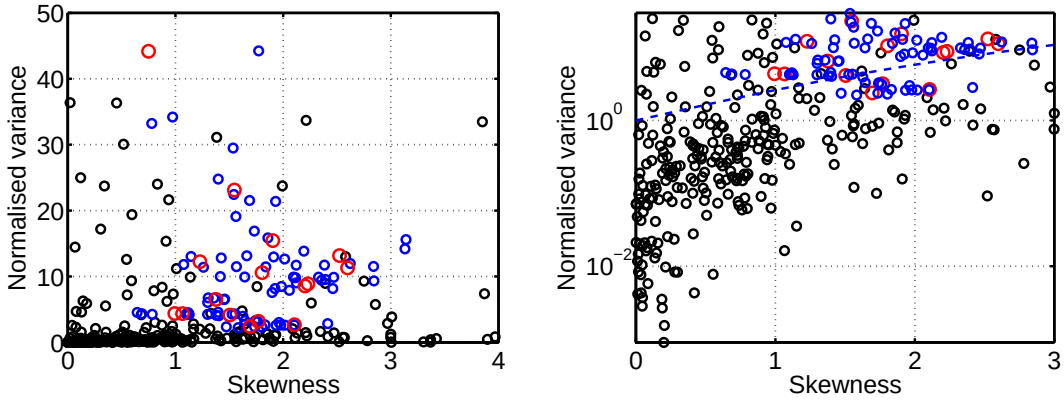

(a) (b)

Figure 6.8: *(a) Skewness/variance relation with data points from each original dataset separately (blue), grouped according to position (red), and from datasets of argon plasma (black). (b) This shows a close up including a theoretical curve for the skewness/variance relation, and with logarithmic y-axis. The dashed theoretical curve is given as* $\sigma^2/\langle\Gamma\rangle^2 = \frac{1}{2}\left(2 + \mathscr{S}^2 + \mathscr{S}\sqrt{4+\mathscr{S}^2}\right)$*, as appropriate for the two level model given by (5.8).*

were less successful than for the skewness/kurtosis relation. The result for both data from my own experiment as well as from those conducted with argon plasma are shown in Figure 6.8. Rather than plotting the skewness found for each set, the absolute value of the skewness has been used. The information gained in this analysis is the same. The only reason it was not done in the previous section is for the sake of completeness. Keeping the sign shows the parabolic shape more clearly, whereas in this case, there is no need for the sign for the skewness.

The results of this particular analysis show little signs of a systematic relation between skewness and variance. Even when zooming in on the smaller values for the variance, as shown in Figure 6.8b) there is no clear correspondence between the theoretical mathematical expression and the actual results. It is useful to keep in mind here that in the case with the skewness/kurtosis relation the theoretical curve $\mathscr{K} = \mathscr{S}^2 + 1$ is an absolute minimum. Values below this line would be impossible. The theoretical line for the skewness/variance relation is merely the corresponding relation for a two-level model. There is no limit on the range of the variance for a general probability distribution, and thus we might obtain values both below and above this line. For a Gaussian random process we find $\mathscr{S} = 0$ and $\sigma^2/\langle\Gamma\rangle^2 \in \{0, \infty\}$.

6.4 Correlation functions

The correlation functions of the various variables would give an indication of the presence of coherent structures. Any large correlation indicates the existence of a structure of some coherence, either in time or in space, and in some cases both.

6.4.1 Autocorrelation functions and power spectra

The autocorrelation functions for density, velocity and flux are presented in Figure 6.9. Here we see that there is a clear periodicity in both density and velocity, though with less correlated regions near the centre. It also appears as though the density is more correlated for $x < 0$, while velocity is most correlated for $x > 0$. They seem to be fluctuating with the same frequency, which is confirmed by the power spectra shown in Figure 6.10. Both have clear peaks for a frequency of about 10 kHz, which is very close to the estimated rotation frequency discussed in Section 4.3. Generally, both velocity and density have peaks for slightly lower frequencies for $x > 0$ than for $x < 0$, though the difference is only of about ~ 1 kHz.

Looking at the autocorrelation of the flux signal there appears to be more fluctuations, but with much lower correlation. Since the flux signal is the product of the density and the velocity we would expect to see at least a second order harmonic oscillation, and possibly also higher order harmonics as well. Turning to the power spectrum of the flux shown in Figure 6.9c) we see in addition to the peak near 10 kHz also significant peaks around 20 kHz. There are also some signs of a third harmonic for positions $7-9$cm. As indicated by both the autocorrelation function and the power spectrum of the flux, this signal appears to be more complex than the velocity and density signals.

A model consistent with the results in Figure 6.9 assumes that the fluctuating density as well as electric field component have a large amplitude part with a very short correlation time, superimposed on an oscillating part with smaller amplitude. This corresponds to the background plasma rotating, combined with the brief occurrence of coherent structures. The two parts seem independent. This argument will in principle apply to all x-positions.

6.4.2 Cross correlation

We investigated the cross correlation of the reference probe signal with signals along the x-axis for floating potential, density, velocity and flux. The results are presented in Figure 6.11. In all cases we see a correlation for both positive and negative positions, with somewhat more chaos near the central positions. Neither

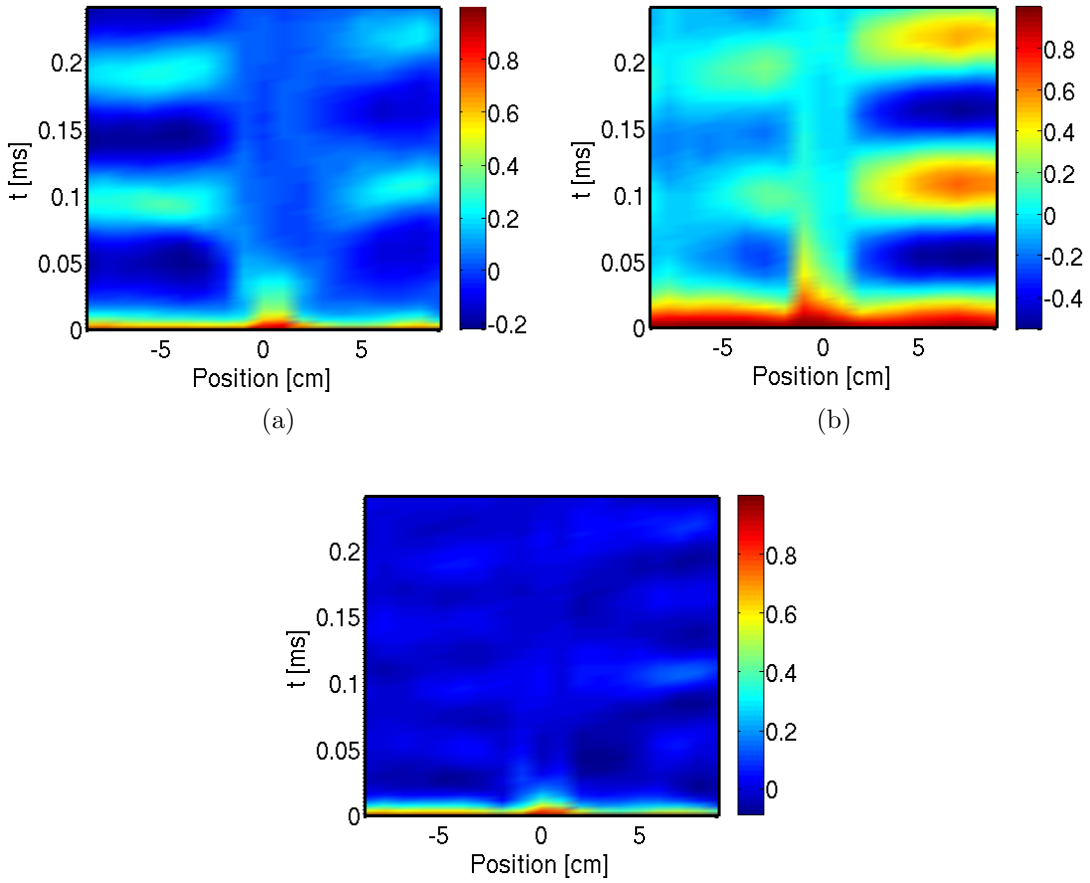

(a) (b) (c)

Figure 6.9: *Autocorrelation functions for density (a), velocity (b), and flux (c) for each position within a time interval of* $[0, 0.25]$ *ms. Only positive values of* t *are included as the autocorrelation function is perfectly symmetric around* $t = 0$ *by definition.*

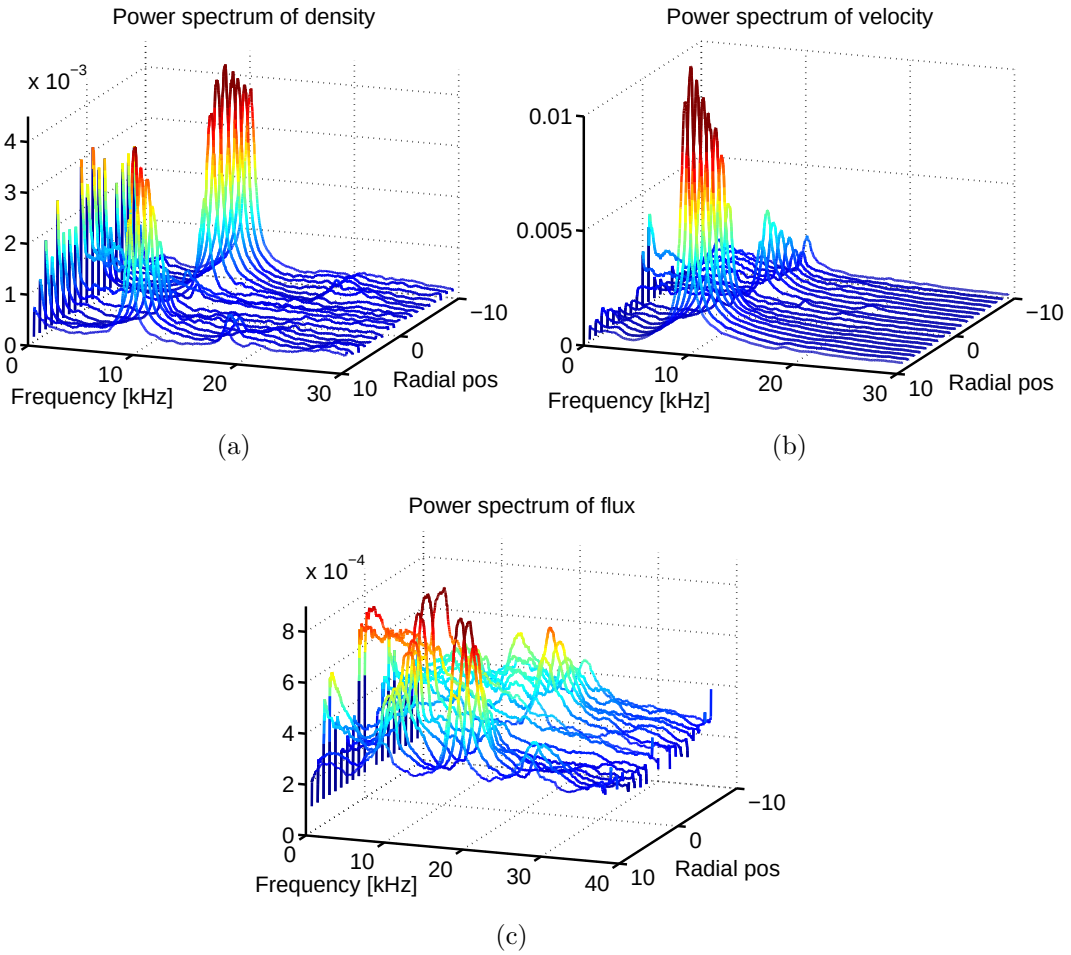

Figure 6.10: *Power spectra for density (a), velocity (b), and flux (c) for each position. A smoothing algorithm has been applied in order to make the plots more clear and easier to interpret.*

of the correlation functions are symmetric about $\tau = 0$, but they display some similarities between positive and negative τ.

For both floating potential and velocity we see that there is a periodically strong correlation, especially for $x > 1$ cm. There is indication of structures that are well correlated in space, as we see clear elongated shapes on both sides of the centre line. These structures are not as well correlated in time, but they occur periodically, which is consistent with a rotation around the centre of the poloidal cross section. Similarly for density we have clear spatially elongated shapes, though here the correlation is strongest for $x < 0$ cm.

In the density correlation function the structure is also tilted somewhat, which indicates that the structure passes different positions at different times, arriving first at the positions closest to the centre, and later at the more extreme positions. It may seem like we have a density enhancement which is "banana-shaped" and rotating around in the poloidal cross section along with the background plasma.

The flux signal is more chaotic, but also here there is a sign of periodic motion. The correlation is stronger for $x > 0$, but there seems to be better spatial correlation for $x < 0$. This may indicate that structures are somewhat deformed over the course of one rotation. Notice that the correlation is never greater than 0.2, thus the flux signal is not as closely correlated with the signal from the reference probe as the density or the velocity signals are.

We assume that the bulk plasma is moving with a nearly constant $\mathbf{E} \times \mathbf{B}/B^2$-velocity for any given radial position r, and also that any coherent structures are transported along with the bulk plasma. This means that any time axis within the graphic display of cross correlation can be said to represent a distance travelled around the poloidal cross section, i.e. $distance \sim time$. Therefore we can depict the cross correlation in a more instructive manner, namely in a circular plot showing how the structure is moving around the centre of the poloidal cross section, rather than how it develops in time as seen by the probes as it passes by. However, there must be two plots for every cross correlation function, since we have data measured in both positive and negative positions, i.e. on both sides of the centre of the circular field. Because of the circular motion of the plasma around the centre, the plot of data from $x < 0$ will correspond to the same structures seen for $x > 0$, only half a revolution later. Thus we have to some extent the opportunity to study both spatial and temporal evolution of coherent structures. It would be inconvenient to combine the plots for $x > 0$ and $x < 0$ into one. Plotting the data from the positive positions, the time $\tau = 0$ will be along the corresponding positions of the measuring probes, with the time axis in the counter-clockwise direction, indicating that any part of a structure found within positive τ is a part that has not yet passed the probe, while anything on negative τ has already passed, and has moved further along with the background velocity. For this to be

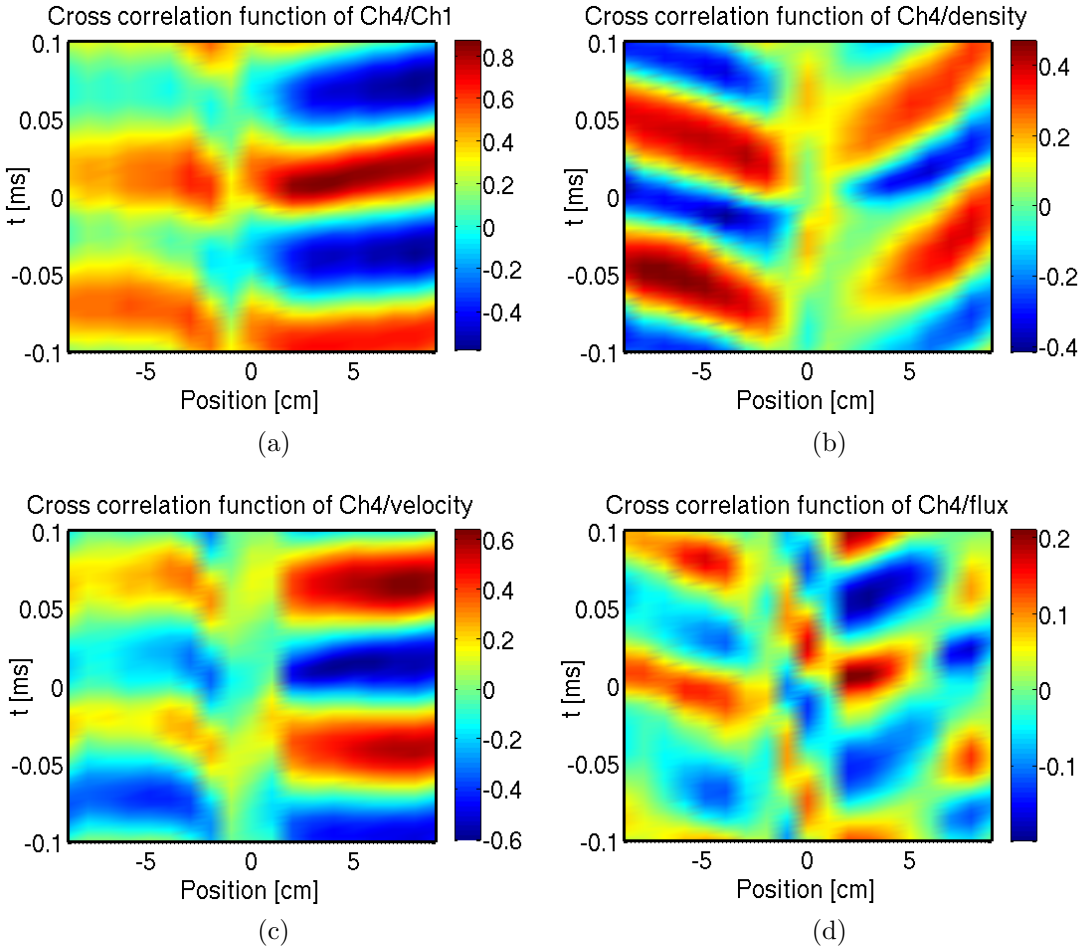

Figure 6.11: *Cross correlation functions between the reference probe (Channel 4) and (a) Channel 1, i.e. one of the probes measuring floating potential, (b) density, (c) velocity and (d) flux for each position within an interval of ±0.1 ms.*

instructive, the time interval needs to correspond to the period of the structures seen in Figure 6.11, which is ~ 100 μs.

The resulting plots are shown in Figure 6.12. Especially in the plots showing density and flux it is clear that we get elongated "banana-shaped" structures that are transported around while also moving outwards, transporting flux towards the wall of the tank. The structures are stretched out and slightly deformed by the circular motion of the background plasma. Looking at the the plots of the flux correlation function (Fig. 6.12(g) and (h)) for $x > 0$, and then for $x < 0$ it appears as though the coherent structure has moved half a revolution around the centre. The structure is also somewhat deformed, having spread out over a larger area, reducing its intensity. The elongated and somewhat less intense structure we see near the outer edge has disappeared. It may have moved beyond the reach of the probes, or it has dissolved. We see the same tendency for the density, where the structure also appears to have spread out somewhat over the course of one half of a revolution, but without any loss in correlation. The velocity is noticeably less correlated after half a revolution.

6.5 Conditional sampling

By using conditional sampling, the average response to a spike in the reference signal can be studied. As with the cross correlation functions, we have chosen to depict this as circular plots as this better illustrates how the resultant structures move around the poloidal cross section. The middle of the interval is placed at the position corresponding to where the data where collected. The notation $x \gtrless 0$ indicates whether that data is collected by the probes on the positive or negative side of the centre of the cross section. The time interval is 104μs corresponding to one rotation period of the plasma column.

Due to the additional conditions used to collect these samples, it is worth noting that when we are looking at an outward burst, i.e. positive flux, we have either a combination of a) $n < 0$ and $u < 0$, or b) $n > 0$ and $u > 0$, given that we are on the low field side ($x > 0$). However, the equivalent conditions that give outward bursts for on the high field side ($x < 0$) is negative flux with individual components a) $n < 0$ and $u > 0$ or b) $n > 0$ and $u < 0$. This is because outward bursts have a velocity in the opposite direction for $x < 0$ compared to $x > 0$, given our chosen local coordinate system.

6.5.1 Outward bursts

As the average flux according the the PDF and moments of the flux distribution is out of the plasma, we begin by investigating outward bursts, i.e. transport of

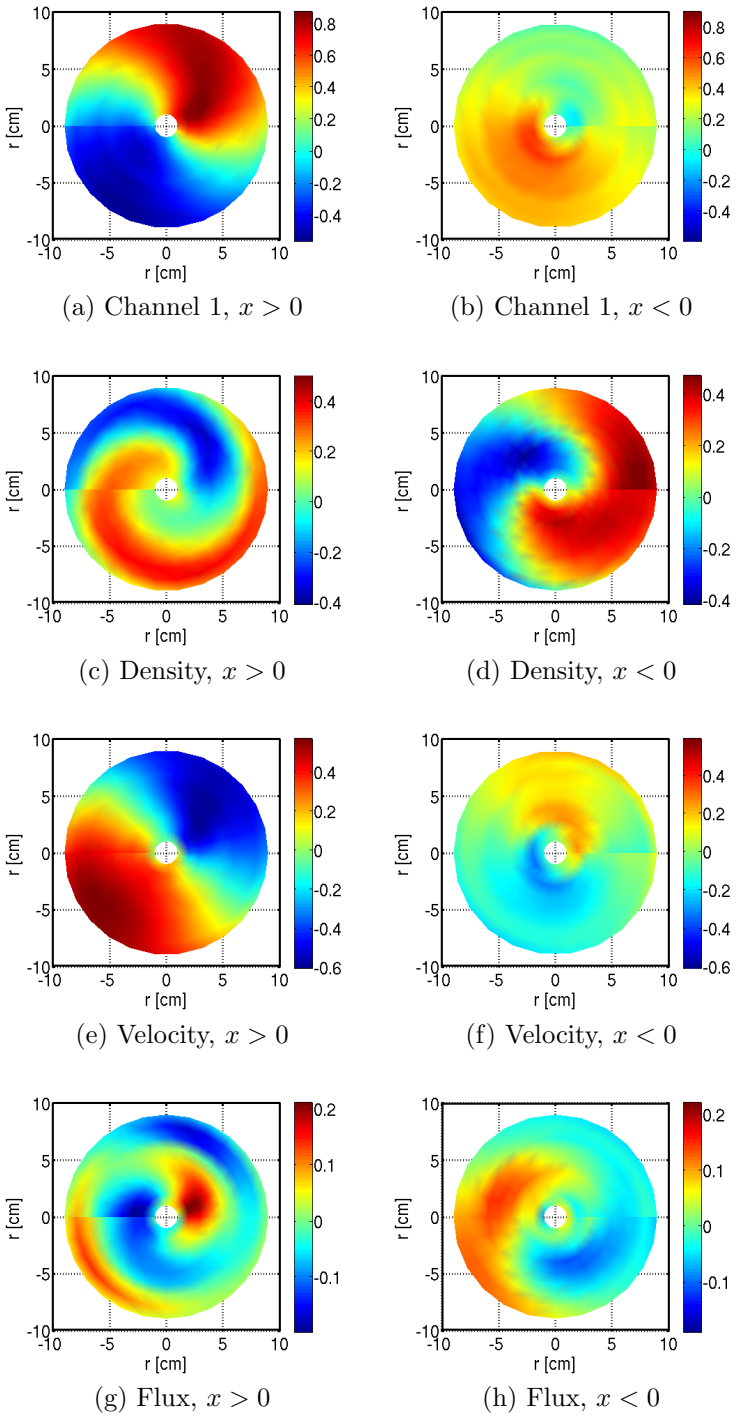

(a) Channel 1, $x > 0$ (b) Channel 1, $x < 0$

(c) Density, $x > 0$ (d) Density, $x < 0$

(e) Velocity, $x > 0$ (f) Velocity, $x < 0$

(g) Flux, $x > 0$ (h) Flux, $x < 0$

Figure 6.12: *Circular presentation of the cross correlation between the reference signal $d\phi/dt$ and floating potential, density, velocity and flux, respectively, for both positive, $x > 0$, and negative, $x < 0$, probe positions.*

plasma out towards the wall of the tank.

The results for several different values of the condition C are shown in Figure 6.13. The secondary conditions are given in the individual captions and are equivalent to density depletions moving inwards.

- $x > 0$
  With $C \geq 0.25\sigma$, where σ is the standard deviation of the reference signal $d\phi/dt$, we see in (a) that the response is mostly dominated by random motion. Too little has been filtered out with such a low condition on the reference signal, so there is only a vague sign of a positive structure standing out from the background plasma in (a). Increasing the condition to $C \geq 0.5\sigma$ gives slightly higher flux for a small area as seen in (c), but else there is little improvement. The resulting response is most likely too noisy. What we see is a slight structure standing out from the background near the positive y-axis. There is also an elongated narrower structure, like a flux channel, oriented almost directly along the positive x-axis.

  Setting $C \geq 1.0\sigma$ we can now clearly see a shape standing out from the background in (e) situated near the positive y-axis, but tilted slightly in the positive x-direction too. This positive flux structure is also somewhat more visible, and increases in size and magnitude along with the condition C, as can be seen in (e), where $C \geq 1.0\sigma$ and (g), where $C \geq 1.5\sigma$. The average maximum flux in (g) is over $800\mathrm{m}^{-3}\mathrm{s}^{-1}$.

  Generally for positive x we have for all conditions C that there is some positive flux of less magnitude (~ 300 $\mathrm{m}^{-3}\mathrm{s}^{-1}$) present all around the cross section especially around the area close to the negative y-axis. This may be an indication that there are several structures present here, but that these others are smaller in magnitude.

  Increasing the condition further to $C \geq 2.0\sigma$, gives much the same results as for $C \geq 1.5\sigma$, only with a somewhat more chaotic motion going on around the larger structure.

- $x < 0$
  Like for $x > 0$ we see in (b) that when $C \geq 0.25\sigma$, there is little sign of any coherent structures standing out from the background, as the condition is set too low. Setting $C \geq 0.5\sigma$ we see a negative structure that appears to be on the opposite side of the cross section from the narrow flow channel seen for $x > 0$. The larger positive structure near the positive y-axis for $x > 0$ does not appear to have an equivalent negative structure for $x < 0$, and has thus been damped.

  In (f), where we have $C \geq 1.0\sigma$, the negative flux structure seen in plots (b) and (d) has increased somewhat in size and also magnitude. This structure

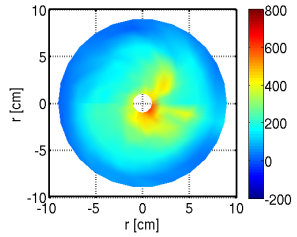

(a) $x > 0$, $C \geq 0.25\sigma$, $\Gamma > 0$, $u < 0$

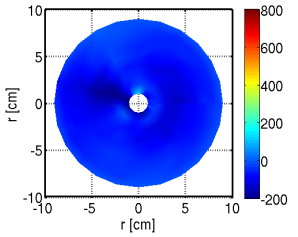

(b) $x < 0$, $C \geq 0.25\sigma$, $\Gamma < 0$, $u > 0$

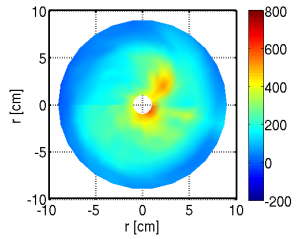

(c) $x > 0$, $C \geq 0.5\sigma$, $\Gamma > 0$, $u < 0$

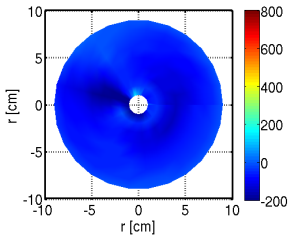

(d) $x < 0$, $C \geq 0.5\sigma$, $\Gamma < 0$, $u > 0$

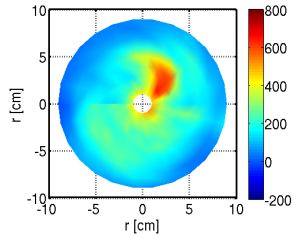

(e) $x > 0$, $C \geq 1.0\sigma$, $\Gamma > 0$, $u < 0$

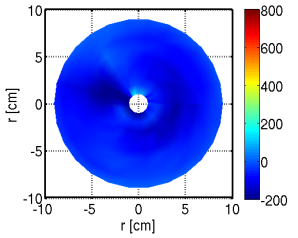

(f) $x < 0$, $C \geq 1.0\sigma$, $\Gamma < 0$, $u > 0$

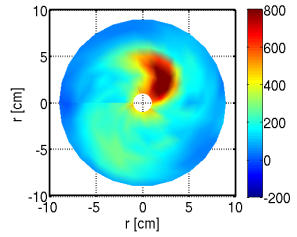

(g) $x > 0$, $C \geq 1.5\sigma$, $\Gamma > 0$, $u < 0$

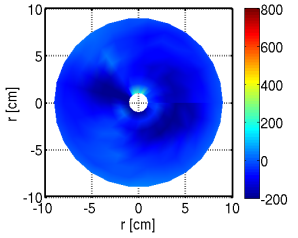

(h) $x < 0$, $C \geq 1.5\sigma$, $\Gamma < 0$, $u > 0$

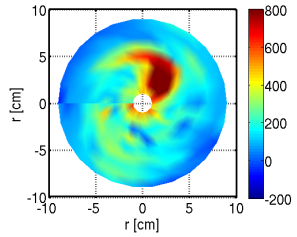

(i) $x > 0$, $C \geq 2.0\sigma$, $\Gamma > 0$, $u < 0$

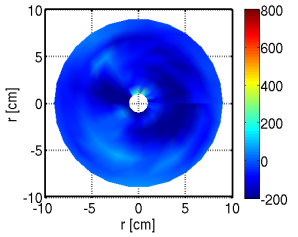

(j) $x < 0$, $C \geq 2.0\sigma$, $\Gamma < 0$, $u > 0$

Figure 6.13: *Conditionally sampled flux for outward burst in the shape of density depletions moving inwards. The reference signal is $d\phi/dt$, and the unit on the colour axis is $m^{-2}s^{-1}$.*

Table 6.1: Table over average number of events per position for each of the conditional samplings. The number of events for each position have been counted, and then used to find an average for $x > 0$ and for $x < 0$.

	$\Gamma > 0$				$\Gamma < 0$			
	$u < 0$		$u > 0$		$u < 0$		$u > 0$	
Condition	$x > 0$	$x < 0$	$x > 0$	$x < 0$	$x > 0$	$x < 0$	$x > 0$	$x < 0$
0.25σ	785	599	1126	627	459	702	781	965
0.5σ	709	594	1111	595	403	659	753	938
1.0σ	466	461	964	419	249	485	629	754
1.5σ	213	255	631	180	111	253	376	405
2.0σ	69	85	265	42	35	81	143	125
2.5σ	20	19	73	10	11	20	38	26

appears to be located near the negative x-axis, indicating that it really is corresponding to the faint narrow structure we see for $x > 0$ along the positive x-axis. In addition, for $x < 0$ we see a weak negative flux structure on the opposite side of the cross section, i.e. near the positive x-axis. This negative structure is more visible when increasing the condition further to $C \geq 1.5\sigma$, as seen in (h). As we saw for $x > 0$ we had a very prominent positive flux structure for $C \geq 1.5\sigma$. However, after half a revolution it has been damped so much it is nearly undetectable. In the corresponding position for $x < 0$ there is some sign of a faint positive flux structure, i.e. plasma transported inwards.

Generally for $x < 0$ we have very little flux compared to $x > 0$. For positive probe positions there are both more prominent coherent structures, but also more significant flux within the entire cross section, whereas for negative probe positions we have very little flux in general, and even the coherent structures we see are rather faint in comparison.

Table 6.1 presents the average number of sampled events per position for each combination of conditions for both $x > 0$ and $x < 0$. Looking at the data in Table 6.1 column 2 and 9 we see here that for positive flux and negative velocities we have quite few events, and so the data that is used to generate the plot shown in Figure 6.13(i) and (j) is not quite sufficient to give good results. If we were to increase the primary condition further, the results would not be good, nor would they offer anything conclusive. One such case is shown in Figure 6.14. Here we see that there are too few events to even out smaller spikes present in some events but

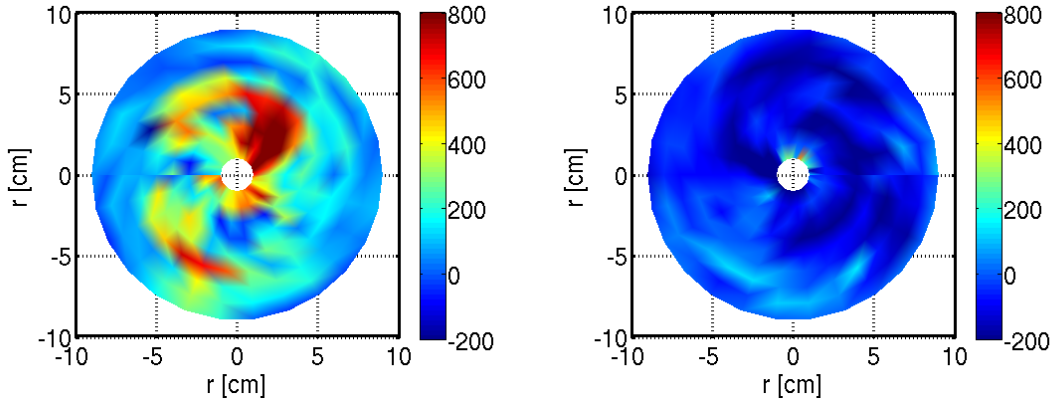

(a) $x > 0$, $\Gamma > 0$, $u < 0$ (b) $x < 0$, $\Gamma < 0$, $u > 0$

Figure 6.14: *Conditionally sampled flux with a large value for the condition, for density depletions moving outwards. Here the number of samples is too small for reliable statistics.*

not in others, causing the response to look chaotic. Too few events are sampled, and thus the result is not statistically significant.

Figure 6.15 shows the results for conditional sampling of density depletions moving inwards with a condition on the $d\phi/dt$ signal of $C \geq 1.5\sigma$, but with automatically scaled colour axis. Not that the innermost data has been excluded from Figure 6.15b) as the flux was very large here, making the colour axis less instructive. In addition the data from the innermost positions is strongly dominated by large fluctuations caused by the filament, thus offering little information on the transport of coherent structures. Now we see the full interval of the oscillations shown for both negative and positive probe positions. For $x > 0$ there is little change. The fluctuations are typically between 0 and ~ 850 $\mathrm{m^{-2}s^{-1}}$, as opposed to the set limits in Figure 6.13 of $[-200, 800]$. For $x < 0$ we have a more interesting image of the structures present, as they are now much more visible. We see the negative flux structures much more clearly. In addition we see that the positive flux structure present in $x > 0$ has been reduced from ~ 800 $\mathrm{m^{-2}s^{-1}}$ at the most to ~ 50 $\mathrm{m^{-2}s^{-1}}$. There is however, some negative structure trailing further behind situated between the negative y-axis and the positive x-axis. This may be some remnant of the original structure, that has been slowed down for some reason. The faint and less structured flux we see all throughout the cross section for $x > 0$ is now also visible for $x < 0$, though it is smaller in magnitude.

Investigating the presence of larger flux events, we have counted the number of times the conditionally sampled flux signal reached a greater value than some fixed number, and also for how long the signal remained at a level higher than

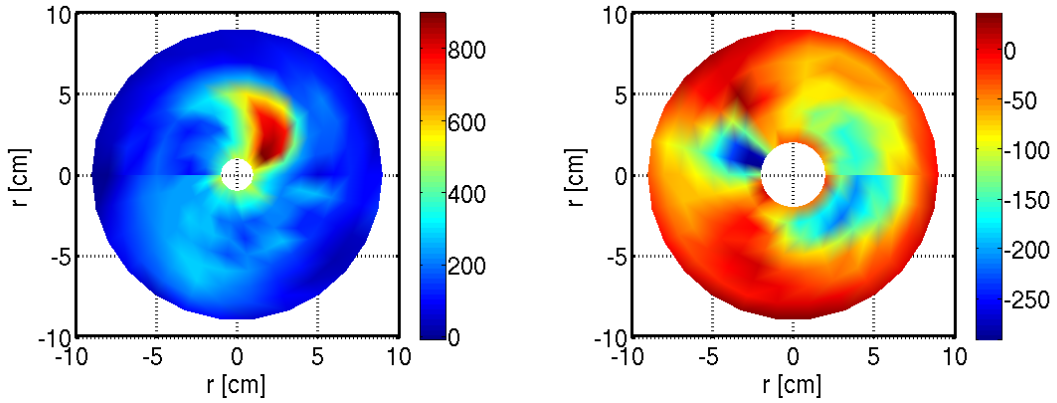

(a) $x > 0$, $\Gamma > 0$, $u < 0$ (b) $x < 0$, $\Gamma < 0$, $u > 0$

Figure 6.15: *Conditionally sampled flux with condition $C \geq 1.5\sigma$ on the reference signal $d\phi/dt$. Here we have used autoscale, in order to show the total interval of the oscillations for both positive and negative positions. The innermost positions are removed for $x < 0$ as the fluctuations here were very large, but offer little information, thus only contribute to hiding the structures of a smaller magnitude present in the data.*

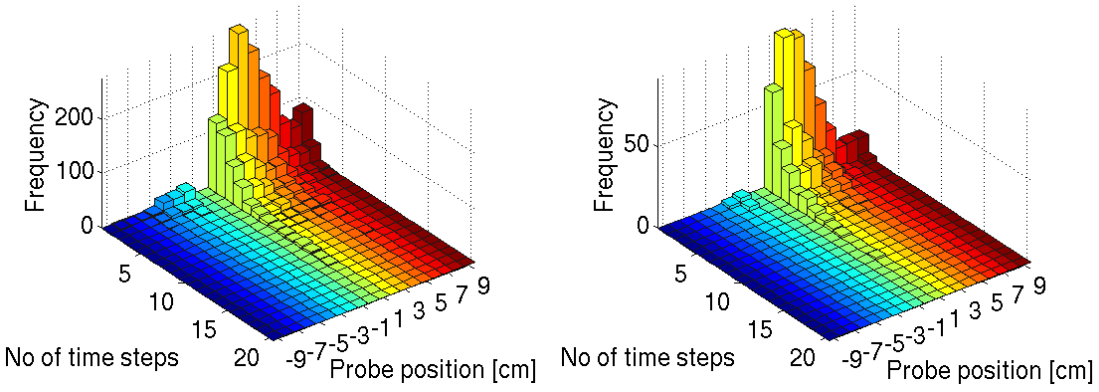

(a) (b)

Figure 6.16: *Distribution of duration of flux bursts for each position for the conditionally sampled flux. Events have been selected for two different threshold levels. In (a) we have chosen a low threshold, and in (b) a high threshold for sampling. The results from the two central positions 0 cm and −1 cm have been excluded due to the great level of disturbance caused by the filament in this area. The primary condition for the original signal was $C \geq 1.5\sigma$. No additional conditions were set.*

this threshold. This was done for each position, summing up the number of events for all sets combined. This is presented in Figure 6.16, where the result for two different values for the threshold were used. As we might expect from the PDFs of the flux, there are more large events for positions close to the filament. These events are also most often rather short, with the largest column representing the case where the event only lasted for one time step, i.e. ~ 4 μs. In Figure 6.16a) we have used a rather small value for the threshold. Increasing it reduces the number of flux spikes, as expected (see Figure 6.16b)). By increasing the threshold by a factor ~ 2, we reduce the number of events by a factor $\sim 2-3$. However, the shape of the distribution is nearly the same in both cases. We also observe a slight shift in which position gives the maximum amount of events, from $x = 3$ cm for a low threshold value, to $x = 2$ cm for a higher threshold value.

Generally we see many more events for $x > 0$ than for $x < 0$, and the few events we do have for $x < 0$ are also shorter. The fact that we have more large flux events for positive probe positions indicates that we have less large flux bursts for $x < 0$. However, the difference in number of events is too large to be accounted for by the simple fact that we have slightly different PDFs for $x < 0$ compared to $x > 0$. Keeping in mind that we had better correlation between the reference signal and data from $x > 0$ than for data from $x < 0$, it seems likely that though there are large bursts for $x < 0$, these are not picked up in the conditional sampling. The large flux burst for $x < 0$ are not sufficiently correlated with the reference signal, and are thus not occurring within the time intervals which are sampled, and therefore we get this very skewed distribution of events and event duration. Note that the two middle positions $x = 0$ cm and $x = -1$ cm are excluded from the figure, as they are dominated by the large fluctuations caused by the filament being so near, and thus the data from these two positions offer little additional insight in this particular investigation.

In Figure 6.17 the equivalent results for density enhancements moving outwards are presented. The results are similar to the ones found when investigating density depletions, but the resulting response in flux is smaller, and there appears to be a flow channel outwards for $x > 0$ at the opposite side to a corresponding negative channel seen for $x < 0$. Though we saw signs of this when investigating the density depletions shown in Figure 6.13 as well, it was mostly averaged out once C was set to values greater than 1.0σ, whereas for density enhancements it is present for all C. In addition there is a negative flux structure for $x < 0$, located in the same area where negative flux was found when investigating density depletions. A minor positive flux structure appears for larger values of C for $x < 0$, indicating inward transport. Looking at the number of events for these data, it is evident that there are more burst that satisfy the conditions corresponding to those presented in Figure 6.17 than the ones presented in Figure 6.13. However, the numerical

value of the flux is generally greater for density depletions propagating inwards.

As mentioned in Section 5.4 we used a reference signal that is the time derivative of the data from the reference probe, as this can be considered to be equivalent to an electric field signal, which would be better related to the flux than a floating potential signal. In Figure 6.18 is the resulting conditional average with the original signal from the reference probe as a reference signal, with $C \geq 1.5\sigma$ as condition for the reference probe signal, looking at density enhancements propagating outwards. Here we see less sign of coherent structures than we do in the corresponding plots presented in Figure 6.17(g) and (h). We do not have the same clear enhancement standing out from the background, like we did with $d\phi/dt$ as a reference, nor do we see the narrow flow channel as clearly. The resulting flux is also even lower than the flux found using the time derivative of the reference probe. We also seem to find negative flux structures for $x < 0$ in different areas of the cross section, compared to what we found using $d\phi/dt$ as a reference signal.

6.5.2 Inward transport

Although the net average transport is *out* of the plasma column, we nevertheless find occasional inward transport as well, see for instance the flux PDF in Figure 6.2d). We can study such events as well using the conditional averaging technique, by changing the additional conditions to correspond to either density depletions moving outwards or enhancements moving inwards.

Figure 6.19 shows the results of conditional sampling and averaging with conditions corresponding to inward transport. For simplicity only a few different values of the main condition C are included here. However, what is interesting here is that we find a flow channel of negative flux for both $u < 0$ and $u > 0$, corresponding to density enhancements flowing inwards and density depletions flowing outwards (for $x > 0$). This channel of negative flux is slightly stronger in magnitude for $u < 0$, but the channel is wider for $u > 0$. In addition we also have the coherent structure of positive flux flowing around along with the bulk plasma. For $x < 0$ we see clear signs of a corresponding positive flux channel at opposite sides to the negative channel seen for $x > 0$, though this structure appears to be stronger for $u < 0$ than $u > 0$, indicating greater magnitude for density depletions moving outwards. In addition we also see a faint negative structure that appears to correspond to the positive structure visible for $x > 0$. Inward transport is rather unexpected as it goes against what might be expected due to turbulent diffusion or blob transport.

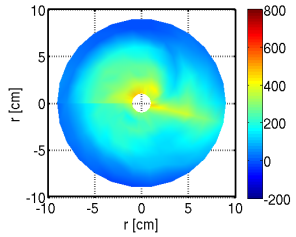

(a) $x > 0$, $C \geq 0.25\sigma$, $\Gamma > 0$, $u > 0$

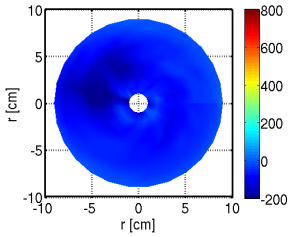

(b) $x < 0$, $C \geq 0.25\sigma$, $\Gamma < 0$, $u < 0$

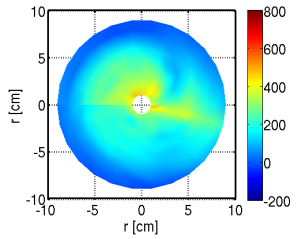

(c) $x > 0$, $C \geq 0.5\sigma$, $\Gamma > 0$, $u > 0$

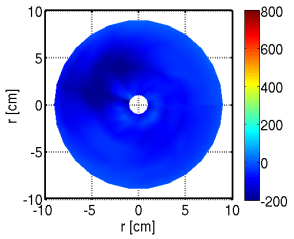

(d) $x < 0$, $C \geq 0.5\sigma$, $\Gamma < 0$, $u < 0$

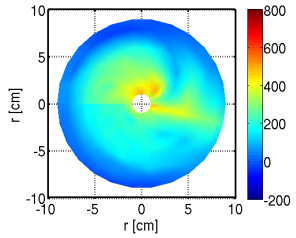

(e) $x > 0$, $C \geq 1.0\sigma$, $\Gamma > 0$, $u > 0$

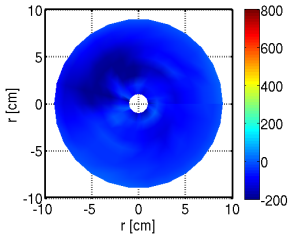

(f) $x < 0$, $C \geq 1.0\sigma$, $\Gamma < 0$, $u < 0$

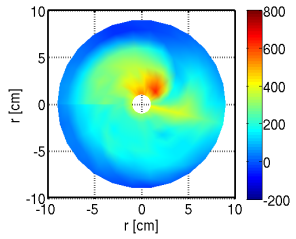

(g) $x > 0$, $C \geq 1.5\sigma$, $\Gamma > 0$, $u > 0$

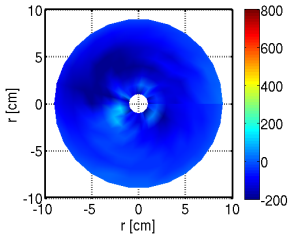

(h) $x < 0$, $C \geq 1.5\sigma$, $\Gamma < 0$, $u < 0$

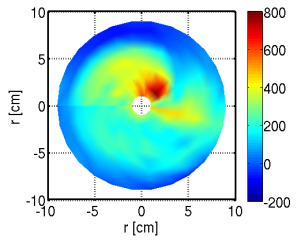

(i) $x > 0$, $C \geq 2.0\sigma$, $\Gamma > 0$, $u > 0$

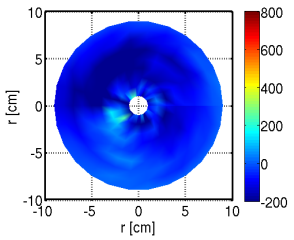

(j) $x < 0$, $C \geq 2.0\sigma$, $\Gamma < 0$, $u < 0$

Figure 6.17: *Conditionally sampled flux for outward burst in the shape of density enhancements moving outwards. The reference signal is $d\phi/dt$, and the unit on the colour axis is $m^{-2}s^{-1}$*

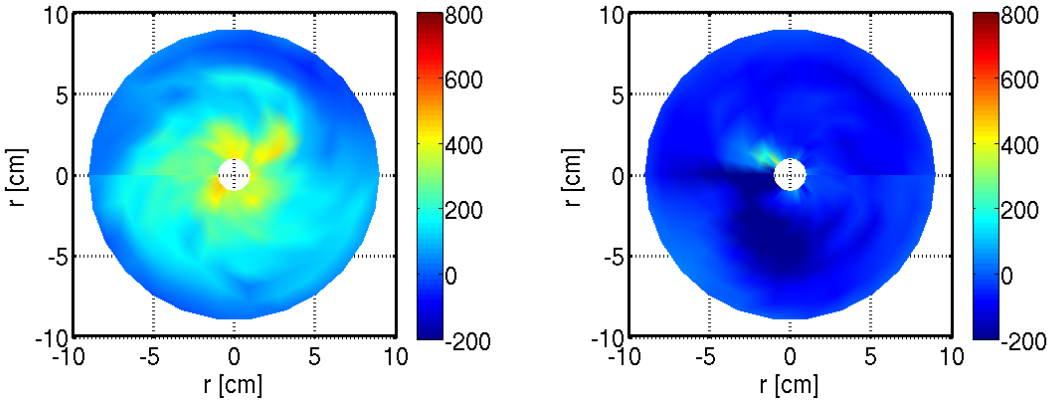

(a) $x > 0$, $C \geq 1.5\sigma$, $\Gamma > 0$, $u > 0$ (b) $x < 0$, $C \geq 1.5\sigma$, $\Gamma < 0$, $u < 0$

Figure 6.18: *Conditionally sampled flux using the original floating potential measured by the reference probe as reference signal. This signal corresponds to a positive density structure propagating outwards.*

6.5.3 Dynamics of the flux-component

We found indications that the bursts of plasma flux damps a great deal with time as the plasma column rotates. To study this feature in more detail we carry out a similar conditional average on the individual components of the flux signal, i.e. $\tilde{n}$ and $\tilde{u}$. By this study we want to find out to what extent the observed damping might be due to a "de-phasing" of the density and velocity. If the velocity and density vary with the same frequency, but are shifted out of phase with each other, the resulting flux fluctuations will decrease in magnitude.

The results for density depletions moving inwards are shown in Figure 6.20, where a) and b) show the density sample and c) and d) the velocity sample. Here we can see that for $x > 0$ the larger negative structure that can be seen in both the density sample and the velocity sample overlap almost perfectly, and we see a clear "bean-shaped" structure in both figures. There is also some positive density structure which overlaps rather well with a large positive velocity structure. The magnitude of these structures is rather small compared to the negative density and velocity structure. This is most likely what caused the smaller flux that was present in the compound signal, giving some positive flux all around the cross section, though much less distinct than the one caused by density depletions. In addition we also see a clear negative density channel in Figure 6.20a) near the positive x-axis, similar to those detected when studying outward transport of density enhancements as well as for inward transport. The conditionally sampled velocity in the same area is negative, though rather small in magnitude (~ -300

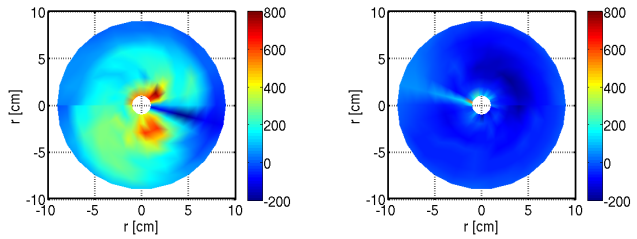

(a) $x > 0$, $C \geq 1.0\sigma$, $\Gamma < 0$, $u < 0$

(b) $x < 0$, $C \geq 1.0\sigma$, $\Gamma > 0$, $u > 0$

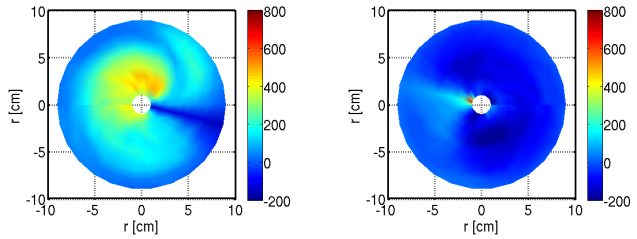

(c) $x > 0$, $C \geq 1.0\sigma$, $\Gamma < 0$, $u > 0$

(d) $x < 0$, $C \geq 1.0\sigma$, $\Gamma > 0$, $u < 0$

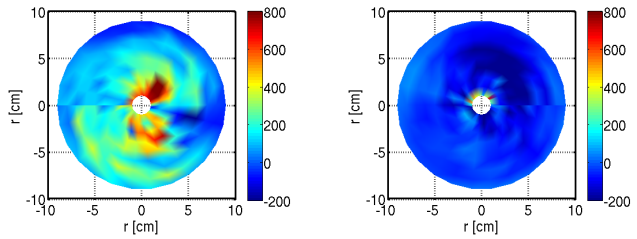

(e) $x > 0$, $C \geq 2.0\sigma$, $\Gamma < 0$, $u < 0$

(f) $x < 0$, $C \geq 2.0\sigma$, $\Gamma > 0$, $u > 0$

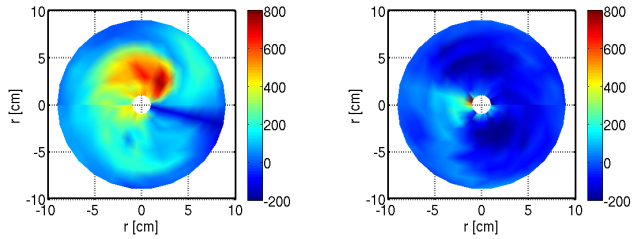

(g) $x > 0$, $C \geq 2.0\sigma$, $\Gamma < 0$, $u > 0$

(h) $x < 0$, $C \geq 2.0\sigma$, $\Gamma > 0$, $u < 0$

Figure 6.19: *Conditionally sampled flux, with additional conditions corresponding to either density enhancement propagating inwards as in a), b), e) and f), or density depletions propagating outwards shown in c), d), g) and h). The reference signal is $d\phi/dt$, and the unit on the colour axis is $m^{-2}s^{-1}$*

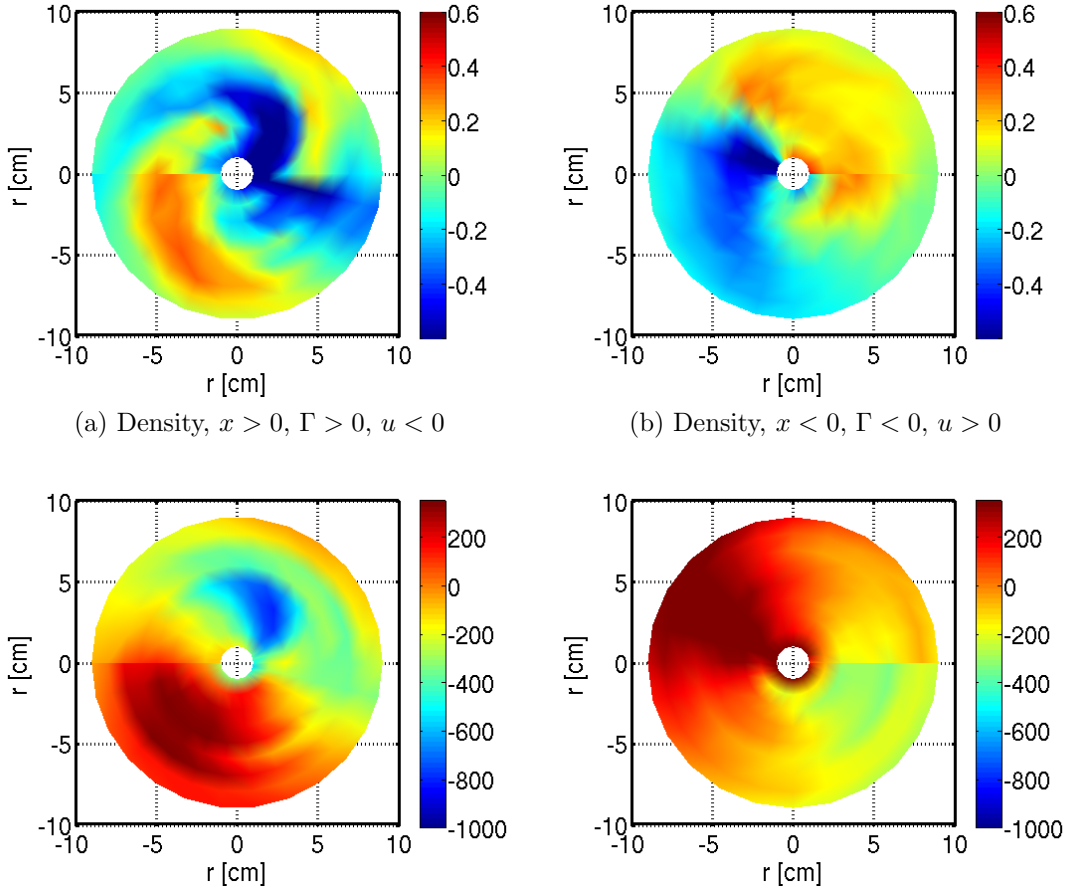

(a) Density, $x > 0$, $\Gamma > 0$, $u < 0$

(b) Density, $x < 0$, $\Gamma < 0$, $u > 0$

(c) Velocity, $x > 0$, $\Gamma > 0$, $u < 0$

(d) Velocity, $x < 0$, $\Gamma < 0$, $u > 0$

Figure 6.20: *Conditionally sampled density and velocity, with additional conditions corresponding to a density depletion propagating inwards. The condition on the reference signal* $d\phi/dt$ *was* $C \geq 1.5\sigma$.

m/s).

However, as one moves half a revolution to the negative positions, i.e. $x < 0$, we see that the density depletion we saw in a) has reduced in magnitude by a factor ~ 2. However, the negative channel that originally was near the positive x-axis, has moved around the cross section to the negative x-axis, and is still nearly equal in magnitude. The positive density structure has mostly maintained its size, though there has been some expansion causing a slight reduction in magnitude. In the velocity sample for $x < 0$ we see that the original negative velocity structure which for these positions would be a corresponding positive structure has moved somewhat further around the cross section. Near the negative y-axis, where we would now expect to find the coherent structure that is so clear and large in magnitude for $x > 0$, we have very small velocities, and the resultant flux will then be greatly reduced, as we see in Figure 6.13h). However, we have significant velocities in the area where the narrow density channel is now found. Hence this structure is what we do see in the compound signal for $x < 0$ and corresponding conditions. The velocity maximum has been reduced by a factor ~ 2 during half a revolution.

Hence it seems like much of the reason for the damping of the flux signal is that the velocity and the density develop at different rates, causing them to de-phase. This de-phasing changes which flux structure is most evident as the plasma column rotates.

6.5.4 Conditional variance

As mentioned in Chapter 5 conditional variance as defined by (5.18) is a measure of reproducibility of a signal. For low values of V_{con} we have high reproducibility and for high values of V_{con} reproducibility is low. However, it is more intuitive to interpret a plot of $C_{rep} = 1 - V_{con}$, as high values correspond to high reproducibility. Figure 6.21 shows this for a given set of conditions. We consider this one figure to be representative for all the different combinations of conditions.

Here we see that there is a fairly high level of reproducibility for the areas in which we find the coherent flux structures. This is the case for both the large rounded structure near the positive y-axis, but also for the narrow channel that we have seen in several figures previously, but which is not that prominent for these particular conditions ($C \geq 1.5\sigma$, $F > 0$ and $u < 0$). This indicates that even though this flow channel is very faint in our conditionally sampled average, it is clearly a significant part of the signal. Anywhere else in the cross section C_{rep} is nearly 0, indicating that these sections are too unpredictable. The highest level of reproducibility found is ~ 0.6.

Having $C_{rep} = 1$ is very unlikely as it means that we can reproduce our results perfectly.

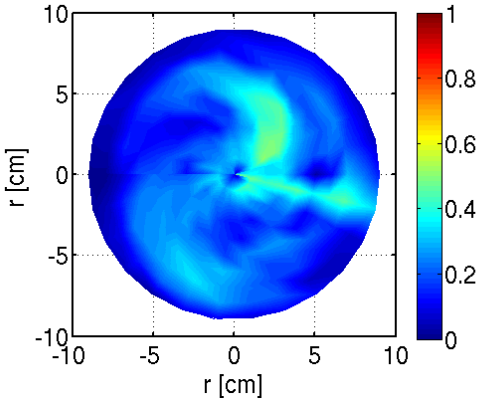

Figure 6.21: *Conditional reproducibility for $x > 0$ of a conditionally sampled flux signal. Mathematically this is $C_{rep} = 1 - V_{con}$. Conditions used are $C \geq 1.5\sigma$, $F > 0$ and $u < 0$. The reference signal was $d\phi/dt$.*

Chapter 7

Discussion and conclusion

In this chapter the results presented in Chapter 6 are discussed and interpreted, attempting to explain what our results mean. The discussion is linked to the different forms of turbulent transport outlined previously. The results are then summarised and some suggestions for future work are outlined. Note that the driving mechanism for the turbulent transport will not be addressed.

7.1 Statistical properties

The statistical properties of the data offer much insight into the average motion we see in the plasma, and are thus useful in studying the motion of the turbulent part of the plasma column as a whole. Single flux bursts are less prominent in this part of the analysis and will be discussed later.

7.1.1 General properties of the plasma fluctuations

Looking at the PDFs of velocity, density and flux it appears as though we have larger values for all variables on the low-field side. The distributions are more peaked for $x < 0$, indicating smaller flux events, corresponding with the expected lower velocities and density perturbations. It is important to keep in mind that our configuration is toroidal, and thus not symmetric around a toroidal axis. The ideal case would be to have an infinitely long cylindrical tank. However, this is impossible in the real world, although many Q-machine experiments (Motley, 1975) operate with long magnetised plasma columns. When using such experimental devices one has to deal with the additional effects caused by plasma reaching the end of the tank. The other realistic option is to use a torus, where there is no end, but where the magnetic field is curved. However, in a torus there is a significant difference between the inner side of the tank and the outer side. When the plasma

column rotates around the toroidal axis, moving from the low-field side to the high-field side, the plasma must be compressed due to conservation of mass. This is because the circumference is greater on the low field side than on the high field side, so the same amount of plasma needs to be denser in order to occupy the same area in the poloidal cross section, while being compressed in the toroidal direction.

The largest fluctuations are found near the centre of the cross section. The plasma source is located near here, and thus there is more turbulence in this area. In addition, the motion seems to be less coherent with respect to the motion of plasma located further away from the source. The plasma discharge at the filament causes much disturbance, and thus there is little sign of coherence here. The larger structures are mostly detectable for positions $|x| \geq 2\text{cm}$.

The joint PDFs of velocity and density demonstrate that there is a correlation between the sign of these to physical quantities, and that this correlation changes when moving from negative positions to positive. For $x > 0$ the correlation is positive, i.e. positive velocity tends to indicate positive density as well and vice versa, whereas for $x < 0$ it is negative. Clearly large positive flux events are favoured for $x > 0$, and here the largest flux events tend to be caused by plasma depletions moving inwards, though the most frequent events are plasma blobs moving outwards. The further away from the centre the probes are positioned, the smaller the fluctuations appear to be, and thus the joint PDF is also more limited.

7.1.2 Skewness kurtosis relations

The investigation of a possible relation between skewness and kurtosis for the flux signal gave excellent results. A clear parabolic connection can be seen similar to what was found by Labit et al. (2007), although they analysed a different signal. Not only was it evident for the particular data from this experiment, but it could also be seen for the data sampled from an argon plasma experiment, also conducted using Blaamann. However, the parabola resulting from the latter data appeared to have different coefficients A and B. This indicates that the general relation $\mathscr{K} = A\mathscr{S}^2 + B$ may well be a general property of the fluctuations in a plasma column, though that it would likely be useful to treat the different types of plasma separately.

It has previously been demonstrated that smoke columns appear to have this characteristic relation between skewness and kurtosis too (Jørgensen et al., 2010). They also found a relation between skewness and normalised variance, that we were unable to reproduce here. Given the electromagnetic nature of plasma fluctuations, it is interesting to see that at least the characteristic relation between skewness and kurtosis can be detected in plasma as well as in a neutral gas.

7.2 Coherent structures

From both the cross correlation functions and the conditional sampling and averaging it seems evident that we have coherent structures in the plasma. These structures appear to be moving around the poloidal cross section along with the clock-wise $\mathbf{E} \times \mathbf{B}/B^2$-velocity of the background plasma, as well as moving in the radial direction. The size of these structures are $\sim$ 4cm across and $\sim$ 7 cm in length. The structure appears to be elongated in the radial direction, as well as somewhat distorted by the circular motion, giving it a bean-like shape. The distribution within the structure indicates a slightly steeper edge in front than in the back, but there is little sign of the typical mushroom-shape associated with plasma blobs. The poloidal background angular velocity is fairly similar in magnitude throughout the entire plasma column, which means the background plasma rotates almost like a rigid body. The coherent structure is transported around with the background plasma, but at the same time it is propagating outwards in the radial direction, getting distorted and eventually dissolving. Typically, one such structure will propagate around the poloidal cross section in 100μs, given the period of the oscillations in the cross correlation function between the flux and the reference probe. The coherent nature of the structure is maintained for $\sim$ 1 revolution.

When we were investigating positive bursts of flux we found more events when looking for enhancements moving outwards than depletions moving inwards. However, the amplitude of the averaged events were larger for $u < 0$. This indicates that the largest flux events are caused by holes moving inwards rather than enhancements moving outwards, but that enhancements moving inwards are more common. This is consistent with the joint probability distribution of the velocity and flux shown in Figures 6.4 and 6.5. For positive positions the tail stretching towards negative u and n is longer and reaches greater numerical values for u, than the corresponding positive tail, while the peak of the distribution is slightly shifted towards combinations of positive density and velocity.

The coherent structures are mainly detected on the outer side of the torus, i.e. the low $\mathbf{B}$-field side. On this side the curvature and ∇B-drifts contribute to the motion of the electrons, while slowing ions down. On the high B-field side, we have to opposite case, with electrons in the bulk plasma being slowed down by the drifts due to inhomogeneities in the magnetic field. Some of the reason for why we mainly see coherent structures for $x > 0$ is that the correlation between the reference signal and the data from the moveable probe is greatly reduced after three quarters of a revolution. For $x > 0$ the plasma has only moved a quarter of a revolution, and therefore we have better correlation, and more evident coherent structures are found. When conditionally sampling data from $x < 0$ it is likely that some of the larger events are not sampled, simply because they are not moving

with the exact same speed as the background plasma, and are therefore not within the conditionally sampled time intervals.

The flux structures are observed to be damped rather quickly, and appear to move approximately one revolution before dissolving. However, the flux correlation signal has a longer correlation period, and thus it appears as though the flux signal is not merely damped by a reduction of $\tilde{u}$ and $\tilde{n}$, but is reduced because the velocity and density fluctuations move out of phase, hence reducing the resulting flux signal. Whether this is due to a global difference in phase throughout the whole signal, or if it is caused by small phase differences within single events is difficult to say. In order to investigate this one would have to look more closely on each event, but limited time prevented me from doing so here.

It is important to remember that the resulting coherent structure found using conditional sampling may differ a great deal from the individual structures. Seeing as the resulting conditional average based on few events shows a much more turbulent picture, with smaller structures appearing in a addition to the structure seen in corresponding plots based on more events, it appears as though the structures in the flux signal constitute a variety of shapes.

It has been shown previously that the conditional averaging technique has a tendency to give too small amplitudes for the coherent structures (Teliban et al., 2007). As we can see on our data as well, the amplitude of the coherent structures appear to increase with increasing trigger level, i.e. the condition C, indicating that we are including events which cause a damping of the amplitude. This tendency can be dealt with by computing the correlation between the selected events, and removing those which cause this amplitude damping. However, one of the advantages of the conditional sampling technique is that it is easy to implement and interpret, thus we have kept it in its simple form, and adding additional conditions on the other signals to improve it instead.

7.3 Anomalous transport

The turbulence we see in these data is characterised by a broad spectrum, with a few narrow spikes in the power spectra. Given that we see evidence of coherent structures in the conditional averages, it is evident that we have bursts and harmonic oscillations which are phase correlated. If they were not, they would have been eliminated through the averaging, rather than emphasised.

The transport we see here appears to be consistent with turbulent transport, though it is quite clear that we are looking at events within the ballistic limit. The ballistic motion is mediated by a coherent plasma flow-channel having a loosely wound spiral form. Our structures maintain their shape for about one revolution, and are transported around in the azimuthal direction with a rotation frequency

of $\sim$ 10 kHz. Hence we are dealing with short timescales. The structures that we detect are elongated and seem consistent with the early time evolution of a structure whose motion is dominated by turbulent diffusion (see Figure 3.1). No diffusion limit is found. This is consistent with the findings of Fattorini et al. (2012).

Despite the fact that previous studies have shown indication of blob motion also in experiments similar to the Blaamann plasma (D'Ippolito et al., 2011), in these data there does not seem to be much proof of it. Even though we have positively skewed density distribution for the outer positions, the corresponding kurtosis is very close to the Gaussian value. There is also little evidence in the data of structures exhibiting the characteristic shape associated with blobs.

7.3.1 Vortex structures

An interesting discovery was the presence of a negative flow channel that was visible for both positive and negative probe positions. This channel is limited in width, but is clearly extended outwards from the very centre of the cross section to the more extreme positions. Considering our background material we would in general only expect transport out of the plasma, and as we have seen, of a burst-like nature. However, inward transport of plasma may be an indication that this particular structure is part of a compound structure that is more complex than a mere flow channel.

Combined with the fact that we find this channel of inward transport in combination with outward transport elsewhere in the cross section indicates that we may have large scale vortex structures here. They are harder to identify as we do not have data from the entire cross section, but only along a string along the local x-axis. It is also important to keep in mind that when conducting the conditional sampling with the additional conditions, it is only the midpoint of each interval that has to satisfy the conditions. We have no guarantee that the structures we see anywhere else in the cross section follow the same criteria. Thus even though we demand that the mid point only samples events corresponding to density enhancements moving outwards, any structure that is not situated near the middle of the time interval in which data has been conditionally sampled, but still exhibiting a positive flux may in fact be a density depletion moving inwards. We have no way of separating the two from each other since they are equivalent when it comes to transport of plasma.

When looking at the conditionally sampled velocity shown in Figure 6.21 we see that velocity tends to be positive on one side of the cross section and negative on the opposite side. This indicates that we have structures moving inwards on one side, and moving outwards on the opposite side, consistent with a vortex transporting plasma around in large circles, while also being transported clockwise around the

cross section by the background $\mathbf{E} \times \mathbf{B}$-drift. Plasma propagating outwards will then be caught in such a vortex, which then drags the plasma back towards the centre of the column, giving this channel of local negative flux. Whether the configuration consists of one or two vortices is difficult to say for certain. Both cases have been identified in previous studies.

Vortices or vortex-like structures in the Blaamann plasma is consistent with other experiments conducted using Blaamann, such as Øynes et al. (1998); Fredriksen et al. (2003b). Interestingly enough it is also consistent with the results of Huld et al. (1991), in which a cylindrical plasma device was used.

7.4 Summary

The aim of this study has been to study the flux of plasma in a simple magnetised torus with no rotational transform. The transport has been studied using various techniques, including studying probability distributions, correlation and use of conditional sampling.

The distribution of the flux was compared to a theoretical model deduced by Carreras et al. (1996). We found that our experimental data are similarly distributed, though the details of the theoretical distribution give less accurate results, as it is an oversimplification of our case. Assuming Gaussian distributed velocity and density becomes too great a simplification to give excellent results. It is also interesting to notice that even though the theoretical model is a universal model that ought to be applicable to all kinds of plasma, we found that in terms of skewness and kurtosis it was not appropriate as a model for argon plasma.

Our study of the turbulent flows within the toroidal Blaamann plasma has revealed coherent structures propagating around with the background plasma, but also transporting plasma out towards the wall of the tank, following spiral orbits. These structures appear in nature to be burst-like, i.e. within the short timescales of turbulent diffusion, and show little indication of being blob-like.

Statistically the average flow is out of the plasma, as is expected given the magnetic configuration of this experiment. We see this also from the estimated average of the flux in each position. However, we have some inward transport in addition, which leads us to believe that we have large scale vortices or vortex-like structures in the plasma. These cause plasma to be transported around in smaller circles, while at the same time propagating around the poloidal cross section along with the background plasma.

7.5 Future perspectives

As there is a limited amount of time one is allowed to spend on a Master thesis, there are a number of goals and ideas that could not be realised in time. However, should the opportunity appear, the ideas believed to be most interesting are listed here. If we should get a chance to continue this study we could look into the following:

- Investigate intermittency in more detail.
- Implement a matched filter, either by searching for a pre-chosen signal shape, or by investigating the curvature of the individual bursts and comparing them for each set and probe position.
- Further investigation of skewness/kurtosis relation could prove interesting. One possibility is to look into the relation for density or velocity fluctuations individually, rather than the combined flux signal.
- Comparing with synthetic data, by simulating a two-dimensional image of the transport that we see, with similar distribution of density and velocity.
- Compare with data from other devices, both simple magnetised tori and tokamaks.
- Conduct a similar investigation of the available argon data, where parts have been analysed already in the present study when discussing a possible universal relation between skewness and kurtosis.
- Out of curiosity one might investigate the conditionally sampled signal for negative spikes, though we would expect the results to be similar to those we have already found for positive spikes.

Appendix A

Source code

Here we include all the Matlab code used to analyse the Blaamann data numerically. All code is based on the methods described in Chapter 5, and is included here to show numerically how it was all implemented. As the programs all are rather short and simple, there is not a separate chapter about them in the thesis. The code is thoroughly commented in order to explain what is the function of each step in every program. In some cases Matlab already had a function that calculated a particular quantity we were interested in. In such cases the Matlab function was used, as that tended to give the most efficient programs.

A.1 Plotting samples of raw data

```
%************************************************
% Program that plots samples of raw data and makes
% a sample plot illustrating conditional sampling.
%************************************************

clear all; close all;

% Physical constants
temp_e = 5.0;
m_e = 9.11e-31;
e = 1.6e-19;
diam = 0.25e-3;
length_p = 7e-3;
% const is needed to get from I_sat to density
const_d = 2/(e*diam*length_p)*sqrt((pi*m_e)/8*temp_e*e);
distance = 7e-3;
B_ref = 0.154; % Needed to get from Ey to velocity
const_v = 1/(distance*B_ref);
const_f = const_d*const_v;

% Find data in spesified folder
%p = path;
%path(p,'fxp02azip0-9cm.zip_FILES')

X = importdata('fxp02ai1000-0608-4cm-dataset1.dat', ' ',
      4);
Ch4 = X.data(:,4);
I_sat = const_d.*X.data(:,3);
Ey = const_v.*X.data(:,5);
F = const_f.*X.data(:,6);

n = size(F);

t = 0:4e-3:(n-1)*(4e-3);

h1 = subplot(3,1,1);
plot(t(2000:3000), I_sat(2000:3000),  'LineWidth', 2, '
     color', [0 0 0.8]);
%xlabel('Time [\mu s]', 'FontSize', 20);
ylabel('Density [m^{-3}]', 'FontSize', 14);
set(gca, 'LineWidth', 2, 'FontSize', 16);
grid on
q = get(h1, 'pos');
q(1) = q(1) + 0.03;
q(4) = q(4) + 0.035;
set(h1, 'pos', q);
xlim([t(2000) t(3000)])
set(gca, 'xticklabel', [])

h2 = subplot(3,1,2);
plot(t(2000:3000), Ey(2000:3000), 'LineWidth', 2, 'color
     ', [0.8 0 0]);
%xlabel('Time [\mu s]', 'FontSize', 20);
ylabel('Velocity [m/s]', 'FontSize', 14);
set(gca, 'LineWidth', 2, 'FontSize', 16);
grid on
%ylim([-3e3 3e3])
q = get(h2, 'pos');
q(1) = q(1) + 0.03;
q(4) = q(4) + 0.035;
set(h2, 'pos', q);
xlim([t(2000) t(3000)])
set(gca, 'xticklabel', [])

h3 = subplot(3,1,3);
plot(t(2000:3000), F(2000:3000), 'LineWidth', 2, 'color'
     , [0 0.4 0.1]);
xlabel('Time [ms]', 'FontSize', 16);
ylabel('Flux [s^{-1}m^{-2}]', 'FontSize', 14);
set(gca, 'LineWidth', 2, 'FontSize', 16);
grid on
ylim([-4.5e3 4.5e3])
q = get(h3, 'pos');
q(1) = q(1) + 0.03;
q(4) = q(4) + 0.035;
set(h3, 'pos', q);
xlim([t(2000) t(3000)])

min = 60;
max = 100;

figure
%h4 = subplot(2,1,1);
h4 = plot(t(min:max), Ch4(min:max), 'LineWidth', 2, '
     color', [0 0 0.7]);
%xlabel('Time', 'FontSize', 20);
ylabel('Reference signal', 'FontSize', 20);
set(gca, 'LineWidth', 2, 'FontSize', 20, 'xticklabel', {
     't-dt', 't', 't+dt'}, 'yticklabel', []);
grid on
set(gca, 'xtick', [t(min+14), t(min+20), t(min+26)],'
     ticklength', [0.001 0.001])
hold on
plot(t(min:max) ,1.3*std(Ch4)*ones(41,1), '--', 'color',
      [1 0 0], 'LineWidth', 2)
xlim([t(min), t(max)])
annotation('line', [0.4 0.4], [0.11 0.92], 'LineStyle',
     '--', 'LineWidth', 2)
annotation('line', [0.635 0.635], [0.11 0.92], '
     LineStyle', '--', 'LineWidth', 2)
legend('Signal', 'Condition')
% q = get(h4, 'pos');
% q(2) = q(2) - 0.06;
% q(4) = q(4) + 0.05;
% set(h4, 'pos', q);
%h5 = subplot(2,1,2);
figure
h5 = plot(t(min:max), F(min:max), 'LineWidth', 2, 'color
     ', [0 0 0.7]);
set(gca, 'LineWidth', 2, 'FontSize', 20, 'xticklabel',
     [], 'yticklabel', []);
grid on
set(gca, 'xtick', [t(min+14), t(min+20), t(min+26)], '
     xticklabel', {'t-dt', 't', 't+dt'}, 'ticklength',
     [0.001 0.001])
xlim([t(min), t(max)])
ylabel('Data signal', 'FontSize', 20)
annotation('line', [0.4 0.4], [0.11 0.92], 'LineStyle',
     '--', 'LineWidth', 2)
annotation('line', [0.635 0.635], [0.11 0.92], '
     LineStyle', '--', 'LineWidth', 2)
% q = get(h5, 'pos');
% q(2) = q(2) + 0.025;
% q(4) = q(4) + 0.05;
% set(h5, 'pos', q);
```

A.2 Probability density functions

A.2.1 Experimental data

```
%************************************************
% Program that calculates the distribution of a
% given variable to be assigned.
% It reads in data from one at a timedataset,
% and from all positions, and presents it in a
% form of stacked plot.
%************************************************

clear all; close all;

tic

% Physical constants
temp_e = 5.0;
m_e = 9.11e-31;
e = 1.6e-19;
diam = 0.25e-3;
length_p = 7e-3;
% const is needed to get from I_sat to density
```

```
const_d = 2/(e*diam*length_p)*sqrt((pi*m_e)/8*temp_e*e);
distance = 7e-3;
B_ref = 0.154; % Needed to get from Ey to velocity
const_v = 1/(distance*B_ref);
const_f = const_d*const_v;

% Number of intervals in histogram
n = 201;
V_edges = linspace(-200, 200, n);
binwidth = abs(V_edges(2)-V_edges(1));
f_k = zeros(n, 19);

N = 10000; % Number of datapoints

for l=-9:1:9

    % Assigns the right folder for data
    % from the corresponding position
    if l<0
        p = path;
        path(p, 'fxp02azip-1--9cm.zip_FILES')
    else
        p = path;
        path(p, 'fxp02azip0-9cm.zip_FILES')
    end

    % Excludes dataset 5 for position -1cm and 0cm,
    % as they are missing. Set 4 for -1cm is
    % removed due to error.
    if l==-1
        S = 3;
    elseif l==0
        S = 4;
    else
        S = 5;
    end

    Ch1 = zeros(N*S, 1);
    Ch2 = zeros(N*S, 1);
    I_sat = zeros(N*S, 1);
    Ch4 = zeros(N*S, 1);
    Ey = zeros(N*S, 1);
    F = zeros(N*S, 1);

    % Read in data
    for i=1:S
        X(i) = importdata(sprintf('fxp02ai1000-0608-%dcm
              -dataset%d.dat', l, i), ' ', 4);
        Ch1((i-1)*N+1:N*i) = X(i).data(:, 1);
        Ch2((i-1)*N+1:N*i) = X(i).data(:, 2);
        I_sat((i-1)*N+1:N*i) = X(i).data(:, 3);
        Ch4((i-1)*N+1:N*i) = X(i).data(:, 4);
        Ey((i-1)*N+1:N*i) = X(i).data(:, 5);
        F((i-1)*N+1:N*i) = X(i).data(:, 6);
    end

    % Assign variable
    v1 = const_f*F;
    y1 = 'Flux';

    % Generates values along x-axis
    dt = 4e-6;
    t = linspace(0, dt*(N-1), N);

    % Sorts data in ascending order
    V = sort(v1, 1);

    %f = zeros(n, 1);

    f_k(:,l+10) = ksdensity(V(:), V_edges, 'function', '
          pdf');
    %f_k(:,l+10) = (histc(v1(:), V_edges))/(S*N*binwidth
          );
end

y = -9:1:9;

figure
h2 = surf(V_edges, y, f_k');
set(h2, 'LineWidth', 2.5, 'EdgeColor', 'interp', '
      FaceColor', 'none', 'MeshStyle', 'Row')
shading flat
colormap jet
%colorbar('location', 'EastOutside');
%caxis([0 30]);
hidden off
title(sprintf('%s distribution', y1), 'FontSize', 20)
grid on
set(gca,'FontSize',20, 'LineWidth', 2)
xlabel(sprintf('%s [m^{-2}s^{-1}]', y1), 'FontSize', 20)
      ;
ylabel('Position [cm]', 'FontSize', 20);
zlabel('Relative Frequency', 'FontSize', 20);
xlim([min(V_edges) max(V_edges)])
ylim([-9.1 9.1])
zlim([0 max(max(f_k))])
view([10 30 35]);
%saveas(h2,sprintf('pdf%s.eps', y1), 'psc2')

toc
```

A.2.2 Theoretical model

```
%************************************************
% Program that calculates the theoretical
% distribution of a the flux signal
% for all positions, and presents it in a
% form of stacked plot.
%************************************************

clear all; close all;

tic

% Physical constants
temp_e = 5.0;
m_e = 9.11e-31;
e = 1.6e-19;
diam = 0.25e-3;
length_p = 7e-3;
% const is needed to get from I_sat to density
const_d = 2/(e*diam*length_p)*sqrt((pi*m_e)/8*temp_e*e);
distance = 7e-3;
B_ref = 0.154; % Needed to get from Ey to velocity
const_v = 1/(distance*B_ref);
const_f = const_d*const_v;

% Number of intervals in histogram
n = 1601;
V_edges = linspace(-200, 200, n);
binwidth = abs(V_edges(2)-V_edges(1));

N = 10000; % Number of datapoints

f_k = zeros(n, 19);

%gamma = 0.85;

smooth_param = [45 45 45 45 45 45 65 65 275 301 301 275
      205 185 115 105 55 55 55];

for l=-9:1:9

    % Assigns the right folder for data
    % from the corresponding position
    if l<0
        p = path;
        path(p, 'fxp02azip-1--9cm.zip_FILES')
    else
        p = path;
        path(p, 'fxp02azip0-9cm.zip_FILES')
    end

    % Excludes dataset 5 for position -1cm and 0cm,
    % as they are missing. Set 4 for -1cm is
    % removed due to error.
    if l==-1
        S = 3;
    elseif l==0
        S = 4;
    else
```

```
        S = 5;
    end

    Ch1 = zeros(N*S, 1);
    Ch2 = zeros(N*S, 1);
    I_sat = zeros(N*S, 1);
    Ch4 = zeros(N*S, 1);
    Ey = zeros(N*S, 1);
    F = zeros(N*S, 1);

    % Read in data
    for i=1:S
        X(i) = importdata(sprintf('fxp02ai1000-0608-%dcm
             -dataset%d.dat', l, i), ' ', 4);
        Ch1((i-1)*N+1:N*i) = X(i).data(:, 1);
        Ch2((i-1)*N+1:N*i) = X(i).data(:, 2);
        I_sat((i-1)*N+1:N*i) = X(i).data(:, 3);
        Ch4((i-1)*N+1:N*i) = X(i).data(:, 4);
        Ey((i-1)*N+1:N*i) = X(i).data(:, 5);
        F((i-1)*N+1:N*i) = X(i).data(:, 6);
    end

    % Assign variable
    v1 = const_f*F;
    y1 = 'Flux';

    sigma_n = std(const_d*I_sat);
    sigma_v = std(const_v*Ey);

    gamma = corrcoef(const_d*I_sat, const_v*Ey);

    % Generates values along x-axis
    dt = 4e-6;
    t = linspace(0, dt*(N-1), N);

    p = (1/pi)*((sqrt(1-gamma(1,2)^2))/(sigma_n*sigma_v)
          )*besselk(0, abs(V_edges(:))./(sigma_n*sigma_v)
          ).*exp(-gamma(1,2)*V_edges(:)./(sigma_n*sigma_v
          ));

    % Sorts data in ascending order
    %V = sort(v1, 1);
    p((n-1)/2+1) = (p((n-1)/2)+p((n-1)/2+2))/2+(p((n-1)
          /2)-p((n-1)/2-1));

    mean(p)

    %f_k(1:9*(n-1)/20,l+10) = smooth(p(1:9*(n-1)/20),
          175);
    %f_k(11*(n-1)/20:n,l+10) = smooth(p(11*(n-1)/20:n),
          175);
    %f_k(9*(n-1)/20+1:11*(n-1)/20-1,l+10) = smooth(p(9*(
          n-1)/20+1:11*(n-1)/20-1), smooth_param(l+10));
    f_k(:, l+10) = smooth(p, smooth_param(l+10));
end

y = -9:1:9;

figure
h = surf(V_edges, y, f_k');
set(h, 'LineWidth', 2.5, 'EdgeColor', 'interp', '
      FaceColor', 'none', 'MeshStyle', 'Row')
shading flat
colormap jet
%colorbar('location', 'EastOutside');
%caxis([0 30]);
hidden off
title(sprintf('%s distribution', y1), 'FontSize', 20)
grid on
set(gca,'FontSize',20, 'LineWidth', 2)
xlabel(sprintf('%s [m^{-2}s^{-1}]', y1), 'FontSize', 20)
      ;
ylabel('Position [cm]', 'FontSize', 20);
zlabel('Relative Frequency', 'FontSize', 20);
xlim([min(V_edges) max(V_edges)])
ylim([-9.1 9.1])
zlim([0 max(max(f_k))])
view([10 30 35]);

toc
```

A.2.3 Joint PDF

```
%************************************************
% Program that calculates the joint PDF of v_x and
% density. This is done directly from the dataset
% by looking at v_x(i) and d(i).
%************************************************

clear all; close all;

tic
% Physical constants
temp_e = 5.0;
m_e = 9.11e-31;
e = 1.6e-19;
diam = 0.25e-3;
length_p = 7e-3;
% const is needed to get from I_sat to density
const_d = 2/(e*diam*length_p)*sqrt((pi*m_e)/8*temp_e*e);
distance = 7e-3;
B_ref = 0.154; % Needed to get from Ey to velocity
const_v = 1/(distance*B_ref);
const_f = const_d*const_v;

% Number of datapoints
N = 10000;

% Number of intervals in histogram
nd = 100;
nv = 100;

% Creates intervals for histogram
D_edges = linspace(-2, 2.5, nd);
V_edges = linspace(-2000, 1200, nv);

% Redefines interval vectors to work
% better when finding the joint PDF
D_edges = [(D_edges) max(D_edges)+(D_edges(2)-D_edges(1)
      )];
V_edges = [(V_edges) max(V_edges)+(V_edges(2)-V_edges(1)
      )];

% Joint PDF
J_dep = zeros(nd,nv);

%empty array for size of distribution
size_dist = zeros(19,1);

for l=1:1:9
    %J_dep(:,:) = 0;
        % Assigns the right folder for data
        % from the corresponding position
    if l<0
        p = path;
        path(p, 'fxp02azip-1--9cm.zip_FILES')
    else
        p = path;
        path(p, 'fxp02azip0-9cm.zip_FILES')
    end

    % Excludes dataset 5 for position -1cm and 0cm,
    % as they are missing. Set 4 from -1cm is
    % removed due to error.
    if l==-1
        S = 3;
    elseif l==0
        S = 4;
    else
        S = 5;
    end

    for q=1:S
        % Read in data from positions 0-9 cm
        X(q) = importdata(sprintf('fxp02ai1000-0608-%dcm
             -dataset%d.dat', l, q), ' ', 4);
        %Ch1(:, q) = X(q).data(:, 1);
        %Ch2(:, q) = X(q).data(:, 2);
        D = const_d*X(q).data(:, 3);
        %Ch4(:, q) = X(q).data(:, 4);
        V = const_v*X(q).data(:, 5);
        %F(:, q) = X(q).data(:, 6);
```

```
        % Calculating joint PDF
        for i=1:N
            for j=1:length(D_edges)-1
                for k=1:length(V_edges)-1
                    if D(i) < D_edges(j+1) && D(i)>=
                          D_edges(j) && V(i)<V_edges(k+1)
                           && V(i)>= V_edges(k)
                        J_dep(j, k) = J_dep(j, k) + 1;
                    end
                end
            end
        end
    end

    %J_dep = J_dep./(S*N);
end

J_dep = J_dep./(N*9*5);

% Plot dependent joint PDF
figure
h1 = image(V_edges(1:nv), D_edges(1:nd), J_dep, '
     CDataMapping', 'Scaled');
shading interp;
%set(h1)
colormap jet;
colorbar
grid on
xlabel('Velocity [m/s]', 'FontSize', 16)
ylabel('Density [m^{-3}]', 'FontSize', 16)
caxis([0 13.5e-4])
%zlabel('Relative Frequency', 'FontSize', 24)
%axis tight
%xlim([V_edges(1) V_edges(nv+1)]);
%ylim([D_edges(1) D_edges(nd+1)]);
%set(gca, 'YDir', 'reverse')
set(gca, 'LineWidth', 2, 'FontSize', 16, 'YDir', 'normal
    ')
%title('Joint PDF', 'FontSize', 20)
%view([0 0 90])

toc
```

A.3 Statisitical moments

A.3.1 All sets treated as one long string of data

```
%***********************************************
% Program for investigating the moments of the
% timeseries, and plotting them aginst position,
% but also againts each other. For each position
% the mean of the moment in question is calculated
% from the mean of all the datasets.
%***********************************************

%clear all; close all;

% Physical constants
temp_e = 5.0;
m_e = 9.11e-31;
e = 1.6e-19;
diam = 0.25e-3;
length_p = 7e-3;
% const is needed to get from I_sat to density
const_d = 2/(e*diam*length_p)*sqrt((pi*m_e)/8*temp_e*e);
distance = 7e-3;
B_ref = 0.154; % Needed to get from Ey to velocity
const_v = 1/(distance*B_ref);
const_f = const_d*const_v;

N = 10000; % Number of datapoints

m = zeros(19, 1);
va = zeros(19, 1);
skew = zeros(19, 1);
kurt = zeros(19, 1);

for k=-9:1:9
    % Assigns the right folder for data from
    % the corresponding position
    if k<0
        p = path;
        path(p, 'fxp02azip-1--9cm.zip_FILES')
    else
        p = path;
        path(p, 'fxp02azip0-9cm.zip_FILES')
    end

    % Excludes dataset 5 for positions 0cm and -1cm,
    % as they is missing, in addition to set 4 for
    % postion -1cm as it is wrong.
    if k==-1
        S = 3;
    elseif k==0
        S = 4;
    else
        S = 5;
    end

    I_sat = zeros(N*S, 1);
    Ey = zeros(N*S, 1);
    F = zeros(N*S, 1);

    % Read in data from positions 0-9 cm
    for i=1:S
        X(i) = importdata(sprintf('fxp02ai1000-0608-%dcm
             -dataset%d.dat', k, i), ' ', 4);
        I_sat((i-1)*N+1:i*N) = const_d*X(i).data(:, 3);
        Ey((i-1)*N+1:i*N) = const_v*X(i).data(:, 5);
        F((i-1)*N+1:i*N) = const_f*X(i).data(:, 6);
    end

    % Assign variable
    v1 = F;
    y1 = 'Flux';

    m(k+10) = mean(v1, 1);
    va(k+10) = var(v1, 1)/(m(k+10))^2;
    skew(k+10) = skewness(v1, 1);
    kurt(k+10) = kurtosis(v1, 1);
end

x = linspace(-9,9,19);
%
% % Makes ordinary plots of moments vs. position
% figure(6)
% h1 = plot(x, m, 'ro');
% set(h1, 'MarkerSize', 10, 'LineWidth', 2)
% grid on
% set(gca, 'LineWidth', 2, 'FontSize', 20)
% xlabel('Position [cm]', 'FontSize', 20)
% ylabel('Mean [arbitrary units]', 'FontSize', 20)
% hold on
% %saveas(h1,sprintf('meanvspos%s.eps', y1), 'psc2')
%
% figure(8)
% h2 = semilogy(x, va, 'ro');
% set(h2, 'MarkerSize', 10, 'LineWidth', 2)
% grid on
% set(gca, 'LineWidth', 2, 'FontSize', 20)
% xlabel('Position [cm]', 'FontSize', 20)
% ylabel('Variance', 'FontSize', 20)
% hold on
% %ylim([0 100])
% %saveas(h2,sprintf('varvspos%s.eps', y1), 'psc2')
%
% figure(3)
% h3 = plot(x, skew, 'ro');
% set(h3, 'MarkerSize', 10, 'LineWidth', 2)
% grid on
```

```
% set(gca, 'LineWidth', 2, 'FontSize', 20)
% xlabel('Position [cm]', 'FontSize', 20)
% ylabel('Skewness', 'FontSize', 20)
% hold on
% %saveas(h3,sprintf('skewvspos%s.eps', y1), 'psc2')
%
% figure(4)
% h4 = plot(x, kurt, 'ro');
% set(h4, 'MarkerSize', 10, 'LineWidth', 2)
% grid on
% hold on
% normline = plot(linspace(-10,10,10), 3*ones(10,1),
    '--');
% set(normline, 'LineWidth', 2)
% set(gca, 'LineWidth', 2, 'FontSize', 20)
% xlabel('Position [cm]', 'FontSize', 20)
% ylabel('Kurtosis', 'FontSize', 20)
% %ylim([0 25])
% %saveas(h4,sprintf('kurtvspos%s.eps', y1), 'psc2')

% % Makes plot of kurtosis vs. skewness squared pluss
    one. Each marker has
% % size and color according to position.
% for l=1:9
%     figure(5)
%     h5 = plot(kurt(l), skew(l)^2+1, 'ro');
%     set(h5, 'MarkerSize', (-4*(l-11)), 'LineWidth', 2)
%     hold on
% end
%
% figure(5)
% h7 = plot(kurt, skew.^2+1, 'ro');
% hold on
% set(h7, 'MarkerSize', 10, 'LineWidth', 2)
% grid on
% set(gca, 'LineWidth', 2, 'FontSize', 20)
% xlabel('Kurtosis', 'FontSize', 20)
% ylabel('Skewness^2 + 1', 'FontSize', 20, 'FontWeight',
     'Bold')
% xlim([0, 20])
% ylim([0, 20])
%
% x1 = linspace(0, 20, 20);
% figure(5)
% stipline = plot(x1, x1, '--');
% set(stipline, 'LineWidth', 2)
% %hold off
% %saveas(h8,'kurtvsskewsq.eps', 'psc2');

% for l=1:9
%     figure(5)
%     h6(l) = plot(kurt(l+10), skew(l+10)^2+1, 'bo');
%     set(h6(l), 'MarkerSize', (4*(l+1)), 'LineWidth',
    2);
% end
%
% legend([h5, h7, h6(1)], 'Negative x-values', 'x=0', '
    Positive x-values', 'Location', 'NorthWest')

% % Makes plot of skewness vs. kurtosis. Each marker has
% % size and color according to position.
% for l=1:9
%     figure(6)
%     h8 = plot(skew(l), kurt(l), 'ro');
%     set(h8, 'MarkerSize', (-4*(l-11)), 'LineWidth', 2)
%     hold on
% end

% figure(1)
% h9 = plot(skew, kurt, 'ro');
% set(h9, 'MarkerSize', 10, 'LineWidth', 2)
% grid on
% set(gca, 'LineWidth', 2, 'FontSize', 20)
% xlabel('Skewness', 'FontSize', 20)
% ylabel('Kurtosis', 'FontSize', 20)
% hold on
%saveas(h9,'skewvskurt.eps', 'psc2');

% for l=1:9
%     figure(6)
%     h10(l) = plot(skew(l+10), kurt(l+10), 'bo');
%     set(h10(l), 'MarkerSize', 4*(l+1), 'LineWidth', 2)
%     hold on
% end
%
% legend([h8, h9, h10(1)], 'Negative x-values', 'x=0', '
    Positive x-values')

% % Makes plot of kurtosis vs. variance squared pluss
    one. Each marker has
% % size and color according to position.
% for l=1:9
%     figure(7)
%     h11 = plot(kurt(l), va(l), 'ro');
%     set(h11, 'MarkerSize', (-4*(l-11)), 'LineWidth',
    2)
%     hold on
% end

% figure(7)
% h12 = plot(kurt, va, 'ro');
% set(h12, 'MarkerSize', 10, 'LineWidth', 2)
% grid on
% set(gca, 'LineWidth', 2, 'FontSize', 20)
% ylabel('Variance/<s>^2', 'FontSize', 20)
% xlabel('Kurtosis', 'FontSize', 20)
% hold on
% %saveas(h12,'kurtvsvar.eps', 'psc2');

% for l=1:9
%     figure(7)
%     h13(l) = plot(kurt(l+10), va(l+10), 'bo');
%     set(h13(l), 'MarkerSize', 4*(l+1), 'LineWidth', 2)
%     hold on
% end
%
% legend([h11, h12, h13(1)], 'Negative x-values', 'x=0',
     'Positive x-values')

% % Makes plot of skewness vs. variance squared pluss
    one. Each marker has
% % size and color according to position.
% for l=1:9
%     figure(8)
%     h14 = plot(skew(l), va(l), 'ro');
%     set(h14, 'MarkerSize', (-4*(l-11)), 'LineWidth',
    2)
%     hold on
% end
%
% figure(8)
% h15 = plot(skew(10), va(10), 'go');
% set(h15, 'MarkerSize', 4, 'LineWidth', 2)
% grid on
% set(gca, 'LineWidth', 2, 'FontSize', 20)
% xlabel('Skewness', 'FontSize', 20)
% ylabel('Variance', 'FontSize', 20)
%
% for l=1:9
%     figure(8)
%     h16(l) = plot(skew(l+10), va(l+10), 'bo');
%     set(h16(l), 'MarkerSize', 4*(l+1), 'LineWidth', 2)
%     hold on
% end
%
% legend([h14, h15, h16(1)], 'Negative x-values', 'x=0',
     'Positive x-values')

figure(2)
h = semilogy(abs(skew), va, 'ro');
set(h, 'MarkerSize', 10, 'LineWidth', 2)
grid on
set(gca, 'LineWidth', 2, 'FontSize', 20)
xlabel('Skewness', 'FontSize', 20)
ylabel('Normalised variance', 'FontSize', 20)
hold on
ylim([0 10])
xlim([0 4])
%saveas(h,'absskewvsvar.eps', 'psc2');
```

A.3.2 All sets treated separately

```
%************************************************
% Program for investigating the moments of the
% timeseries, and plotting them aginst position,
% but also againts each other. For each position the
% mean of the moment in question is calculated from
% the mean of all the datasets.
%************************************************

%clear all; close all;

N = 10000; % Number of datapoints
% Physical constants
temp_e = 5.0;
m_e = 9.11e-31;
e = 1.6e-19;
diam = 0.25e-3;
length_p = 7e-3;
% const is needed to get from I_sat to density
const_d = 2/(e*diam*length_p)*sqrt((pi*m_e)/8*temp_e*e);
distance = 7e-3;
B_ref = 0.154; % Needed to get from Ey to velocity
const_v = 1/(distance*B_ref);
const_f = const_d*const_v;

m = zeros(19*5-3, 1);
va = zeros(19*5-3, 1);
skew = zeros(19*5-3, 1);
kurt = zeros(19*5-3, 1);

counter = 0;
for k=-9:1:9
    % Assigns the right folder for data from the
        corresponding position
    if k<0
        p = path;
        path(p, 'fxp02azip-1--9cm.zip_FILES')
    else
        p = path;
        path(p, 'fxp02azip0-9cm.zip_FILES')
    end

    % Excludes dataset 5 and 4 for position -1cm,
    % and set 5 for 0 cm, as they are missing.
    % Set 4 for -1cm is also removed due to error.
    if k==-1
        S = 3;
    elseif k==0
        S = 4;
    else
        S = 5;
    end

    I_sat = zeros(N, S);
    Ey = zeros(N, S);
    F = zeros(N, S);

    % Read in data from positions 0-9 cm
    for i=1:S
        X(i) = importdata(sprintf('fxp02ai1000-0608-%dcm
            -dataset%d.dat', k, i), ' ', 4);
        I_sat(:, i) = const_d*X(i).data(:, 3);
        Ey(:, i) = const_v*X(i).data(:, 5);
        F(:, i) = const_f*X(i).data(:, 6);
    end

    % Assign variable
    v1 = F;
    y1 = 'Flux';

    Mean = zeros(S, 1);
    Variance = zeros(S, 1);
    Skewness = zeros(S, 1);
    Kurtosis = zeros(S, 1);

    for j=1:S
        Mean(j) = mean(v1(:,j));
        Variance(j) = var(v1(:,j), 1)/(Mean(j)^2);
        % The 1 indicates that the calculated standard
            % deviation devides by n and not n-1.
        Skewness(j) = skewness(v1(:,j), 1);
        Kurtosis(j) = kurtosis(v1(:,j), 1);
    end

    if k==-1 && S==3
        m(41:43) = Mean;
        va(41:43) = Variance;
        skew(41:43) = Skewness;
        kurt(41:43) = Kurtosis;
        counter = 1;
    elseif k==-1 && S==4
        m(41:44) = Mean;
        va(41:44) = Variance;
        skew(41:44) = Skewness;
        kurt(41:44) = Kurtosis;
    elseif k==0 && counter==1
        m(44:47) = Mean;
        va(44:47) = Variance;
        skew(44:47) = Skewness;
        kurt(44:47) = Kurtosis;
    elseif k==0 && counter==0
        m(45:48) = Mean;
        va(45:48) = Variance;
        skew(45:48) = Skewness;
        kurt(45:48) = Kurtosis;
    elseif k<-1
        m((k+10)*S-S+1:(k+10)*S) = Mean;
        va((k+10)*S-S+1:(k+10)*S) = Variance;
        skew((k+10)*S-S+1:(k+10)*S) = Skewness;
        kurt((k+10)*S-S+1:(k+10)*S) = Kurtosis;
    elseif k>0 && counter==1
        m((k+10)*S-S-2:(k+10)*S-3) = Mean;
        va((k+10)*S-S-2:(k+10)*S-3) = Variance;
        skew((k+10)*S-S-2:(k+10)*S-3) = Skewness;
        kurt((k+10)*S-S-2:(k+10)*S-3) = Kurtosis;
    else
        m((k+10)*S-S-1:(k+10)*S-2) = Mean;
        va((k+10)*S-S-1:(k+10)*S-2) = Variance;
        skew((k+10)*S-S-1:(k+10)*S-2) = Skewness;
        kurt((k+10)*S-S-1:(k+10)*S-2) = Kurtosis;
    end

end

x1 = linspace(-9,9,19);
x2 = [-9 -8 -7 -6 -5 -4 -3 -2 1 2 3 4 5 6 7 8 9];
x = sort([x1,x1,x1,x2,x2, 0]);

% % Makes ordinary plots of moments vs. position
% figure(6)
% h1 = plot(x, m, 'o');
% set(h1, 'MarkerSize', 7, 'LineWidth', 2)
% grid on
% set(gca, 'LineWidth', 2, 'FontSize', 20)
% xlabel('Position [cm]', 'FontSize', 20)
% ylabel('Mean', 'FontSize', 20)
% hold on
%
% figure(8)
% h2 = plot(x, va, 'o');
% set(h2, 'MarkerSize', 7, 'LineWidth', 2)
% grid on
% set(gca, 'LineWidth', 2, 'FontSize', 20)
% xlabel('Position [cm]', 'FontSize', 20)
% ylabel('Variance', 'FontSize', 20)
% %ylim([0 100])
% hold on
%
% figure(3)
% h3 = plot(x, skew, 'o');
% set(h3, 'MarkerSize', 7, 'LineWidth', 2)
% grid on
% set(gca, 'LineWidth', 2, 'FontSize', 20)
% xlabel('Position [cm]', 'FontSize', 20)
% ylabel('Skewness', 'FontSize', 20)
% hold on
%
% figure(4)
% h4 = plot(x, kurt, 'o');
% set(h4, 'MarkerSize', 7, 'LineWidth', 2)
% grid on
% set(gca, 'LineWidth', 2, 'FontSize', 20)
```

```
% xlabel('Position [cm]', 'FontSize', 20)
% ylabel('Kurtosis', 'FontSize', 20)
% hold on
%
% % % Makes plot of kurtosis vs. skewness squared pluss
    one. Each marker has
% % % size and color according to position.
% % for l=1:9
% %     figure(5)
% %     h5 = plot(kurt(l), skew(l)^2+1, 'ro');
% %     set(h5, 'MarkerSize', (-4*(l-11)), 'LineWidth',
    2)
% %     hold on
% % end
%
% figure(5)
% h7 = plot(kurt, skew.^2+1, 'o');
% hold on
% set(h7, 'MarkerSize', 7, 'LineWidth', 2)
% grid on
% set(gca, 'LineWidth', 2, 'FontSize', 20)
% xlabel('Kurtosis', 'FontSize', 20)
% ylabel('Skewness^2 + 1', 'FontSize', 20, 'FontWeight',
     'demi')
% xlim([0, 20])
% ylim([0, 20])
%
% x_lin = linspace(0, 20, 20);
% figure(5)
% stiplin = plot(x_lin, x_lin, '--');
% set(stiplin, 'LineWidth', 2, 'Color', [0 0 0.4])
%
% modelFun2 =  @(q,x) q(1).*x+q(2);
% startingVals2 = [1 1];
% coefEsts2 = nlinfit(kurt, skew.^2+1, modelFun2,
    startingVals2);
% xgrid = linspace(0,20,20);
% line(xgrid, modelFun2(coefEsts2, xgrid), 'Color',[0
    0.4 0], 'LineWidth', 2);
% hold off
%
% % for l=1:9
% %     figure(5)
% %     h6(l) = plot(kurt(l+10), skew(l+10)^2+1, 'bo');
% %     set(h6(l), 'MarkerSize', (4*(l+1)), 'LineWidth',
     2);
% % end
% %
% % legend([h5, h7, h6(1)], 'Negative x-values', 'x=0',
    'Positive x-values', 'Location', 'NorthWest')

% % Makes plot of skewness vs. kurtosis. Each marker has
% % size and color according to position.
% for l=1:9
%     figure(6)
%     h8 = plot(skew(l), kurt(l), 'ro');
%     set(h8, 'MarkerSize', (-4*(l-11)), 'LineWidth', 2)
%     hold on
% end
%
% figure(1)
% h9 = plot(skew, kurt, 'bo');
% set(h9, 'MarkerSize', 7, 'LineWidth', 2)
% grid on
% set(gca, 'LineWidth', 2, 'FontSize', 20)
% xlabel('Skewness', 'FontSize', 20)
% ylabel('Kurtosis', 'FontSize', 20)
% hold on
% xlim([-4 4])
% ylim([0 30])
%
% modelFun =  @(p,x) p(1).*x.^2+p(2);
% startingVals = [1 1];
% coefEsts = nlinfit(skew, kurt, modelFun, startingVals)
    ;
% xgrid = linspace(-6,6,100);
% line(xgrid, modelFun(coefEsts, xgrid), 'Color',[0 0.4
    0], 'LineWidth', 2);
% %hold off
%
% figure(1)
% terline = plot(xgrid, xgrid.^2+1, '--');
% set(terline, 'LineWidth', 2)
```

```
% for l=1:9
%     figure(6)
%     h10(l) = plot(skew(l+10), kurt(l+10), 'bo');
%     set(h10(l), 'MarkerSize', 4*(l+1), 'LineWidth', 2)
%     hold on
% end
%
% legend([h8, h9, h10(1)], 'Negative x-values', 'x=0', '
    Positive x-values')

% % Makes plot of kurtosis vs. variance squared pluss
    one. Each marker has
% % size and color according to position.
% for l=1:9
%     figure(7)
%     h11 = plot(kurt(l), va(l), 'ro');
%     set(h11, 'MarkerSize', (-4*(l-11)), 'LineWidth',
    2)
%     hold on
% end

% figure(7)
% h12 = plot(kurt, va, 'o');
% set(h12, 'MarkerSize', 7, 'LineWidth', 2)
% grid on
% set(gca, 'LineWidth', 2, 'FontSize', 20)
% ylabel('Variance', 'FontSize', 20)
% xlabel('Kurtosis', 'FontSize', 20)
% hold on

% for l=1:9
%     figure(7)
%     h13(l) = plot(kurt(l+10), va(l+10), 'bo');
%     set(h13(l), 'MarkerSize', 4*(l+1), 'LineWidth', 2)
%     hold on
% end
%
% legend([h11, h12, h13(1)], 'Negative x-values', 'x=0',
     'Positive x-values')

% % Makes plot of skewness vs. variance squared pluss
    one. Each marker has
% % size and color according to position.
% for l=1:9
%     figure(8)
%     h14 = plot(skew(l), va(l), 'ro');
%     set(h14, 'MarkerSize', (-4*(l-11)), 'LineWidth',
    2)
%     hold on
% end
%
% figure(8)
% h15 = plot(skew(10), va(10), 'go');
% set(h15, 'MarkerSize', 4, 'LineWidth', 2)
% grid on
% set(gca, 'LineWidth', 2, 'FontSize', 20)
% xlabel('Skewness', 'FontSize', 20)
% ylabel('Variance', 'FontSize', 20)
%
% for l=1:9
%     figure(8)
%     h16(l) = plot(skew(l+10), va(l+10), 'bo');
%     set(h16(l), 'MarkerSize', 4*(l+1), 'LineWidth', 2)
%     hold on
% end
%
% legend([h14, h15, h16(1)], 'Negative x-values', 'x=0',
     'Positive x-values')

figure(2)
h = semilogy(abs(skew), va, 'bo');
set(h, 'MarkerSize', 7, 'LineWidth', 2)
grid on
set(gca, 'LineWidth', 2, 'FontSize', 20)
xlabel('Skewness', 'FontSize', 20)
ylabel('Normalised variance', 'FontSize', 20)
hold on

x_lin2 = 0:0.1:3;
semilogy(x_lin2, 0.5*(2+x_lin2.^2+x_lin2.*sqrt(4+x_lin2
    .^2)), '--', 'LineWidth', 2)
ylim([0 30])
```

```
xlim([0 3])
% hold off
hold on
```

A.3.3 Including the Argon plasma data

```
%************************************************
% Program that reads in data from the Argon
% plasma experiment, and calculates skewness,
% variance, mean and kurtosis. Due to some
% sets missing, a method that skips these
% had to be implemented.
%************************************************

clear all; close all;

% Number of points per set
N = 10000;

% Empty array for flux
f = zeros(N, 1);

% Number of datasets
S = 23;

for j=1:6
    % Empty arrays for skewness and kurtosis
    variance = zeros(S, 1);
    skew = zeros(S, 1);
    kurt = zeros(S, 1);

    p = path;
    path(p,'arbvarhp')

    for i=1:23
        if i==12 && j==2
            continue
        end
        % Read data
        fid = fopen(sprintf('arb%d00hp.TXT', j));
        if j==2 && i>12
            C1 = textscan(fid, '%f %f %f %f', 'delimiter
                 ', ' ', 'HeaderLines', (i-1)
                 *10003-8958);
        else
            C1 = textscan(fid, '%f %f %f %f', 'delimiter
                 ', ' ', 'HeaderLines', 42+(i-1)*10003);
        end
        fclose(fid);
        % Calculate flux
        f(:) = -(C1{1}-C1{2}).*C1{3};
        % Calculate skewness and kurtosis of flux
        variance(i) = var(f, 1)/(mean(f))^2;
        skew(i) = skewness(f);
        kurt(i) = kurtosis(f);
    end

%     figure(1)
%     h1 = plot(skew, kurt, 'ko');
%     grid on
%     xlabel('Skewness', 'FontSize', 20)
%     ylabel('Kurtosis', 'FontSize', 20)
%     %title('Skewness-kurtosis relation for flux', '
      FontSize', 20)
%     set(h1, 'LineWidth', 2, 'MarkerSize', 7)
%     set(gca, 'LineWidth', 2, 'FontSize', 20)
%     xlim([-4, 4])
%     ylim([0, 30])
%     hold on

    figure(2)
    h3 = semilogy(abs(skew), variance, 'ko');
    grid on
    xlabel('Skewness', 'FontSize', 20)
    ylabel('Normalised variance', 'FontSize', 20)
    %title('Skewness-variance relation for flux', '
         FontSize', 20)
    set(h3, 'LineWidth', 2, 'MarkerSize', 7)
    set(gca, 'LineWidth', 2, 'FontSize', 20)
    %xlim([-4, 4])
    %ylim([0, 25])
    hold on
end

for j=1:6
    % Empty arrays for skewness and kurtosis
    variance = zeros(S, 1);
    skew = zeros(S, 1);
    kurt = zeros(S, 1);

    p = path;
    path(p,'arbvarlp')

    if j==4
        for i=3:23
            % Read data
            fid = fopen(sprintf('arb%d00lp.TXT', j));
            C1 = textscan(fid, '%f %f %f %f', 'delimiter
                 ', ' ', 'HeaderLines', 11048+(i-3)
                 *10003);
            fclose(fid);
            % Calculate flux
            f(:) = -(C1{1}-C1{2}).*C1{3};
            % Calculate skewness and kurtosis of flux
            variance(i) = var(f)/(mean(f))^2;
            skew(i) = skewness(f);
            kurt(i) = kurtosis(f);
        end
    else
        for i=1:23
            % Read data
            fid = fopen(sprintf('arb%d00lp.TXT', j));
            C1 = textscan(fid, '%f %f %f %f', 'delimiter
                 ', ' ', 'HeaderLines', 42+(i-1)*10003);
            fclose(fid);
            % Calculate flux
            f(:) = -(C1{1}-C1{2}).*C1{3};
            % Calculate skewness and kurtosis of flux
            variance(i) = var(f)/(mean(f))^2;
            skew(i) = skewness(f);
            kurt(i) = kurtosis(f);
        end
    end

%     figure(1)
%     h2 = plot(skew, kurt, 'ko');
%     grid on
%     xlabel('Skewness', 'FontSize', 20)
%     ylabel('Kurtosis', 'FontSize', 20)
%     %title('Skewness-kurtosis relation for flux', '
     FontSize', 20)
%     set(h2, 'LineWidth', 2, 'MarkerSize', 7)
%     set(gca, 'LineWidth', 2, 'FontSize', 20)
%     xlim([-4, 4])
%     ylim([0, 30])
%     hold on
%
    figure(2)
    h5 = semilogy(abs(skew), variance, 'ko');
    grid on
    xlabel('Skewness', 'FontSize', 20)
    ylabel('Normalised variance', 'FontSize', 20)
    %title('Skewness-variance relation for flux', '
         FontSize', 20)
    set(h5, 'LineWidth', 2, 'MarkerSize', 7)
    set(gca, 'LineWidth', 2, 'FontSize', 20)
    %xlim([-4, 4])
    %ylim([0, 25])
    hold on
end

for j=10:5:15
    % Empty arrays for skewness and kurtosis
    variance = zeros(S, 1);
    skew = zeros(S, 1);
    kurt = zeros(S, 1);

    p = path;
```

```
    path(p,'arbvarlp')

    for i=1:23
        if j==15 && i==10
            continue
        end
        % Read data
        fid = fopen(sprintf('arb%d0pla.TXT', j));
        if j==15 && i>10
            C1 = textscan(fid, '%f %f %f %f', 'delimiter
                 ', ' ', 'HeaderLines', (i-1)
                 *10003-8955);
        else
            C1 = textscan(fid, '%f %f %f %f', 'delimiter
                 ', ' ', 'HeaderLines', 45+(i-1)*10003);
        end
        fclose(fid);
        % Calculate flux
        f(:) = -(C1{1}-C1{2}).*C1{3};
        % Calculate skewness and kurtosis of flux
        variance(i) = var(f)/(mean(f))^2;
        skew(i) = skewness(f);
        kurt(i) = kurtosis(f);
    end

%     figure(1)
%     h2 = plot(skew, kurt, 'ko');
%     grid on
%     xlabel('Skewness', 'FontSize', 20)
%     ylabel('Kurtosis', 'FontSize', 20)
%     %title('Skewness-kurtosis relation for flux', '
      FontSize', 20)
%     set(h2, 'LineWidth', 2, 'MarkerSize', 7)
%     set(gca, 'LineWidth', 2, 'FontSize', 20)
%     xlim([-4, 4])
%     ylim([0, 30])
%     hold on

    figure(2)
    h4 = semilogy(abs(skew), variance, 'ko');
    grid on
    xlabel('Skewness', 'FontSize', 20)
    ylabel('Normalised variance', 'FontSize', 20)
    %title('Skewness-variance relation for flux', '
         FontSize', 20)
    set(h4, 'LineWidth', 2, 'MarkerSize', 7)
    set(gca, 'LineWidth', 2, 'FontSize', 20)
    %xlim([-4, 4])
    %ylim([0, 25])
    hold on
end
```

A.4 Autocorrelation and FFT

```
%************************************************
% Program calculating the Fast Fourier Transform
% of a variable's autocorrelation function.
% This is done for every position, and the auto
% correlation function is calculated for each set,
% and averaged.
%************************************************

clear all; close all;

tic

% Physical constants
temp_e = 5.0;
m_e = 9.11e-31;
e = 1.6e-19;
diam = 0.25e-3;
length_p = 7e-3;
% const is needed to get from I_sat to density
const_d = 2/(e*diam*length_p)*sqrt((pi*m_e)/8*temp_e*e);
distance = 7e-3;
B_ref = 0.154; % Needed to get from Ey to velocity
const_v = 1/(distance*B_ref);
const_f = const_d*const_v;

n = 10000;

% Generates values along x-axis
dt = 4e-6;
t = linspace(0, dt*(n-1), n);

% Empty array for the auto correlation function
C_v1 = zeros(n, 1);
% Empty array for the fourier transforms
fft_v1 = zeros(n, 1);
yy = zeros(1200, 19);

Fs = 250; % Samplingsfrekvens
frek = (Fs/2)*linspace(0,1,n/2);

for l=-9:1:9
    % Assigns the right folder for data
    % from the corresponding position
    if l<0
        p = path;
        path(p, 'fxp02azip-1--9cm.zip_FILES')
    else
        p = path;
        path(p, 'fxp02azip0-9cm.zip_FILES')
    end

     % Excludes dataset 5 for positions 0cm and -1cm,
     % as they are missing. Set 4 for -1cm is
     % removed due to error.
    if l==-1
        S = 3;
    elseif l==0
        S = 4;
    else
        S = 5;
    end

    v1_d = zeros(n, S);

    var_v1 = zeros(S, 1);

    for k=1:S
        X(k) = importdata(sprintf('fxp02ai1000-0608-%dcm
              -dataset%d.dat', l, k), ' ', 4);
        Ch1 = X(k).data(:,1);
        Ch2 = X(k).data(:,2);
        d = X(k).data(:, 3);
        Ch4 = X(k).data(:, 4);
        v  = X(k).data(:, 5);
        f = X(k).data(:, 6);

        % Assign variable
        v1 = const_d.*d;
        y1 = 'density';

        % Calculate means
        mean_v1 = mean(v1);
        % Calculate std
        var_v1(k) = var(v1);

        %Autocorrelation function
        for i=1:n
            R_v1 = 0;
            for j=1:n-i+1
                R_v1 = R_v1 + ((v1(j)-mean_v1)*(v1(j+i
                      -1)-mean_v1));
                %R_v1 = R_v1 + (v1(j))*(v1(j+i-1));
            end
            v1_d(i,k) = R_v1;
        end
    end

    v1_dd = sum(v1_d,2);

    C_v1(:) = v1_dd./(n*sum(var_v1));

    % Fouriertransform
    fft_v1(:) = fft(C_v1(:), n)/n;
```

```
    y = 2*abs(fft_v1(1:1200));
    yy(:,l+10) = smooth(y, 25);
end

r = -9:1:9;

% figure
% h = surf(t(1:50), r, C_v1(1:50, :));
% title(sprintf('Autocorrelation function of %s/%s', y1,
      y2), 'FontSize', 20)
% grid on
% colormap jet
% shading interp
% colorbar('location', 'EastOutside')
% set(gca,'FontSize',20, 'LineWidth', 2, 'box', 'on', '
     YDir', 'reverse')
% view([270,90])
% %caxis([-0.2 0.2])
% %xlim([0, n*dt])
% xlabel('t [ms]', 'FontSize', 20)
% ylabel('Position [cm]', 'FontSize', 20)
% %zlabel('Correlation', 'FontSize', 20)
% axis ij;
% axis tight;
% %saveas(h,sprintf('autocorr%s.eps', y1), 'psc2')

% plot power spectrum
figure
h1 = mesh(r, frek(1:1200), yy);
%h1 = plot(frek(1:1500), yy);
grid on
set(h1, 'MeshStyle', 'Column', 'LineWidth', 2)
set(gca, 'LineWidth', 2, 'FontSize', 18)
hidden off
%ylim([0 30])
caxis([0.0 4e-3])
xlabel('Radial pos', 'FontSize', 18);
ylabel('Frequency [kHz]', 'FontSize', 18);
title(sprintf('Power spectrum of %s', y1), 'FontSize',
     18)
view([80,30,30])
%axis tight
zlim([0 4.5e-3])
%saveas(h1,sprintf('powerspec%s.eps', y1), 'psc2')

toc
```

A.5 Cross correlation

```
%************************************************
% Program for calculating the crosscorrelation
% between two signals given i the command window.
% The variables are given from a preset file in a
% given folder. Only one file read at a time.
% The cross correlation function is calculated
% for both positive and negative time values, and
     plotted
% againts a time axis.
%************************************************

clear all; close all;

tic

% Physical constants
temp_e = 5.0;
m_e = 9.11e-31;
e = 1.6e-19;
diam = 0.25e-3;
length_p = 7e-3;
% const is needed to get from I_sat to density
const_d = 2/(e*diam*length_p)*sqrt((pi*m_e)/8*temp_e*e);
distance = 7e-3;
B_ref = 0.154; % Needed to get from Ey to velocity
const_v = 1/(distance*B_ref);
const_f = const_d*const_v;

%S = 5; % Number of datasets
n = 10000; % Number of datapoints

tau=100;

C_v1v2 = zeros(2*tau+1, 19);
%C_v1v3 = zeros(2*tau-1, 19);
%C_diff = zeros(2*tau-1, 19);

v1v2 = zeros(2*tau+1, 1);

for l=-9:1:9
    % Assigns the right folder for data from
    % the corresponding position
    if l<0
        p = path;
        path(p, 'fxp02azip-1--9cm.zip_FILES')
    else
        p = path;
        path(p, 'fxp02azip0-9cm.zip_FILES')
    end

    % Excludes dataset 5 for position -1cm and 0cm,
    % and set 4 for -1 cm, as they are missing.
    if l==-1
        S = 3;
    elseif l==0
        S = 4;
    else
        S = 5;
    end

    % Empty matrises for data from different channels
    Ch1 = zeros(n, S);
    Ch2 = zeros(n, S);
    d = zeros(n, S);
    Ch4 = zeros(n, S);
    v = zeros(n, S);
    f = zeros(n, S);

    % Load data
    for k=1:S
        X(k) = importdata(sprintf('fxp02ai1000-0608-%dcm
             -dataset%d.dat', l, k), ' ', 4);
        Ch1(:,k) = X(k).data(:,1);
        Ch2(:,k) = X(k).data(:,2);
        d(:,k) = const_d*X(k).data(:, 3);
        Ch4(:,k) = X(k).data(:, 4);
        v(:,k)  = const_v*X(k).data(:, 5);
        f(:,k) = const_f*X(k).data(:, 6);
    end

    % Assign variable 1 and 2
    v1 = Ch4;
    y1 = 'Ch4';
    v2 = const_f*f;
    y2 = 'Flux';

    % Calculate means and variance
    mean_v1 = zeros(S, 1);
    mean_v2 = zeros(S, 1);
    var_v1 = zeros(S, 1);
    var_v2 = zeros(S, 1);
    for k=1:S
        mean_v1(k) = mean(v1(:,k));
        mean_v2(k) = mean(v2(:,k));
        var_v1(k) = var(v1(:,k));
        var_v2(k) = var(v2(:,k));
    end

    % Cross correlation
    v1v2_d = zeros(2*tau+1, S);

    v1v2(:) = 0.0;

    % Calculates the cross correlation for both
    % positive and negative tau
    for k=1:S
        for i=0:tau
            R_v1v2 = 0;
            for j=1:n-i
                %R_v1v2 = R_v1v2 + (v1(j,k)-mean_v1(k))
                      *(v2(j+i,k)-mean_v2(k));
```

```
                R_v1v2 = R_v1v2 + v1(j,k)*v2(j+i,k);
            end
            v1v2_d(i+tau+1,k) = R_v1v2;
        end
        for q=0:tau
            R2_v1v2 = 0;
            for p=q+1:n
                %R2_v1v2 = R2_v1v2 + (v1(p,k)-mean_v1(k)
                      )*(v2(p-q,k)-mean_v2(k));
                R2_v1v2 = R2_v1v2 + v1(p,k)*v2(p-q,k);
            end
            v1v2_d(tau-q+1,k) = R2_v1v2;
        end
    end

    v1v2 = sum(v1v2_d,2);

    % Divide by std of the two variables and the length
         of the dataset
    C_v1v2(:,l+10) = v1v2./(n*sqrt(sum(var_v1)*sum(
         var_v2)));
end

% Generates values along x-axis
dt = 4e-3;
t = linspace(-tau*dt, tau*dt, 2*tau+1);
y_1 = -9:1:9;

% Plot cross correlation function
figure(1)
h = surf(t, y_1, C_v1v2');
title(sprintf('Cross correlation function of %s/%s', y1,
      y2), 'FontSize', 20)
grid on
colormap jet
shading interp
colorbar('location', 'EastOutside')
set(gca,'FontSize',20, 'LineWidth', 2, 'box', 'on', '
     YDir', 'reverse')
view([270,90])
%caxis([0 0.6])
%xlim([0, n*dt])
xlabel('t [ms]', 'FontSize', 20)
ylabel('Position [cm]', 'FontSize', 20)
%zlabel('Correlation', 'FontSize', 20)
axis ij;
axis tight;
%saveas(h,sprintf('crosscorr%s%s.eps', y1,y2), 'psc2')

x = -9:1:9;
y3 = 'negative';
theta = (2*pi)/(t(2*tau+1)-t(1)).*t;

[thg,rg] = meshgrid(theta, x(1:9));
%f = inline('C_v1v2', 'theta','r');
%u = feval(f,thg,rg);

[x,y,z] = pol2cart(thg,rg,C_v1v2(:,1:9)');

figure(2); clf;
h2 = surf(x,y,z);
colorbar('location', 'EastOutside')
set(gca, 'FontSize', 20, 'LineWidth', 2, 'box', 'on')
xlabel('r [cm]', 'FontSize', 20)
ylabel('r [cm]', 'FontSize', 20)
view(2)
caxis([-0.19 0.22])
axis square;
shading interp
%saveas(h2,sprintf('crosscorrpolar%s%s%s.eps', y1,y2,y3)
     , 'psc2')

toc
```

A.6 Conditional sampling

```
%***********************************************
% Program that finds the indexes where the data
% from Ch4 are greater than the standard deviation
% times a given constant. These indices are used to
% select snippets of data from another set. This
% is called conditional sampling.
%***********************************************

clear all; close all;

tic

% Physical constants
temp_e = 5.0; %eV
m_e = 9.11e-31;
e = 1.6e-19;
diam = 0.25e-3;
length_p = 7e-3;
% const is needed to get from I_sat to density
const_d = 2/(e*diam*length_p)*sqrt((pi*m_e)/8*temp_e*e);
distance = 7e-3;
B_ref = 0.154; % Needed to get from Ey to velocity
const_v = 1/(distance*B_ref);
const_f = const_d*const_v;

% Number of data points
N = 10000;

% Width of interval to be selected from variable 2
delta_t = 52e-6;

% Sampling rate
Fs = 250e3;

% Number of datapoints to select
dl = delta_t*Fs;

Ds = 19; % Antall datasett

% Empty arrays
phi_con1 = zeros(2*dl+1,Ds);
phi_con2 = zeros(2*dl+1,Ds);
phi_con_med1 = zeros(2*dl+1,Ds);
phi_con_med2 = zeros(2*dl+1,Ds);
sigma_con1 = zeros(2*dl+1,Ds);
sigma_con2 = zeros(2*dl+1,Ds);

% counter for number of events
counter = zeros(19, 1);

%curv_edges = linspace(-0.2e-3, 0.2e-3, 100);

t_hist = (1:1:20);
Dt_kk = zeros(length(t_hist), 19);

for l=-9:1:9
    phi_con1(:, l+10) = 0;
    phi_con2(:, l+10) = 0;
    phi_con_med1(:, l+10) = 0;
    phi_con_med2(:, l+10) = 0;
    sigma_con1(:, l+10) = 0;
    sigma_con2(:, l+10) = 0;
    % Assigns the right folder for data
    % from the corresponding position
    if l<0
        p = path;
        path(p, 'fxp02azip-1--9cm.zip_FILES')
    else
        p = path;
        path(p, 'fxp02azip0-9cm.zip_FILES')
    end

    % Excludes dataset 5 for position -1cm and 0cm
    % as they are missing,
    % as well as set 4 from -1cm since it is wrong.
    if l==-1
       S = 3;
```

```
elseif l==0
   S = 4;
else
   S = 5;
end

q = 1;

for k=1:S
    % imports datafiles
    X = importdata(sprintf('fxp02ai1000-0608-%dcm-
         dataset%d.dat', l, k), ' ', 4);
    Ch1 = X.data(:, 1);
    Ch2 = X.data(:, 2);
    I_sat = (const_d).*X.data(:, 3);
    Ch4 = X.data(:, 4);
    V = (const_v).*X.data(:, 5);
    F = (const_f).*X.data(:, 6);

    % Assign variables
    n=N-1;
    v1 = zeros(n, 1);
    for w=1:n
        v1(w) = (Ch4(w+1)-Ch4(w))/2;
    end
    y1 = 'Channel 4';
    v2 = F(2:n+1);
    y2 = 'Flux';

    % Filter
    % selects intervals where condition is met
    j = 1; % interval no.
    len = 0; % counts length of time interval
    dt = 0; % center of interval
    gamma = 1.5*std(v1); % Threshold value
    %cond = '0.5std'; % string for figure title
    for i=dl+1:n-1-dl % loop starts at dl+1 to
                      % ensure that no interval
                      % includes negative indices.
        if v1(i) < gamma
            continue % returns to top of the loop
                 again.
        end
        if v1(i)>=gamma % tests for value of
             reference signal
            len = len+1; % Counter
            if v1(i+1)< gamma % checks if loop has
                 reached
                                % end of current
                                     interval.
                                % NB must have same
                                     inequality
                                % as top if-test!
                % selects central point of interval.
                      If interval
                % consits of odd number of points,
                     mid point is
                % selected. If interval consists of
                     even number of
                % points, the greater of the two mid
                      points is
                % selected.
                if mod(len,2) == 1
                    dt(j) = i-((len-1)/2);
                else
                    i1 = i-len/2;
                    i2 = i-len/2+1;
                    [C I] = max(abs((v1([i1,i2]))));
                    if I==1
                        dt(j) = i1;
                    else
                        dt(j) = i2;
                    end
                end
                len = 0; % sets length counter to
                     zero
                if V(dt(j))<0 && F(dt(j))>0
                    % test to ensure this interval
                         does not overlap with
                    % previous interval
                    if j>1 && dt(j)-dl-1<dt(j-1)+dl
                        +1
                        continue
                    end
                    j = j+1; % counts on to next
                         interval
                end
            end
        end
    end
    counter(l+10) = counter(l+10)+j-1;

    % Defining empty arrays for storing the
    % subsets of v1 and v2, both as a new string
    % with only these datapoints, and as a string
    % with correct number of zeros between
    % intervals to correspond to initial time series
         .
    var1 = zeros(2*dl+1, length(dt));
    var2 = zeros(2*dl+1, length(dt));
    va1 = zeros(n, 1);
    va2 = zeros(n, 1);

    % Finding the valies of the two series
    % for the intervals where the
    % condition is met.
    for p=1:(length(dt))
        va1(dt(p)-dl:dt(p)+dl) = v1(dt(p)-dl:dt(p)+
            dl);
        va2(dt(p)-dl:dt(p)+dl) = v2(dt(p)-dl:dt(p)+
            dl);
        var1(1:1:2*dl+1, p) = v1(dt(p)-dl:dt(p)+dl);
        var2(1:1:2*dl+1, p) = v2(dt(p)-dl:dt(p)+dl);
    end

    % Counts the number of large flux events left
         after conditional
    % sampling.
    dt(:,:) = 0;
    threshold = 1400;
    ddt = 0;
    for i=1:n-1
        if va2(i)>threshold
            ddt = ddt+1; % Counter
            if va2(i+1) < threshold
                dt(q, k) = ddt; % Store size of
                     interval
                q = q+1; % Continues on to next
                     interval
                ddt = 0;
            end
        else
            dt(q, k) = 0;
            continue
        end
    end


    % Averaging over the intervals, and adding
    % together for each dataset, finding the
    % conditional average, median and std.
    phi_con1(1:1:2*dl+1, l+10) = phi_con1(1:1:2*dl
         +1, l+10) + mean(var1, 2);
    % The number 2 specifies the dimension
    % along which the mean is found, here along
    % the second dimension, i.e. over the events,
    % not over time.
    phi_con2(1:1:2*dl+1, l+10) = phi_con2(1:1:2*dl
         +1, l+10) + mean(var2, 2);
    %phi_con2_sq(1:1:2*dl+1,l+10) = phi_con2_sq
         (1:1:2*dl+1,l+10) + mean(var2.^2, 2);
    phi_con_med1(1:1:2*dl+1, l+10) = phi_con_med1
         (1:1:2*dl+1, l+10) + median(var1, 2);
    phi_con_med2(1:1:2*dl+1, l+10) = phi_con_med2
         (1:1:2*dl+1, l+10) + median(var2, 2);
    %sigma_con1(1:1:2*dl+1, l+10) = sigma_con1
         (1:1:2*dl+1, l+10) + var(var1, 1, 2);
    sigma_con2(1:1:2*dl+1, l+10) = sigma_con2(1:1:2*
         dl+1, l+10) + var(var2, 1, 2)./(mean(var2
         .^2, 2));
end

[s1 s2] = size(dt);
Dt = zeros(s1, 1);
Dt_k = zeros(length(t_hist), S);
```

```
    % Generates histogram matrix from the filter for
         each threshold value
    for k=1:S
        Dt = 1*sort(dt(:,k),1);
        Dt_k(:,k) = (histc(Dt(:), t_hist(:)));
        Dt(:) = 0.0;
    end
    dt(:,:) = 0;
    Dt_kk(:,l+10) = sum(Dt_k, 2);

    % Saving the conditional average for each position,
    % and dividing by the number of datasets.
    phi_con1(:, l+10) = phi_con1(:, l+10)./S;
    phi_con2(:, l+10) = phi_con2(:, l+10)./S;
    phi_con_med1(:, l+10) = phi_con_med1(:, l+10)./S;
    phi_con_med2(:, l+10) = phi_con_med2(:, l+10)./S;
    sigma_con1(:, l+10) = sigma_con1(:, l+10)./S;
    sigma_con2(:, l+10) = sigma_con2(:, l+10)./S;
end

Dt_kk(:,10) = NaN;
Dt_kk(:, 9) = NaN;

% defining a time axis and a position axis
t = linspace(-10^3*delta_t, 10^3*delta_t, 2*dl+1);
r = -9:1:9;

%
% circular plot
%r = -9:1:9;
theta = (2*pi)/(t(length(t))-t(1)).*t;

[thg,rg] = meshgrid(theta, r(1:9));

[x,y,z] = pol2cart(thg,rg,phi_con2(:,1:9)');

figure;
h2 = surf(x,y,z);
colorbar('location', 'EastOutside')
set(gca, 'FontSize', 28, 'LineWidth', 2, 'box', 'on')
xlabel('r [cm]', 'FontSize', 28);
ylabel('r [cm]', 'FontSize', 28);
%caxis([-1000 350])
shading interp
view(2)
axis equal
xlim([-10 10])
ylim([-10 10])

[thg2,rg2] = meshgrid(theta, r(11:19));

[x2,y2,z2] = pol2cart(thg2,rg2,phi_con2(:,11:19)');

figure
h3 = surf(x2,y2,z2);
colorbar('location', 'EastOutside')
set(gca, 'FontSize', 28, 'LineWidth', 2, 'box', 'on')
xlabel('r [cm]', 'FontSize', 28);
ylabel('r [cm]', 'FontSize', 28);
%caxis([-1000 350])
shading interp
view(2)
axis equal
xlim([-10 10])
ylim([-10 10])

[thg3,rg3] = meshgrid(theta, r(10:19));

[x3,y3,z3] = pol2cart(thg3,rg3,1-sigma_con2(:,10:19)');

figure
h4 = surfc(x3, y3, z3);
colorbar('location', 'EastOutside');
set(gca, 'FontSize', 28, 'LineWidth', 2, 'box', 'on');
xlabel('r [cm]', 'FontSize', 28);
ylabel('r [cm]', 'FontSize', 28);
shading interp
caxis([0, 1])
hidden off
view(2)
axis equal

xlim([-10 10])
ylim([-10 10])

[thg4,rg4] = meshgrid(theta, r(1:10));

[x4,y4,z4] = pol2cart(thg4,rg4,1-sigma_con2(:,1:10)');

figure
h5 = surfc(x4, y4, z4);
colorbar('location', 'EastOutside');
set(gca, 'FontSize', 28, 'LineWidth', 2);
xlabel('r [cm]', 'FontSize', 28);
ylabel('r [cm]', 'FontSize', 28);
shading interp
caxis([0, 1])
hidden off

% [thg5,rg5] = meshgrid(theta, r(11:19));
%
% [x5,y5,z5] = pol2cart(thg5,rg5,phi_con_med2(:,11:19)')
    ;
%
% figure
% h6 = surfc(x5, y5, z5);
% colorbar('location', 'EastOutside');
% set(gca, 'FontSize', 28, 'LineWidth', 2, 'box', 'on');
% xlabel('r [cm]', 'FontSize', 28);
% ylabel('r [cm]', 'FontSize', 28);
% shading interp
% %caxis([0, 1])
% hidden off
% view(2)
% axis equal
% xlim([-10 10])
% ylim([-10 10])
%
% [thg6,rg6] = meshgrid(theta, r(1:9));
%
% [x6,y6,z6] = pol2cart(thg6,rg6,phi_con_med2(:,1:9)');
%
% figure
% h7 = surfc(x6, y6, z6);
% colorbar('location', 'EastOutside');
% set(gca, 'FontSize', 28, 'LineWidth', 2, 'box', 'on');
% xlabel('r [cm]', 'FontSize', 28);
% ylabel('r [cm]', 'FontSize', 28);
% shading interp
% %caxis([0, 1])
% hidden off
% view(2)
% axis equal
% xlim([-10 10])
% ylim([-10 10])

figure
b=bar3(t_hist, Dt_kk, 'hist');
%xlim([-9 9]);
set(b, 'EdgeColor', [0.1 0.1 0.1])
xlabel('Probe position [cm]', 'FontSize', 20)
ylabel('No of time steps', 'FontSize', 20)
zlabel('Frequency', 'FontSize', 20)
set(gca, 'FontSize', 20,'xtick', 1:2:19, 'xticklabel',
     -9:2:9)
%title(sprintf('%s', y1))
grid on
ylim([0.5 max(t)+0.5])
axis tight



toc
```

Bibliography

A. S. Bishop. *Project Sherwood The U.S. Program in Controlled Fusion*. Addison-Wesley Publishing Company, Inc., Reading, Massachusetts, USA, 1958.

T. Brundtland. A description of the vacuum chamber for the blaamann plasma experiment. *Vacuum*, 43(3):185–187, 1992.

B. A. Carreras, C. Hidalgo, E. Sánchez, M. A. Pedrosa, R. Balbín, I. García-Cortés, B. van Milligen, D. E. Newman, and V. E. Lynch. Fluctuation-induced flux at the plasma edge in toroidal devices. *Physics of Plasmas*, 3(7):2664–2672, 1996.

F. F. Chen. *Introduction to Plasma Physics and Controlled Fusion*. Plenum Press, 2 edition, 1984. ISBN 0-306-41332-9.

W. Crookes. The Bakerian Lecture: On the Illumination of Lines of Molecular Pressure, and the Trajectory of Molecules. *Philosophical Transactions*, 170: 135–164, 1879.

D. A. D'Ippolito, J. R. Myra, and S. J. Zweben. Convective transport by intermittent blob-filaments: Comparison of theory and experiment. *Physics of Plasmas*, 18(6), 2011.

L. Fattorini, Å. Fredriksen, H. L. Pécseli, C. Riccardi, and J. K. Trulsen. Tubulent transport in a toroidal magnetized plasma. *Plasma Physics and Controlled Fusion*, 54(8), 2012.

Å. Fredriksen, C. Riccardi, L. Cartegni, D. Draghi, R Trasarti-Battistoni, and H. E. Roman. Statistical analysis of turbulent flux and intermittency in the nonfusion magnetoplasma blaamann. *Physics of Plasmas*, 10(11):4335–4340, 2003a.

Å. Fredriksen, C. Riccardi, L. Cartegni, and H. L. Pécseli. Coherent structures, transport and intermittency in a magnetized plasma. *Plasma Physics and Controlled Fusion*, 45(5):721–733, 2003b.

O. E. Garcia. Blob Transport in the Plasma Edge: a Review. *Plasma and Fusion Research: Review Articles*, 4(19):1–7, 2009.

O. E. Garcia. Stochastic modeling of intermittent scrape-off layer plasma fluctuations. *Physical Review Letters*, 108(26), 2012.

R. J. Goldston and P. H. Rutherford. *Introduction to Plasma Physics*. Institute of Physics Publishing Ltd, 1995. ISBN 0-7503-0183-X.

W. Horton. Drift waves and transport. *Reviews of modern physics*, 71(3):735–778, 1999.

T. Huld, A. H. Nielsen, H. L. Pécseli, and J. Juul Rasmussen. Coherent structures in twodimensional plasma turbulence. *Physics of Fluids B-Plasma Physics*, 3 (7):1609–1625, 1991.

H. Johnsen, H. L. Pécseli, and J. Trulsen. Conditional eddies in plasma turbulence. *Physics of Fluids*, 30(7):2239–2254, 1987.

H. E. Jørgensen, T. Mikkelsen, and H. L. Pécseli. Concentration fluctuations in smoke plumes released near ground. *Boundary-Layer Meteorology*, 137(3):345–372, 2010.

S. I. Krasheninnikov, D. A. D'Ippolito, and J. R. Myra. Recent theoretical progress in understanding coherent structures in edge and sol turbulence. *Journal of Plasma Physics*, 74(5):679–717, 2008.

B. Labit, I. Furno, A. Fasoli, A. Diallo, S. H. Müller, G. Plyushchev, M. Podestà, and F. M. Poli. Universal statistical properties of drift-interchange turbulence in TORPEX plasmas. *Physical Review Letters*, 98(25), 2007.

I. Langmuir. Oscillations in ionized gases. *Proceedings of the National Academy of Sciences of the United States of America*, 14(8):627–637, 1928.

M. A. Lieberman and A. J. Lichtenberg. *Principles of Plasma Discharges and Materials Processing*. John Wiley & Sons, Inc., Hoboken, New Jersey, USA, 2 edition, 2005. ISBN 978-0-471-72001-0.

P. C. Liewer. Measurements of microturbulence in tokamaks and comparisons with theories of turbulence and anomalous transport. *Nuclear Fusion*, 25(5):543–621, 1985.

R. W. Motley. *Q Machines*. Academic Press, New York, USA, 1975.

H. M. Mott-Smith and I. Langmuir. The Theory of Collectors in Gaseous Discharges. *Physical Review*, 28:727–763, 1926.

K. Odajima. Effects of Radial Electric Field on Drift Wave Instability in a Weakly Ionized Plasma. *Journal of the Physical Society of Japan*, 44(5):1685–1693, 1978.

ITER Organization. The iter project. `www.iter.org`, 2012.

H. L. Pécseli and J. Trulsen. On the interpretation of experimental methods for investigating nonlinear wave phenomena. *Plasma Physics and Controlled Fusion*, 35:1701–1715, 1993.

H. L. Pécseli. *Fluctuations in Physical Systems*. Cambridge University Press, 2000. ISBN 0 521 65592 7.

H. L. Pécseli. *Waves and Oscillations in Plasmas*. Taylor & Francis, UK, 2012.

P. H. Roberts. On the application of a statistical approximation to the theory of turbulent diffusion. *Journal of Mathematics and Mechanics*, 6(6):781–799, 1957.

K. Rypdal, E. Grønvoll, F. Øynes, Å. Fredriksen, R. J. Armstrong, J. Trulsen, and H. L. Pécseli. Confinement and turbulent transport in a plasma torus with no rotational transform. *Plasma Physics and Controlled Fusion*, 36(7):1099–1114, 1994.

I. Teliban, D. Block, A. Piel, and F. Greiner. Improved conditional averaging technique for plasma fluctuation diagnostics. *Plasma Physics and Controlled Fusion*, 49(4):485–497, 2007.

L. Tonks. Birth of plasma. *American Journal of Physics*, 35(9):857–858, 1967.

F. Øynes, H. Pécseli, and K. Rypdal. Fluctuations in a magnetized toroidal plasma without rotational transform. *Physical Review Letters*, 75(1):81–84, 1995.

F. J. Øynes, O. M. Olsen, H. L. Pécseli, Å. Fredriksen, and K. Rypdal. Experimental study of low-frequency electrostatic fluctuations in a magnetized toroidal plasma. *Physical Review E*, 57(2):2242–2255, 1998.